UNIVERSITY OF CALIFORNIA,
IRVINE

The effect of low-frequency climate variability on stratosphere-troposphere coupling during boreal winter

DISSERTATION

submitted in partial satisfaction of the requirements
for the degree of

DOCTOR OF PHILOSOPHY

Earth System Science

by

Dillon Elsbury

Dissertation Committee:
Professor Gudrun Magnusdottir, Chair
Associate Professor Michael Pritchard
Distinguished Professor Michael Prather

2021

TABLE OF CONTENTS

Page

LIST OF FIGURES iv

LIST OF TABLES x

LIST OF ACRONYMS xi

ACKNOWLEDGEMENTS xii

VITA xiii

ABSTRACT OF THE DISSERTATION xvi

1. Introduction 1
- 1.1 Stratosphere-troposphere coupling 1
- 1.2 Coupling at high latitudes, mid-latitudes, and in the tropics 2
- 1.3 Top-down coupling in the mid-latitudes 4
- 1.4 Bottom-up coupling in the mid-latitudes 6
- 1.5 Scope of the dissertation 8

2. The Atmospheric Response to Positive IPV, Positive AMV and their Combination in Boreal Winter
- 2.1 Introduction 12
- 2.2 Models and experiments 14
- 2.3 Results 17
  - 2.3.1 Mid-latitude wintertime atmospheric response 17
  - 2.3.2 Modulation of the North Pacific upper troposphere by +AMV 21
  - 2.3.3 Planetary wave responses to IPV and AMV variability 27
  - 2.3.4 Polar stratospheric response 29
- 2.4 Discussion and conclusion 34
- 2.5 Sensitivity to the QBO 35

3. Variation in the Holton-Tan effect by longitude
- 3.1 Background 40
  - 3.1.2 Why the Holton-Tan effect may vary over longitude 43
- 3.2 Methods 44
  - 3.2.1 Diagnostic tools 44
  - 3.2.2 Model 46
  - 3.2.3 Control Experiment 46
  - 3.2.4 Climatological polar stratosphere (CPS) experiment 49
  - 3.2.5 Transient QBO Response Experiments 50
- 3.3 Results 51
  - 3.3.1 QBO indexing scheme and Holton-Tan effect 51
  - 3.3.2 Modulation of planetary waves by the QBO 54
  - 3.3.3 Tropospheric response: competition between the direct and indirect effect 59
  - 3.3.4 Timing of the polar vortex response: importance of the North Pacific 63
  - 3.3.5 Stratospheric wave response 65

3.3.6 Reanalysis results 72
3.4 Conclusions and Discussion 74
3.5 Limitations of this study 76
4. Underestimation of the Holton-Tan effect by the CMIP6 models
4.1 Introduction 78
4.2 Methods 80
4.3 Results 82
4.3.1 Zonal mean zonal wind 82
4.3.2 Zonally asymmetric middle stratospheric teleconnection 84
4.3.3 Middle stratosphere in the CMIP6 models 89
4.4 Discussion 94
4.4.1 Importance of the QBO-MMC 94
4.4.2 Limitations of this argument 95
4.5 Conclusions 96
5. Conclusions
5.1 Summary of the research 99
5.2 Ongoing research 101
5.2.1 The poleward shift of the North Pacific jet during QBOE 101
Bibliography 113

LIST OF FIGURES

Page

Figure 1.1: Dec. - Jan. (DJ) 300 hPa zonal wind responses to the QBO (a) and the 60 days following 12 DJ SSWs (b). Hatching denotes responses corresponding to p-values < 0.05 via s student's t-test, when comparing easterly QBO DJ season to westerly QBO DJ seasons (a) and U300 deviations from the seasonal cycle to climatology (b). The QBO is indexed at 70 hPa using winds between 5°S and 5°N. The response is calculated as easterly QBO DJ seasons minus westerly QBO DJ seasons. All ENSO years in which the Nino 3.4 index exceeds +/- 1 sigma are excluded when creating panel (a). The Charlton and Polvani (2007) SSW definition is used for panel (b). The U300 standard deviation (c) and climatology (d) are also shown 3

Figure 2.1: The prescribed sea surface temperature patterns for each combination of IPV and AMV variability. Climatological conditions (Fig. 1f) are shown in a different color scale 15

Figure 2.2: Dec. - Mar. 200 hPa eddy geopotential height anomalies. Climatological zonal means are removed to calculate the eddy component. Anomalies are calculated as the difference between each experiment and the control, denoted "climatology" (e). Hatching denotes p-values < 0.05 via a student's t-test 17

Figure 2.3: As in Figure 2.2, but for sea level pressure. The contour interval on (2.1e) is 2.5 hPa 19

Figure 2.4: Dec. - Mar. PNA indices for each perturbation run calculated using standardized Z500 values and the formula provided by Wallace and Gutzler. On the x-axis, "A" refers to AMV, "C" to cold phase, "I" to IPV, and "W" to warm phase. So AWIC is the +AMV, -IPV experiment. Median values are indicated by each black bar across a boxplot, means are shown by purple diamonds, and printed below each boxplot. Box with negative means are shown in orange. Above each whisker, "**" refers to p-values < 0.05 with a student's t-test 20

Figure 2.5: Dec. - Mar. 250 hPa velocity potential and divergent wind anomalies. Anomalies are calculated as the difference between each experiment and the control, denoted "climatology" (a). Stippling denotes p-values < 0.05 via a student's t-test. Statistically significant divergent wind vectors are shown in gray 22

Figure 2.6: Dec. - Mar. omega (multiplied by -1) responses averaged between 5°N to 5°S. Red means ascent and blue mean descent. The climatological contours in gray use interval +/- 0.02 Pa/second with the zero contour not shown. For the climatology (f), the number of contour intervals is doubled (interval of +/- 0.01 Pa/s) 23

Figure 2.7: Extended winter HadISST SST 1926-2010 climatology (a), +IPV anomalies (d), and +AMV anomalies (g). Positive (warm) anomalies are red and negative (cold) anomalies are blue. The climatology (a) is shown in a different color scale. The middle column contains ERA-20C Z200x anomalies (m) for the +IPV (e), +AMV (h), and a similar climatology shown in a different color scale (b). Positive (negative) anomalies correspond to increases (decreases) in the height field. The last column contains ERA-20C sea level pressure anomalies (hPa) for the +IPV (f), +AMV (i), and a similar climatology (c). Hatching with black dots indicates statistical significance at or above 95% 25

Figure 2.8: Dec. - Mar. 100 hPa vertical wave activity flux anomalies. All wavenumbers are included in the calculation. Anomalies are calculated as the difference between each experiment and the control, denoted “climatology” (e). Hatching denotes p-values < 0.05 via a student’s t-test 27
Figure 2.9: Extended winter daily geopotential height anomalies averaged over the polar cap north of 65°N. These cross sections exhibit time (days) on the x-axis and pressure levels on the y-axis. Shown are the anomalies for the (a) +IPV, (b) +AMV, and (c) +AIV perturbations. Hatching denotes anomalies statistically significant at or above 95%. Two additional composites are calculated: (d) the sum of +IPV and +AMV. (e) is the difference between the +AIV anomalies and the aforementioned linear sum (d) 31
Figure 2.10: The change in frequency of cold extremes for +IPV in (a) early and (b) late winter. (c-d) The same as (a-b) except for +AIV. Increases in frequency are shaded in blue and decreases in red. Cold extremes are days during which the daily temperature falls below the climatological 10^{th} percentile temperature value for that specific day and location 33
Figure 2.11: Dec. - Jan. outgoing longwave radiation (top) and 200 geopotential height (bottom) responses to the QBO in a 300 member set of 1-year timeslice experiments (described in the next chapter). The QBO is defined using the weakest 33% of winds (easterlies) at 10 hPa (a,f), 20 hPa (b,g), and so on. Response corresponding to p-values < 0.05 are hatched. The contour interval is +/- 1 W m^{-2} for the OLR and +/- 3 m for the geopotential height 36
Figure 2.12: Dec. - Mar. 100 hPa vertical wave activity flux anomalies. (c) The response to +IPV forcing. The QBO index defined as the Dec.-Jan. time averaged, zonally averaged, and latitudinally averaged winds between 5°S and 5°N. The upper (lower) tercile of winds make up the westerly (easterly) winters. (a) and (c) show atmospheric responses to a westerly QBO defined at 50 hPa and 30 hPa, respectively. (b) shows the atmospheric response to positive IPV regardless of the background QBO state. (d) Climatological DJFM 100 hPa wave activity flux with +/-.004 m^2s^2 contours 38
Figure 3.1: ERA5 1979-2019 Dec. - Jan. (DJ) zonal mean zonal wind anomalies are shaded. Gray hatching denotes statistical significance, p-values < 0.05 via a student’s t-test, when comparing easterly QBO anomalies to westerly QBO anomalies. Warm (cool) temperature anomalies are shown in black with +/- 1 K contours. The 30 hPa phase angle index of Huang et al. (2012) is used. Anomalies are calculated as QBOE months (19) minus QBOW months (25). QBOE is defined as phases 1-4 and QBOW as phases 5-8. Years in which the Nino 3.4 index is equal to or exceeds +/- 1 sigma are excluded 41
Figure 3.2: Dec. - Jan. averages of the normalized wave activity flux (WAF) responses. A QBO_{30} index is used. The vertical WAF component (WAFz) is shown in color and standardized. Significance is stippled with gray dots coinciding with p-values < 0.05 from a student’s t-test. Black contours show the standardized WAF divergence (WAFd). The intervals are +/- 0.1 standard deviations. The zero contour is not shown. Significance for WAFd is calculated the same way as for WAFz, but it is hatched. Panel (f) shows the average of the 500 QBO_{30} DJ periods. Significance is calculated by comparing the 500 QBO_{30} DJ periods to the 1000 non-easterly QBO_{30} DJ periods. Composite (f) is most similar to composites included in the rest of this chapter. 48

Figure 3.3: December and January (DJ) zonal mean responses to each of the five QBO indices. The isobar used to index the QBO is in the title of each composite. Zonal wind anomalies are shaded and extra contour levels are used about zero to show the tropospheric wind response: gray stippling is used to denote statistical significance. Wave activity flux (WAF) divergence is shown in black contours with intervals of +/ .001, .0025, .005, .01, .025, .05, .1, .25, .5 m/s/day. Standardized (by climatological standard deviation) vertical and meridional WAF responses are shown as vectors. Only statistically significant responses are shown for all fields other than zonal wind. Fig. 1f shows the climatological response: zonal wind is shaded, WAF divergence is shown similarly with intervals of +/ .01, .025, .05, .1, .25, .5, 1, 2.5, 5 m/s/day, and WAF vectors are instead shown as gray 51

Figure 3.4: Zonally averaged anomalies of each longitudinal sector are shown with the same graphical conventions used to create Figure 1. The columns from left to right show the North Atlantic, Siberia, North Pacific, and North America responses. Each row corresponds to a different isobar used to index the QBO. The isobar is given on the right of each row 55

Figure 3.5: Polar stereographic views of the anomalous 850 hPa vertical WAF in the CTL (top) and in CPS (bottom). The isobar used to index the QBO is found above the composites. Stippling is used to denote statistical significance. DJ climatologies in black contours are shown on the right with intervals of +/- 0.03 m^2s^{-2} 56

Figure 3.6: Polar stereographic views of the 50 hPa vertical WAF anomalies in the CTL (top) and in CPS (bottom). The isobar used to index the QBO is found above the composites. Stippling is used to denote statistical significance. Anomalous WAF divergence is overlaid with contour intervals of 0.0026 m/s/day with the zero-contour omitted. Only the statistically significant responses are shown. DJ climatologies in black contours are shown on the right with intervals of +/- 0.003 m^2s^{-2}. The difference between the CTL and CPS anomalies is shown in the bottom row 57

Figure 3.7: Polar stereographic views of the 200 hPa zonal wind response to the QBO in the CTL (top) and in CPS (bottom). Wind anomalies are shaded and stippling is used to denote statistical significance. The isobar used to index the QBO is found above the row 1 plot. The DJ climatological wind is superimposed in black contours with contour levels of 10, 20, 30 … m/s with no zero-contour line 59

Figure 3.8: Pacific sector (135°E to 135°W) zonal mean zonal wind (black contours, 0.25 m/s interval) and temperature responses (shading) to the QBO. The first row features the CTL response, middle is for CPS, and the bottom is the difference between CTL and CPS responses to the QBO. The isobar used to index the QBO is found above these composites. Only responses corresponding to p-values < 0.05 are shown 61

Figure 3.9: October to January (ONDJ) daily 10 hPa geopotential height anomalies (m) over the polar cap (60°N-90°N) and split amongst the four equally sized sectors: North Pacific (135°E to 135°W), North America (135°W to 45°W), North Atlantic (45°W to 45°E), and Siberia (45°E to 135°E). The five different colors used identify the isobar used to index the QBO with QBOW indices corresponding to blue and QBOE indices corresponding to red. The QBO is indexed using only December and January, however October and November are included for the analysis 64

Figure 3.10: Polar stereographic views of the 50 hPa response to the QBO in the seasonal mean. Each column corresponds to a different isobar used to index the QBO. This isobar is denoted in the title of the composites in row one. Row one shows the geopotential height responses, row two the PV responses, and row three the 3D WAF responses. Geopotential height anomalies are shaded and stippling denotes statistical significance. PV anomalies are shown in contours with an interval of +/- 0.5 PVU and gray shading denotes statistical significance. For the 3D WAF, the vertical component is shaded, the meridional and zonal components are shown as vectors, and WAF divergence is shown in blue contours with intervals of +/- 0.0026 m/s/day, excluding the zero contour. Only statistically significant responses are shown 66

Figure 3.11: Polar stereographic views of the 50 hPa atmospheric response to turning on the QBO in the branched experiments. Anomalies are calculated as QBO_{50} – QBO_{10}, which highlights the response to easterly QBO. Row one shows the response over days 11-30, row two: days 31-50, row three: days 51-70, and row four: 71-92. From left to right, column one shows the 3D WAF response. The vertical component is shaded, the meridional and zonal components are shown as vectors, and WAF divergence is shown in contours with an interval of +/- 0.00864 m/s/day, excluding the zero contour. Only statistically significant responses are shown. Column two shows the 510 K PV response. The contour interval in +/- 1 PVU and gray shading denotes statistical significance. Column three shows the geopotential height response in shading and hatching denotes statistical significance. Column four shows the 200 hPa zonal wind response with hatching used to denote statistical significance 68

Figure 3.12: 510 K Potential vorticity (PV) and 50 hPa 3D WAF composites of “upward” and “downward” events in the North Atlantic stratosphere. Refer to text for details on how these plots are created. From left to right, column one shows responses for upward events and column two shows that for downward events. Row one shows the anomalous PV response, row two the anomalous WAF response, and row three the full PV field corresponding to these events. This is indicated to the left of column one. Composite (a) shows the domain over which the vertical WAF is averaged to create the indices for upward and downward events: 60°W to the Prime Meridian and 45°N to 75°N 71

Figure 3.13: As in Figure 10, but for ERA5. The geopotential height anomaly colorscale ranges from +100 to -100 meters now to account for the stronger responses in ERA5 73

Figure 4.1: DJ zonal mean zonal wind anomalies. Thin contours show anomalies between +/- 8.5 m/s with intervals of +/- 1m/s. Thick contours correspond to +10, 15, 20 … m/s. Gray shading denotes statistical significance, p-values < 0.05 via a student’s t-test, when comparing QBO_{E50} anomalies to all other anomalies. To the right of model titles is the number of DJ periods averaged together to make each composite and the 10 hPa latitudinal width of the QBO. Widths are calculated by applying the “half-maximum” method of Richter et al. (2020) and Bushell et al. (2020) to the anomalous 10 hPa response from each plot. Warm (cool) temperature anomalies are shown on Fig. 4.1q with +/- 1 K contours 83

Figure 4.2: ERA5 DJ 850 Kelvin PV anomalies. Anomalies are deviations from the seasonal cycle for QBO_{E50} indices. Hatching denotes statistical significance, p-values < 0.05 via a student' t-test, when comparing QBO_{E50} anomalies to all other anomalies. The contour interval in line and shading for all panels is +/- 10 PVU. Fifteen DJ seasons are used to make the composite (a). Panel (b) shows the standard deviation of the field with contour intervals 10, 20, 30… PVU 85

Figure 4.3: The first three empirical orthogonal functions of the ERA5 850 Kelvin potential vorticity are shown. The variance accounted for by each principal component is printed in the title of each frame 85

Figure 4.4: Anomalies after imposing a QBO_{E50} profile in the transient runs. (a-c): Zonal mean meridional PV gradient for successive 30-day periods after branching: dashed-negative (solid-positive) contours begin at negative (positive) $1x10^{-7}$ $K{\cdot}m{\cdot}kg^{-1}{\cdot}s^{-1}$ and decrease (increase) by negative (positive) $5x10^{-7}$ $K{\cdot}m{\cdot}kg^{-1}{\cdot}s^{-1}$ intervals. The responses at each isentrope are multiplied by $(\theta/350)^{-9/2}$ to account for logarithmic change in PV with height. (d-f): Latitude-time Hövmollers of 850 Kelvin PV (+/- 10 PVU) averaged over 0°E-120°E (d), 120°E-240°E (e), and (f) 240°E-360°E. Gray shading denotes statistical significance in (a-f), p-values < 0.05 via a student's t-test, when comparing QBO_{E50} and control responses. (g-h) Maps of 850 K PV (+/- 10 PVU) anomalies with hatching denoting statistical significance 87

Figure 4.5: DJ 850 K PV anomalies for the 18 datasets. Contour intervals are +/- 10 m/s. Hatching denotes statistical significance, p-values < 0.05 via a student's t-test, when comparing QBO_{E50} anomalies to all other anomalies. Black and blue rectangles denote where the anomalous $_P$ is highly correlated with polar cap warming (Table 4.1) 89

Figure 4.6: December and January time averaged 850 K zonal wind anomalies (m/s) for each of the 18 datasets. Lined contour intervals are +/- 6 m/s excluding the 0 m/s contour. Shaded contours are +/- 3.6 m/s. Hatching denotes statistical significance, p-values < 0.05 via a student's t-test, when comparing QBO_{E50} anomalies to all other anomalies. The QBO_{W10} index is defined as the temporally, zonally, and cosine weighted meridionally averaged 5°S-5°N 10 hPa DJ zonal wind exceeding (less than) 2.5 m/s. The number of DJ periods used to create each composite is printed next to each model title 91

Figure 4.7: Left: The anomalous meridional PV gradient over Asia is compared to the anomalous 10 hPa polar cap (60°N+) temperature. P_ϕ is not divided by the radius of Earth when calculating it. Right: The anomalous 10 hPa QBO, longitudinally averaged and cosine weighted latitudinally averaged zonal winds between 5°S-5°N, of Figure 1 are compared to P_ϕ over Asia 93

Figure 4.8: The anomalous zonally averaged meridional potential vorticity (PV) gradient between 40°N and 60°N and 60°E and 120°E is compared to the 10 hPa latitudinal width of the anomalous zonal wind anomalies in of Figure 4.1 in the chapter. All averaging over time is during December and January (DJ). The latitudinal width is calculated using similar methods to Richter et al. (2020) and Bushell et al. (2020). The peak value of the QBO westerlies between 5°S-5°N is identified. This is the maximum. Half of the maximum defines the northern and southern hemisphere bounds of the QBO. To cleanly identify the latitudinal width to a tenth of a degree latitude, the 10 hPa transect is linearly interpolated from 96 latitude points per dataset to 1800. Transient reversals of the QBO phase that last for 1~4 months are removed from the 10 hPa zonal wind timeseries as is done in the previously mentioned papers 96

Figure 5.1: ERA5 Dec. - Jan. (DJ) 300 hPa zonal wind (top) and 300 hPa geopotential height responses to the QBO. Plots are shown in color, and the lined contour interval is indicated above each plot. The QBO is defined using its easterly phase at 70 hPa - this level is found to maximize the North Pacific response. All ENSO years in which the Nino 3.4 index exceeds +/- 1 sigma are excluded. Hatching indicates p-values < 0.05 with a student's t-test on panels (a) and (d) 103
Figure 5.2: As in Fig. 5.1, but for 200 hPa temperature (top) and 250 hPa temperature (bottom). As an indication of the tropopause, the climatological 200 hPa 2-PVU line is shown in royal blue and the climatological 250 hPa 2-PVU line is shown in cyan on panels (a) and (d) 105
Figure 5.3: Horizontal eddy momentum flux (m^2s^2) responses are shown in row 1 and mean meridional mass streamfunction (10^9 kg/s) responses are shown in row 2. As in Figs. 5.1 and 5.2, the response to the QBO is shown in column 1, the standard deviation in column 2, and the climatologies in column 3. Contour intervals are noted in each plot's title. Statistical significance is shown by gray fill in panel (a) and is hatched in panel (d). Temperature responses are shaded on panel (d) with an arbitrary colorscale of +/- 0.5 Kelvin and significance is stippled for this field 107
Figure 5.4: As in Fig. 5.2, but for 300 hPa (top) and 400 hPa (bottom) 109
Figure 5.5: 300 hPa omega responses (top) and horizontal eddy momentum flux (m^2s^2) responses are shown (bottom). For omega, blue coincides with ascent and red coincides with descent. For panels (a) and (d), hatching denotes statistical significance. The blue line is at 58°N, to illustrate where that large positive horizontal eddy momentum flux anomaly from Fig. 5.3a is - it appears to be over northwestern Canada 110

LIST OF TABLES

Page

Table 2.1 Number and frequency of stratospheric sudden warmings in events per extended winter season. Both number of events and frequency are calculated using daily data (Nov. – Mar.) over the entire 200-year period 30

Table 3.1. The number of months making up the QBO index for each level between 10 hPa and 70 hPa is seen on the diagonal of this matrix. Other cells show the number of the months overlapping between different QBO indices. For example, 285 of the 990 months making up the QBO 30 hPa index overlap with the QBO 10 hPa index 52

Table 3.2. The number of SSWs occurring per QBO index between 10 hPa and 70 hPa are bolded and located on the diagonal of this matrix. Other cells show the number of SSWs that overlap with an adjacent QBO index 53

Table 4.1: Pearson correlation coefficients between the 10 hPa polar cap (cosine weighted latitudinal average poleward of 60°N) temperature anomalies of each model and the corresponding anomalous longitudinally averaged meridional potential vorticity (PV) gradient between 40°N and 60°N. Each row of Table 1 corresponds to a different 60° longitudinal domain.Bolded correlations correspond to p-values < 0.05 when comparing QBO_{E50} anomalies to all other anomalies. Calculations are for all CMIP6 models and ERA5 reanalysis 92

List of Acronyms

Below is a list of selected acronyms used frequently throughout the dissertation

AGCM	Atmospheric Global Climate Model
AIV	+ Atlantic Multidecadal Variability and + Interdecadal Pacific Variability
AMOC	Atlantic Meridional Overturning Circulation
AMV	Atlantic Multidecadal Variability
CAM	Community Atmosphere Model
CMIP	Coupled Model Intercomparison Project
CPS	Climatological Polar Stratosphere
DCPP	Decadal Climate Prediction Project
DJ	December - January
DJFM	December – January – February - March
ENSO	El Nino Southern Oscillation
EOF	Empirical Orthogonal Function
EP Flux	Eliassen-Palm Flux
HEMF	Horizontal Eddy Momentum Flux
HTE	Holton-Tan Effect
IPV	Interdecadal Pacific Variability
ITCZ	Intertropical Convergence Zone
MJO	Madden-Julian Oscillation
NAM	Northern Annular Mode
NAO	North Atlantic Oscillation
OLR	Outgoing Longwave Radiation
PAMIP	Polar Amplification Model Intercomparison Project
PDO	Pacific Decadal Oscillation
PNA	Pacific North American (pattern)
PV	Potential Vorticity
QBO	Quasi-Biennial Oscillation
QBOE	Easterly phase of Quasi-Biennial Oscillation
QBOW	Westerly phase of Quasi-Biennial Oscillation
QBO-MMC	Quasi-Biennial Oscillation Mean Meridional Circulation
SC-WACCM	Specified Chemistry version of WACCM
SIC	Sea Ice Concentration
SIT	Sea Ice Thickness
SST	Sea Surface Temperature
SSW	Sudden Stratospheric Warming
S2S	Subseasonal to Seasonal
U10/U300	Zonal Wind at 10 hPa/300 hPa
WACCM	Whole Atmosphere Community Climate Model
WAF	Wave Activity Flux

ACKNOWLEDGEMENTS

Thank you for being an excellent person and advisor, Gudrun. I appreciate the simple things you did, like lending your books, all the way up to guiding me, leading our group, and sharing your Earth System Science expertise. Your appreciation for Rossby waves made me excited about them too. You assembled a great lab group. I really enjoyed my time here with Ana Sena, Zachary Labe, Tien-Yiao Hsu, Wenchang Yang, Yuna Lim, and Yannick Peings. I would not have had the privilege of meeting them without you steering the ship.

Thank you, Yannick. You have been the best second advisor. I think that an expertise of yours is global climate modeling and I appreciate the privilege of learning this from you. You and Gudrun always brought positive energy to our meetings and interactions. I am going to miss hanging out in the cubicle farm and looking at plots.

To Ana, Zack, Tien-Yiao, Wenchang, and Yuna, it was a pleasure to meet each of you, work with you, and also, to not work on occasion. Some of favorite memories from working together involved the occasional nonverbal agreement to just stop working and chat. Daniel Ruiz, the social butterfly that he is, could not resist joining in on this either. Each of you taught me plenty.

I really appreciate my dissertation committee members, Michael Pritchard and Michael Prather, as well as my advancement committee members Jin-Yi Yu, and Adeyemi Adeleye. Thank you for letting me stop by your offices on occasion. Those conversations were helpful for me and I appreciate your guidance. While I am expecting a serious challenge, I cannot wait to study atmospheric chemistry, Michael, and I am excited to see where you take tropical dynamics, Mike. Claudia Czimczik, Francois Primeau, and Juno Hsu have been similarly helpful and open to talking over the years. I am grateful to be a member of the Department of Earth System Science. There is a culture of empathy in the department in my experience. Thank you to the faculty, researchers, postdocs, students, and friends (👍🏾) that cultivate this culture.

I would also like to acknowledge the decades of support and love from my mom, Monica. I want to thank you for what you have done, but it is difficult because you did it all. I appreciate you more each day.

Thank you to Gregory Osterman, Arturo Keller, and Kendra Garner for showing me that science can be a passion and a job. In particular, thank you Amy Mainzer and Riley Duren. I appreciate the decade plus of laughs, facts, and guidance that I have received from you two.

Funding has been provided by the National Science Foundation (NSF), Division of Atmospheric Geopspace Sciences (AGS-1624038) and NSF Division of Graduate Education (DGE-1839285). Additional funding has also been provided by the Department of Energy, Office of Biological Environment Research (DE-SC0019407). Further, the Department of Earth System Science at UC Irvine has funded part of this work. I also acknowledge high-performance computing support for Cheyenne (doi:10.5065/D6RX99HX) and Yellowstone (ark:/85065/d7wd3xhc) provided by NCAR's CISL, sponsored by the NSF.

Finally, I would like to thank the American Meteorological Society and Wiley for permission to include work published in their journals within Chapters 2 and 3 of this dissertation.

VITA

Dillon Elsbury

Education

Ph.D. in Earth System Science — June 2021
University of California, Irvine

M.Sc. in Earth System Science — February 2019
University of California, Irvine

B.Sc. in Environmental Studies — June 2015
University of California, Santa Barbara

Research Interest

Large-scale atmospheric circulation | Climate variability | Stratosphere-troposphere coupling | Atmospheric Predictability | Extreme Weather | Watersheds | Astronomy

Scientific Research Experience

Graduate Research Assistant — September 2016-June 2021
Advisor: Gudrun Magnusdottir at University of California, Irvine

- Assessed the impact of the Quasi-Biennial Oscillation and sea surface temperature variability on stratosphere-troposphere coupling and extreme weather events by using global climate models

Staff Reseach Associate — October 2015-September 2016
Keller Research Team at University of California Santa Barbara

- Used the Water Analysis Risk Management Framework (WARMF) model to make predictions of nitrogen and phosphorous loads entering the Mississippi River

Staff Research Associate — June 2015 – September 2016
Chemical Life Cycle Collaborative at University of California Santa Barbara

- Developed fate and transport model to predict the dispersion of organic chemical pollutants through waterways and soils in six major United States cities

Student Intern — Summers of 2014, 2013, 2012, 2010
NASA Jet Propulsion Laboratory: Orbiting Carbon Observatory (OCO-2) and Wide Field Infrared Survey Explorer (WISE) teams

- 2014: OCO-2: Colocated atmospheric carbon dioxide observations made by satellite with “true” ground-based observations to verify that retrieval algorithm used by the team was working
- 2013: OCO-2: Used remotely sensed fluorescence data to study changes in terrestrial vegetation over time with a focus on the response of plants to the 2012-2013 North American drought
- 2012: OCO-2: Investigated the sensitivity of the retrieval algorithm and data quality to spatiotemporal biases associated with aerosols
- 2010: WISE: Performed quality assurance of the asteroid observations made by the satellite and investigated the orbital distribution of the observed comets

Publications

Elsbury, D., Peings, Y., and Magnusdottir, G., 2021. Variation in the Holton-Tan effect by longitude, *Quarterly Journal of the Royal Meteorological Society, v. 147(736), 1767-1787*

Elsbury, D., Peings, Y., and Magnusdottir, G., 2019. The Atmospheric Response to Positive IPV, Positive AMV, and Their Combination in Boreal Winter, *Journal of Climate, v. 32(14), 4193*

Publications in preparation

Elsbury, D., Peings, Y., and Magnusdottir, G., 2021. CMIP6 models underestimate the Holton-Tan effect, *Geophysical Research Letters* (Submitted).

Professional affiliations

2017 – Present: American Geophysical Union - Member
2020 – Present: Few Affiliations Club – President

Fellowships and awards

Spring 2018 – Spring 2021: NSF Graduate Research Fellowship (awarded and accepted)
January 2017 – June 2018: NSF Research Traineeship Grant for Machine Learning and Physical Science Sciences (honorary fellow)

Presentations

Elsbury, D., Peings, Y. and Magnusdottir, G. (December 2019). *Variation in the Holton-Tan effect by longitude*. American Geophysical Union Fall Meeting 2019. Oral presentation, San Francisco, California.

Elsbury, D., Rapp, C., Minallah, S., and Martinez, C. (July 2019). *Sequential Severe Weather and Flood Events of 16-20 May 2016*. NCAR ASP Summer Colloquium. Oral presentation at NCAR.

Elsbury, D., Peings, Y. and Magnusdottir, G. (December 2017). *Atmospheric Response to multi-decadal sea surface temperature variability in the Pacific Ocean (IPV) and the Atlantic Ocean (AMV)*. American Geophysical Union Fall Meeting 2017. Presented poster, New Orleans, Louisiana.

Elsbury, D., Garner, K. and Keller, A. (June 2016). *Fate and Transport Module.* Chemical Life Cycle Collaborative (CLiCC) Chemical Life Cycle Assessment Workshop 2016. Led session at University of California, Santa Barbara.

Garner, K., Elsbury, D. and Sonar, . (September 2015). *Fate and Transport Module.* Chemical Life Cycle Collaborative (CLiCC) Annual Program Review 2015. Oral Presentation at University of California, Santa Barbara.

Elsbury, D. and McGurk, G. (June 2015). *Reservations and Renewable Energy: The Suitability of Native American Lands for Renewable Energy Development.* Spatial Science Poster and Plenary Session. Presented poster at University of California, Santa Barbara.

Elsbury, D. and Osterman, G. (August 2014). *Colocating XCO2 Observations to Investigate the ACOS XCO2 Bias.* JPL Summer Internship Final Presentations. Oral presentation given at NASA JPL.

Elsbury, D., Osterman, G. and Frankenberg, C. (August 2013). *Chlorophyll Fluorescence as an OCO-2 Product.* JPL Summer Internship Final Presentations. Oral presentation given at NASA JPL.

Elsbury, D., Osterman, G. and Frankenberg, C. (July 2013). *Chlorophyll Fluorescence as an OCO-2 Product.* JPL Earth Science Director's Review. Oral presentation given at NASA JPL.

Elsbury, D. and Osterman, G. (August 2012). *Carbon Dioxide and Aerosol Optical Depth Validation for the Orbiting Carbon Observatory 2.* JPL Summer Internship Final Presentations. Oral presentation given at NASA JPL.

Elsbury, D., Mainzer, A. and Masiero, J. (August 2010). *Understanding the Orbital Distribution of Comets.* JPL Summer Internship Final Presentations. Oral presentation given at NASA JPL.

Teaching experience

Spring 2018: Teaching Assistant, "The Atmosphere"

Winter 2018: Teaching Assistant, "Air Pollution"

Outreach experience and events

Spring 2019 – Present: Half-Baked, informal seminar series host.
February 2020 – Science Olympiad. Created, proctored, and graded meteorology exam.
January 2020 – Climate Solutions Conference. Mentored group of presenters

Professional workshops

July 2019 – NCAR Advance Summer Program on Quantifying and Communicating Uncertainty in High Impact Weather Prediction

Technical strengths

Python, MATLAB, Bash, CDO, NCO, NCL ArcGIS, SQL, making plots

ABSTRACT OF THE DISSERTATION

The effect of low-frequency climate variability on stratosphere-troposphere coupling during boreal winter

by

Dillon Elsbury

Doctor of Philosophy in Earth System Science

University of California, Irvine, 2021

Professor Gudrun Magnusdottir, Chair

The exchange of heat, momentum, and chemical species between the stratosphere and troposphere affects weather and climate. Stratosphere-troposphere coupling often refers to *weather* events. As a result, there are many studies focusing on dynamical coupling between the two layers at daily to seasonal timescales. Less is known about how low frequency *climate* variability in the Earth system affects stratosphere-troposphere coupling.

The purpose of this dissertation is to assess how three forms of low frequency climate variability, the Quasi Biennial Oscillation (QBO), Interdecadal Pacific Variability (IPV), and Atlantic Multidecadal Variability (AMV), influence stratosphere-troposphere coupling. The main tools used are multi-century, high-top, atmospheric global climate model perturbation experiments and reanalysis. Two specific goals are to (1) assess what teleconnections are elicited by each mode of variability and (2) identify how these teleconnections enhance or suppress stratosphere-troposphere coupling. The stratospheric circulation is often associated with wintertime extreme weather events. Benchmarking how these modes of variability affect stratosphere-troposphere coupling may enhance predictability of these events.

Studies have assessed the atmospheric response to IPV and AMV individually, but not together. Here, all combinations of IPV and AMV are imposed in a set of perturbation experiments to assess their combined effects on the boreal winter atmosphere. The atmospheric response to IPV dominates the response forced by AMV. In nature, the AMV is currently in its positive phase and the IPV is thought to be transitioning to its positive phase. Therefore, more targeted study is done for the positive AMV experiment, positive IPV experiment, and their combination. Positive IPV promotes a deeper Aleutian Low, which is partially cancelled by the atmospheric response to positive AMV, which promotes ridging over the North Pacific. While the polar stratospheric response to positive IPV is broadly similar with or without positive AMV, the downward propagation of the polar stratospheric warming during positive IPV is significantly reduced when the positive AMV is included.

Since the QBO has a known teleconnection with the polar stratosphere, the Holton-Tan effect, a brief attempt is made to subsample the IPV and AMV results by QBO phase. It becomes unclear how the QBO is suppressing or enhancing the IPV and AMV teleconnections. As a result, I pivot towards using a hierarchy of model experiments to isolate the impact of the QBO on planetary waves and the tropospheric and stratospheric circulations. The QBO is found to promote amplification of planetary waves at the tropopause, contrasting with the amplification of planetary waves in the troposphere promoted by IPV and AMV. The QBO forces regional teleconnections. There is consistent evidence that the North Pacific atmosphere is more tightly coupled with the QBO compared to other longitudes. The QBO promotes latitudinal shifting of the tropospheric jet stream, especially in the North Pacific. However, the polar stratospheric response to the QBO moderates this effect. While the QBO promotes an interesting set of teleconnections in the lower stratosphere, the dominant teleconnection between the QBO and polar vortex occurs in the middle stratosphere (30 kilometers).

Chapter 1

Introduction

1.1 Stratosphere-troposphere coupling

Studies continuously show that the stratosphere can influence the circulation in the troposphere and near the surface of Earth (Kodera et al., 1990; Perlwitz & Graf, 1995; Thompson & Wallace, 1998; Charlton & Polvani, 2007; Garfinkel & Hartmann, 2011a,b; Jia et al., 2017). Stratosphere-troposphere coupling often occurs at weather timescales or throughout a season. But this coupling is sensitive to low frequency internal climate variability in the Earth System - slow fluctuations on the order of a few years to many decades. Our records of the atmospheric state, which are around 40 to 60 years, are often too short to retrieve robust results showing how low frequency climate variability affects transient instances of stratosphere-troposphere coupling. To overcome this problem, we can use long integrations with global climate models (GCMs) to evaluate how climate affects weather. In this dissertation, low frequency internal climate variability refers to (1) the Quasi-Biennial Oscillation (QBO), (2) Interdecadal Pacific sea surface temperature Variability (IPV), and (3) Atlantic Multidecadal sea surface temperature Variability (AMV). The purpose of this work is to assess how wintertime stratosphere-troposphere coupling is influenced by these climate modes. The following stratosphere-troposphere coupling pathways are considered: (1) downward propagating Northern Annular Mode variability, (2) sudden stratospheric warmings, (3) QBO coupling with the mid-latitude troposphere directly, and (4) QBO coupling with the polar stratosphere and subsequently the troposphere.

1.2 Coupling at high latitudes, mid-latitudes, and in the tropics

At high latitudes, downward propagating Northern Annular Mode (Baldwin & Dunkerton, 1999; Domeisen et al., 2020) variability couple the polar stratospheric flow with the lower tropospheric circulation. Sudden stratospheric warmings (SSWs), rapid decelerations of the wintertime polar stratospheric flow associated with polar cap warming, are prominent components of NAM variability (Charlton and Polvani 2007; Butler et al. 2017). SSWs promote ridging of the canonical Icelandic Low and decreases in atmospheric height over the canonical Azores High, a negative North Atlantic Oscillation (NAO) response, in which the North Atlantic jet-stream shifts equatorward (Fig. 1b). This may promote multi-month (White et al. 2021) temperature and precipitation fluctuations over mid-latitudes (Butler et al. 2017). While SSWs are extreme *weather* events, their frequency and perhaps the type of SSW (Liu et al. 2014) is sensitive to the lower frequency *climate* variability in the Earth System. Atlantic Multidecadal sea surface temperature Variability (AMV, Omrani et al. 2014; Peings and Magnusdottir 2016) and Interdecadal Pacific sea surface temperature Variability (IPV, Kren et al. 2016) influence the wintertime polar stratospheric circulation. Further, the average 28-month Quasi-Biennial Oscillation (QBO) in tropical stratospheric winds between easterlies and westerlies (Baldwin et al. 2001) also affects NAM variability and the frequency of SSWs (Labitzke 2005; Lu et al. 2014; Dimdore-Miles et al. 2021; Anstey et al. 2021). This may be why the U300 response to the QBO (Fig. 1.1a) and the U300 response to SSWs (Fig. 1.1b) are so similar.

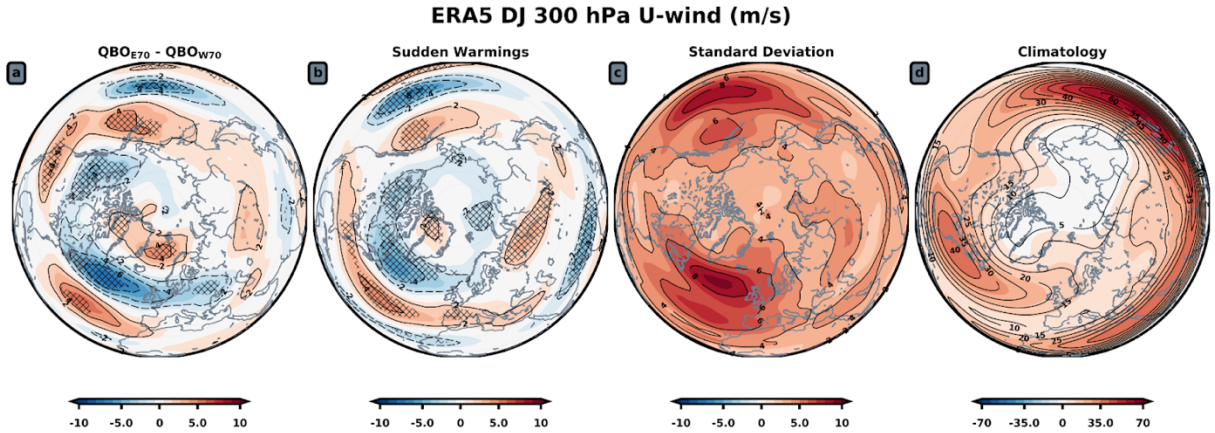

Figure 1.1: Dec. - Jan. (DJ) 300 hPa zonal wind responses to the QBO (a) and the 60 days following 12 DJ SSWs (b). Hatching denotes responses corresponding to p-values < 0.05 via s student's t-test, when comparing easterly QBO DJ season to westerly QBO DJ seasons (a) and U300 deviations from the seasonal cycle to climatology (b). The QBO is indexed at 70 hPa using winds between 5°S and 5°N. The response is calculated as easterly QBO DJ seasons minus westerly QBO DJ seasons. All ENSO years in which the Nino 3.4 index exceeds +/- 1 sigma are excluded when creating panel (a). The Charlton and Polvani (2007) SSW definition is used for panel (b). The U300 standard deviation (c) and climatology (d) are also shown.

At mid-latitudes, there are multiple ways for the stratosphere and troposphere to interact. The QBO has a "subtropical route" of influence whereby the QBO is thought to affect the tropospheric subtropical jet (Garfinkel et al. 2011a,b; Gray et al. 2018; Hitchman et al. 2021). When the easterly component of the QBO is located in the tropical lower stratosphere around 50 or 70 hPa (QBOE), reanalysis shows a poleward shift of the upper tropospheric jet in Fall (Inoue et al. 2011; Inoue et al. 2013) and during winter (Garfinkel et al. 2011a,b; White et al. 2015; Wang et al. 2018; Hitchman et al. 2021). This result is reproduced in Fig. 1a, for which all of the years when the December-January Nino 3.4 index exceeds +/-1 sigma have been removed. An interesting finding from Fig. 1a is that the observed zonal mean poleward shift of the jet (e.g., White et al. 2015) seems to be a North Pacific feature. The direct influence of the QBO on the tropospheric jet, namely the Pacific jet, is debated as multi-model studies do not consistently show this response (Anstey et al. 2021). Further research is needed here as there is widespread interest in leveraging the QBO for subseasonal to seasonal (S2S) forecasts of NAM variability (Garfinkel et al., 2018; Anstey et al. 2021), forecasting the Madden-Julian

Oscillation (MJO, (Lim et al., 2019; Kim et al., 2019), and forecasting the associated QBO-MJO impacts on weather in the mid-latitudes (Mundhenk et al., 2018).

The tropics are an interesting hotspot for low frequency fluctuations in stratosphere-troposphere coupling. The QBO modulates tropical convection by means not comprehensively understood (Son et al., 2017; Martin et al., 2019; Haynes et al., 2021). The QBO also demonstrates multi-decadal fluctuations in reanalysis (Lu et al. 2014) and model experiments (Dimdore-Miles et al. 2021). Speculating then, the QBO may have a moderate low frequency impact on convection. The 11-year solar cycle is also relevant. It affects the temperature of the stratosphere (Kodera et al. 1990; Labitzke 2005) and influences the tropospheric circulation (Haigh et al. 2005; Kidston et al. 2015). If climate change is regarded as a low frequency forcing, Arctic amplification (Labe, 2020) and the observed upper tropospheric warming (Santer et al., 2017; Li et al., 2019) may interact to influence the mid-latitude tropospheric circulation (Manzini et al., 2014; Peings et al., 2019). Further, the response of the Brewer Dobson Circulation to stratospheric cooling associated with increasing greenhouse gas emissions (Butchart et al., 2010) may promote changes in the tropospheric jets (Scaife et al., 2014).

1.3 Top-down coupling in the mid-latitudes

Stratosphere-troposphere coupling occurs on intraseasonal, interannual, and decadal timescales (Thompson and Wallace 1998; Kidston et al. 2015). SSWs illustrate top-down coupling between the stratosphere and troposphere well. SSWs are dramatic intraseasonal events that affect the global circulation – they occur about six times per decade in the northern hemisphere (Charlton and Polvani 2007; Butler et al., 2017). In the southern hemisphere, they are rare, with one major warming in September of 2002 (Newman & Nash, 2005; Charlton et al., 2005) and one minor warming in September of 2019 (Noguchi et al. 2020). SSWs occur when

planetary scale waves break on the edge of the polar vortex, prompting easterly torque, counteracting the climatological westerly flow (McIntyre, 1982; McIntyre & Palmer, 1983). In the case of a split polar vortex, the tropospheric response is instantaneous while for a displaced polar vortex, it takes approximately two weeks for the troposphere to respond (White et al. 2021). SSWs have nonlocal effects on the atmospheric circulation. While SSWs occur at polar latitudes, they affect the Brewer Dobson Circulation and therefore tropical lower stratospheric stability and convection (Eguchi et al., 2015; Noguchi et al. 2020). The tropospheric jet-stream shifts equatorward in response to the polar stratospheric warming (Limpasuvan et al. 2004; Baldwin et al. 2021). The duration of the tropospheric response appears to be dependent on how deep the polar stratospheric warming makes it into the lower stratosphere where the multi-week radiative damping rates “preserve” the temperature anomaly (Kodera et al. 1990; Kuroda & Kodera, 2001; Hitchcock et al., 2013; Kodera et al., 2016). In the event that the lower polar stratosphere is anomalously cold, everything reverses. The tropospheric jet shifts poleward (Polvani and Kushner 2002; Shaw & Perlwitz, 2014), mainly over the Atlantic (Nie et al., 2008), and the polar stratosphere is more depleted of ozone (Lawrence et al., 2020). This shifting of the tropospheric jet equatorward in response to changing conditions in the stratosphere is the key manifestation of mid-latitude stratosphere-troposphere coupling. Meridional excursions in the jet enhance its sinuosity, promoting cold spells (Röthlisberger et al., 2016, 2019; Matthias & Kretschmer, 2020).

Meridional excursions of the jet characterize annular mode variability (Kushner, 2010). Kodera et al. (1990) and Perlwitz and Graf (1995) were some of the first to show that stratospheric winds are associated with meridional movement of the tropospheric jet stream. Interest in annular modes skyrocketed once Thompson and Wallace (1998, 2000) defined annular modes as principal components of sea level pressure and geopotential height variability. Baldwin and Dunkerton (1999), Christiansen, (2001), and Kuroda and Kodera (2001) demonstrated that

stratospheric variability is downward propagating and leads changes in the tropospheric circulation. When viewed in a zonal mean, annular mode variability characterizes meridional excursions in the eddy-driven portion of the jet (Christiansen, 2001; Lorenz & Hartmann, 2001; Lorenz & Hartmann, 2003; Eichelberger & Hartmann, 2007). Jet variability is enhanced following changes to lower stratospheric temperature (Polvani and Kushner 2002; Haigh et al. 2005; Simpson et al. 2009; Domeisen et al., 2013; Hitchcock et al. 2014). A feedback between synoptic eddies and the lower frequency flow (Lorenz and Hartmann 2001, 2003) maintains the tropospheric wind response to lower stratospheric temperature change, but it is not clear what role the stratosphere plays in this response (Hitchcock and Simpson 2016; White et al. 2019). Further, there is uncertainty over how the tropospheric jets will adjust in a changing climate (Gerber et al., 2010; Simpson et al. 2018).

1.4 Bottom-up coupling in the mid-latitudes

Upward propagating planetary waves from the troposphere enter the stratosphere from mid-latitudes and propagate equatorward in climatology, breaking in the so-called mid-latitude 'surf-zone' (Matsuno, 1970; McIntyre & Palmer, 1984; Lu et al. 2020). A wave will propagate along a steep gradient in the south-to-north positive definite isentropic potential vorticity (PV) field (McIntyre 1982; McIntyre 1992), which normally takes the wave up the edge of the polar vortex (Lu et al. 2020). When the wave breaks, PV is mixed irreversibly, with more PV pooling in lower latitudes and PV being diluted at higher latitudes. Algorithms made to identify wave breaking usually look for signs of flattening or complete reversals of the meridional PV gradient (Abatzoglou & Magnusdottir, 2006; Hitchman & Huesmann, 2009; Barnes and Hartmann 2012). Meridional transport of stratospheric trace gases, namely ozone, occurs when planetary waves break (Leovy et al., 1985). Diabatic circulations arise in response to the wave breaking, driving cross isentropic mass flow in the stratosphere (Haynes & McIntyre, 1987). These circulations

may be viewed in the transformed-Eulerian mean sense, which lends itself to longitudinal averaging (e.g, Dunkerkton et al. 1981), but longitudinal averages hide the zonal asymmetry that Lagrangian circulations and Stokes drift reveal (Dunkerton, 1978; Haynes & McIntyre, 1987; Kinoshita et al., 2019). While these circulations will not be viewed explicitly in this dissertation, the coupled variability of planetary waves and their effect on the mean flow will be a consistent theme.

There are three non-mutually-exclusive views on how planetary scale waves are forced. One is through linear interference - this one emphasizes the troposphere. A planetary scale stationary wave pattern exists in the troposphere. It is a set of semi-permanent undulations in the wind-field forced by topography, land-sea contrast, and zonally asymmetric diabatic heating (Plumb 1985; Garfinkel et al., 2020). When an anomalous wave forced by anomalous boundary condition comes into phase with the climatological wave pattern, the combined wave may be amplified such that it can propagate into the stratosphere (Smith et al., 2010; Fletcher & Kushner, 2011). A second view emphasizes that the stratosphere regulates upward wave propagation (Plumb, 2010; Hitchcock & Haynes, 2016; Cámara et al., 2017). Recent studies find that deceleration of the polar stratospheric flow, during SSWs for instance, is more often preceded by anomalous wave activity in the *stratosphere* rather than the *troposphere* (Birner & Albers, 2017; Cámara et al., 2019) and that the origin (stratosphere or troposphere) of the wave determines the tropospheric response to the stratospheric warming (White et al., 2019). This view is consistent with studies emphasizing the balance between radiative forcing and planetary wave breaking as the two controls of internal stratospheric variability (Holton & Mass, 1976; Scott & Polvani, 2004, 2006). A third view, which connects the previous two, is that the tropopause (Chen & Robinson, 1992) or lower stratosphere (Martineau et al., 2018) acts as a valve for upward propagating waves. This view emphasizes the tropopause as a wave source with a potential role for synoptic scale eddies (Scinocca & Haynes, 1998; Boljka & Birner, 2020).

Coy et al. (2009) and Coy & Pawson (2015) show nice examples of synoptic scale disturbances entering the stratosphere and amplifying just before SSWs.

1.5 Scope of the dissertation

This dissertation aims to improve our understanding of how low frequency internal climate variability promotes stratosphere-troposphere coupling during boreal winter. An underlying motivation for this work is to contribute to a better understanding of how weather and climate intersect, so-called subseasonal to seasonal (S2S) variability. The stratosphere is well-suited for this. Studies consistently show that better representing the stratosphere in climate models by enhancing its resolution (Scaife et al. 2012; Barton et al. 2019) or by forcing the modeled stratosphere towards its observed state (Jia et al. 2017; Choi and Son 2019; Noguchi et al. 2020) enhances the modeled representation of the troposphere (Butler et al., 2019). Better understanding the stratosphere is good for tropospheric predictability. However, there are two key problems: (1) our observational record is short and (2) the atmospheric circulation is chaotic. Therefore, the QBO, IPV, and AMV are imposed in simplified perturbation experiments, which are run for sufficiently long periods, to isolate the teleconnections they force.

Chapter 2 begins with a brief introduction of how IPV and AMV influence climate. Getting into the results, I first show the wintertime atmospheric response to all nine combinations of IPV and AMV variability, one of the first times this is done. Considering the current positive polarity of the AMV in nature and the expected phase transition to positive IPV, more targeted analysis is presented for positive IPV, positive AMV, and their combination. I close with a brief example of why it is interesting to split the IPV and AMV results by QBO phase, but also why it is tricky to do so. The two questions addressed in this chapter are:

1. What is the wintertime atmospheric response to every combination of IPV and AMV?
2. How do the atmospheric responses to each mode compete or reinforce each other while promoting stratosphere-troposphere coupling?

Parts of this chapter are published in *Journal of Climate*:

Elsbury, D., Peings, Y., Saint-Martin, D., Douville, H., & Magnusdottir, G. (2019). The atmospheric response to positive IPV, positive AMV, and their combination in boreal winter. *Journal of Climate*, *32*(14), 4193-4213, doi: doi.org/10.1175/JCLI-D-18-0422.1

Chapter 3 begins with a discussion of the QBO anatomy and what is known about its teleconnection with the wintertime polar vortex. Most of this information is derived from studies using zonally averaged fields. The literature consistently shows that the QBO modulates planetary waves in a way that weakens (strengthens) the polar vortex when the easterly (westerly) portion of the QBO is located in the tropical lower stratosphere. However, none of the studies show where, what longitudinal sector, this planetary scale wave activity flux is coming from. Without a better understanding of how the QBO *alone* affects planetary waves, it is difficult to infer how the QBO and another mode of variability like the IPV or AMV combine to affect the planetary waves. Therefore, the following questions are asked:

1. How does the impact of the QBO on the extratropical circulation vary over longitude? What longitudinal sector does the planetary scale wave activity flux forced by the QBO come from?
2. What is the impact of the QBO on the wintertime atmosphere versus the impact of the stratospheric polar vortex on the wintertime atmosphere? Both have been shown to influence the position of the tropospheric jet-stream.

Hundreds of timeslice experiments reveal that the QBO and internal polar stratospheric variability compete to alter the tropospheric circulation, the stratospheric circulation, and the planetary wave response to the QBO. This competition between the QBO and polar stratospheric variability is most pronounced for the North Pacific tropospheric jet-stream. While studies have shown that the QBO modulates the position of the North Pacific jet (Inoue et al. 2011, 2013; Garfinkel and Hartmann 2011a,b; Wang et al. 2018), a new result discussed in this chapter is that the polar stratospheric response to the QBO also modulates the position of the jet. These effects compete with each other.

This work is published in the *Quarterly Journal of the Royal Meteorological Society*:

Elsbury, D., Peings, Y., & Magnusdottir, G. (2021). Variation in the Holton–Tan effect by longitude. *Quarterly Journal of the Royal Meteorological Society*, doi.org/10.1002/qj.3993

Chapter 4 builds on Chapter 3 by evaluating how the CMIP6 models represent the Holton-Tan effect. The CMIP6 models studied spontaneously generate the QBO. As a result, there is considerable variability in how the models represent the QBO and its associated teleconnections like the Holton-Tan effect. The models underestimate stratosphere-troposphere coupling in response to the QBO. I ask the following questions to investigate why:

1. How well do the models simulate the teleconnection between the QBO and the polar stratosphere?
2. What attributes of the QBOs themselves are most important for simulating the QBO teleconnections?

This work has been submitted and is currently being reviewed for *Geophysical Research Letters*.

Chapter 5 begins with a summary of the key findings from each chapter. Following that, I work to better resolve the impact of the QBO on the North Pacific jet-stream by using reanalysis data.

Note that Chapter 2 and Chapter 3 are similar to their corresponding papers published in Journal of Climate and the Quarterly Journal of the Royal Meteorological Society, respectively. While Chapter 3 is very consistent with its corresponding published paper, many results have been included in Chapter 2 that do not appear in the corresponding paper.

Chapter 2

The Atmospheric Response to Positive, IPV, Positive AMV and their Combination in Boreal Winter

2.1 Introduction

Decadal to multidecadal fluctuations of sea surface temperature (SST) in the Pacific and North Atlantic drive variations in climate and are potential sources of predictability for regional temperature and precipitation (Kerr, 2000; England et al., 2014; Dong & Dai, 2015; Cassou et al., 2018). Traditionally the leading mode of interannual to multidecadal SST variability in the Pacific is called the Pacific Decadal Oscillation (PDO), corresponding to the first empirical orthogonal function of monthly SST anomalies in the Pacific poleward of 20°N (Mantua et al., 1997). However, here the focus is on Interdecadal Pacific Variability (IPV: "variability" instead of "oscillation"), the basin-wide manifestation of the PDO. IPV extends from 60°N to 45°S with an alternating tripole pattern of SST anomalies. The mode alternates between warm and cool conditions over 20-30 year periods (Henley et al., 2015; Mantua et al., 1997). The IPV is a regulator of global mean surface air temperature and precipitation. It affects climate variability over every continent (Dong and Dai 2015; Joshi & Rai, 2015; Meehl et al., 2019). The network of IPV teleconnections is similar to that forced by the El Niño Southern Oscillation (ENSO), as the IPV is a multidecadal representation of Pacific SST (Horel & Wallace, 1981; García-Serrano et al., 2017). IPV is thought to be associated with accelerations and decelerations in the rate of global mean surface air temperature change (Meehl et al., 2013; Kosaka & Xie, 2013; Henley & King, 2017).

In the Atlantic, SST alternates between warm and cool conditions with a periodicity of 60-80 years, although paleoclimate records show that individual phases have ensued for longer (Kerr 2000; Trenberth & Shea, 2006; Knudsen et al., 2011). This mode of variability, referred to as Atlantic Multidecadal Variability (AMV) is thought to be mainly driven by internal fluctuations of the ocean-atmosphere system, although it is also influenced by natural and anthropogenic external forcings (greenhouse gases, aerosols, volcanoes, solar radiation) (Knight, 2005; (Ting et al., 2009; Otterå et al., 2010; Booth et al., 2012; Terray, 2012; Knudsen et al. 2014; Tandon & Kushner, 2015). The mechanism for AMV, and in particular the role of ocean dynamics, is debated (Clement et al., 2015; O'Reilly et al., 2016; Cane et al., 2017). However, numerous modeling studies suggest a role for ocean dynamics, and especially for the Atlantic Meridional Overturning Circulation (AMOC) that is associated with meridional oceanic heat transport and AMV-like SST anomalies in the North Atlantic (Delworth et al., 1993; Knight et al. 2005; Danabasoglu et al., 2016; Delworth et al., 2017). Phase shifts of AMV are important to consider because AMV elicits an extensive network of teleconnections. The AMV promotes multidecadal fluctuations in tropical cyclone activity (Vimont & Kossin, 2007), Sahel monsoon rainfall (Wang et al., 2012) and temperature/precipitation over North America and Europe (Enfield et al., 2001; Sutton & Hodson, 2005; Wang et al., 2012). The AMV has also been shown to be associated with long-term trends in the North Atlantic Oscillation (NAO), (Hurrell & Van Loon, 1997), and the AMV has been suggested as a driver of multidecadal variability in North Atlantic weather regimes and extreme weather over Europe (Peings & Magnusdottir, 2014; Omrani et al., 2014).

While the IPV and AMV have been investigated in isolation, their combined influence on the large-scale circulation has received less attention. The work here looks at the combined influence of these modes on the wintertime atmospheric circulation, the polar stratosphere, and stratosphere-troposphere coupling. The polar stratosphere is known to respond to positive IPV

(Woo et al., 2015; Kren et al., 2016) and positive AMV (Omrani et al., 2014; Peings & Magnusdottir, 2016) individually. This is important to consider now because the AMV is currently in its positive phase and the IPV is thought to be transitioning to its positive phase (Meehl et al., 2016).

The layout of the paper is as follows. The next section describes the model used and the experiments performed. Section 3 will show the December - March (DJFM) large-scale atmospheric response in the mid-latitudes and tropics. The destructive influence of positive AMV on the atmospheric response to positive IPV is identified. The polar stratospheric response to the modes is diagnosed afterwards and then the influence of the modes on extreme mid-latitude weather is discussed in light of stratosphere-troposphere coupling. Following a conclusion in Section 4, there is a discussion in Section 5 of why subsampling these results by QBO phase is not trivial.

2.2 Models and experiments

The Whole Atmosphere Community Climate Model (WACCM) is used in this study (Marsh et al. 2013). Community Atmosphere Model version 4 (CAM4) physics is used and so is specified chemistry (SC-WACCM4), which decreases the computational cost of the runs while retaining a similar climatology with the standard version (Smith et al. 2014). A repeating 28-month cycle of the Quasi-Biennial Oscillation (QBO) is prescribed. The model domain extends from the surface to 5.1×10^{-6} hPa, ~ 145 kilometers with 66 vertical levels and a horizontal resolution of 1.9° latitude by 2.5° longitude. The external radiative forcings (greenhouse gases, aerosols, solar radiation) are kept constant to present-day values.

A total of nine experiments are run, including every combination of IPV and AMV polarity. Given that each mode can exist in a negative, neutral, or positive state, there are nine combinations of SST variability. About half of the results highlight the atmospheric response to all nine experiments. The other half focus on the responses to positive IPV (+IPV), positive AMV (+AMV), and their combination (+AIV).

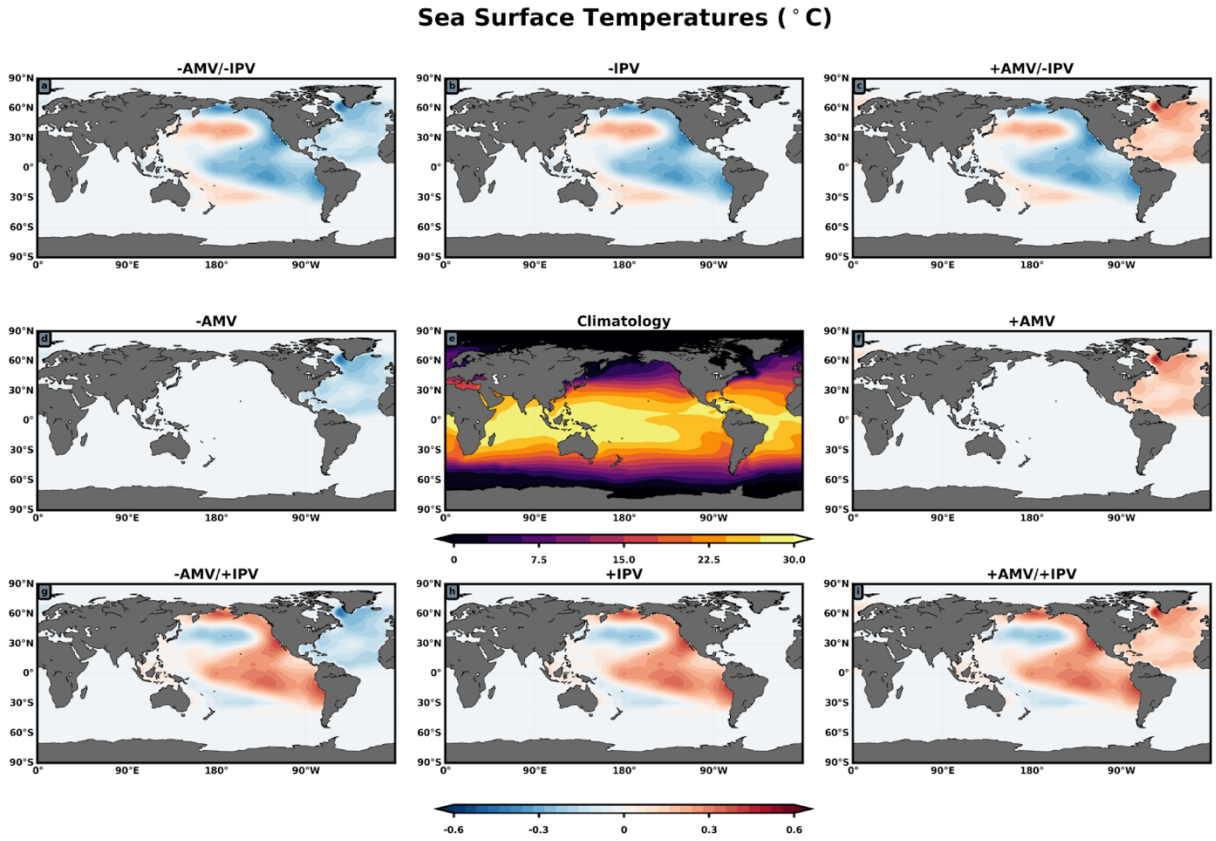

Figure 2.1: The prescribed sea surface temperature patterns for each combination of IPV and AMV variability. Climatological conditions (Fig. 2.1e) are shown in a different color scale.

The neutral IPV, neutral AMV experiment is the control (Fig. 2.1e). It consists of a 200-year experiment (after a one-year spin-up) forced with climatological monthly mean SST/sea ice concentration (1979-2008 average annual cycle from Hadley Centre Sea Ice and Sea Surface Temperature dataset, HadiSST, Rayner, 2003). Each perturbed experiment is run with its

corresponding SST anomaly superimposed onto the climatological SST field, with a buffer zone at the edge to avoid steps in the SST spatial distribution.

The prescribed IPV and AMV SST patterns are those designed for the Decadal Climate Prediction Project (DCPP) (Boer et al., 2016). To calculate the anomalies associated with each mode, the influence of external drivers of decadal climate variability is removed from the observed SSTs. This external component includes natural (solar and volcanic) and anthropogenically (greenhouse gases and aerosols) forced SST variations (Boer et al. 2016). This component is removed using the protocol described by Ting et al. (2009). The anomalies imposed in these experiments correspond to +/- 1 standard deviation of the AMV and IPV indices (Fig. 1.1). The response to IPV and AMV SST anomalies is derived by subtracting the 200-year mean of the control run from the 200-year mean of each perturbation run. A two-sided student t-test is used to assess statistical significance for each response.

2.3. Results

2.3.1 Mid-latitude wintertime atmospheric response

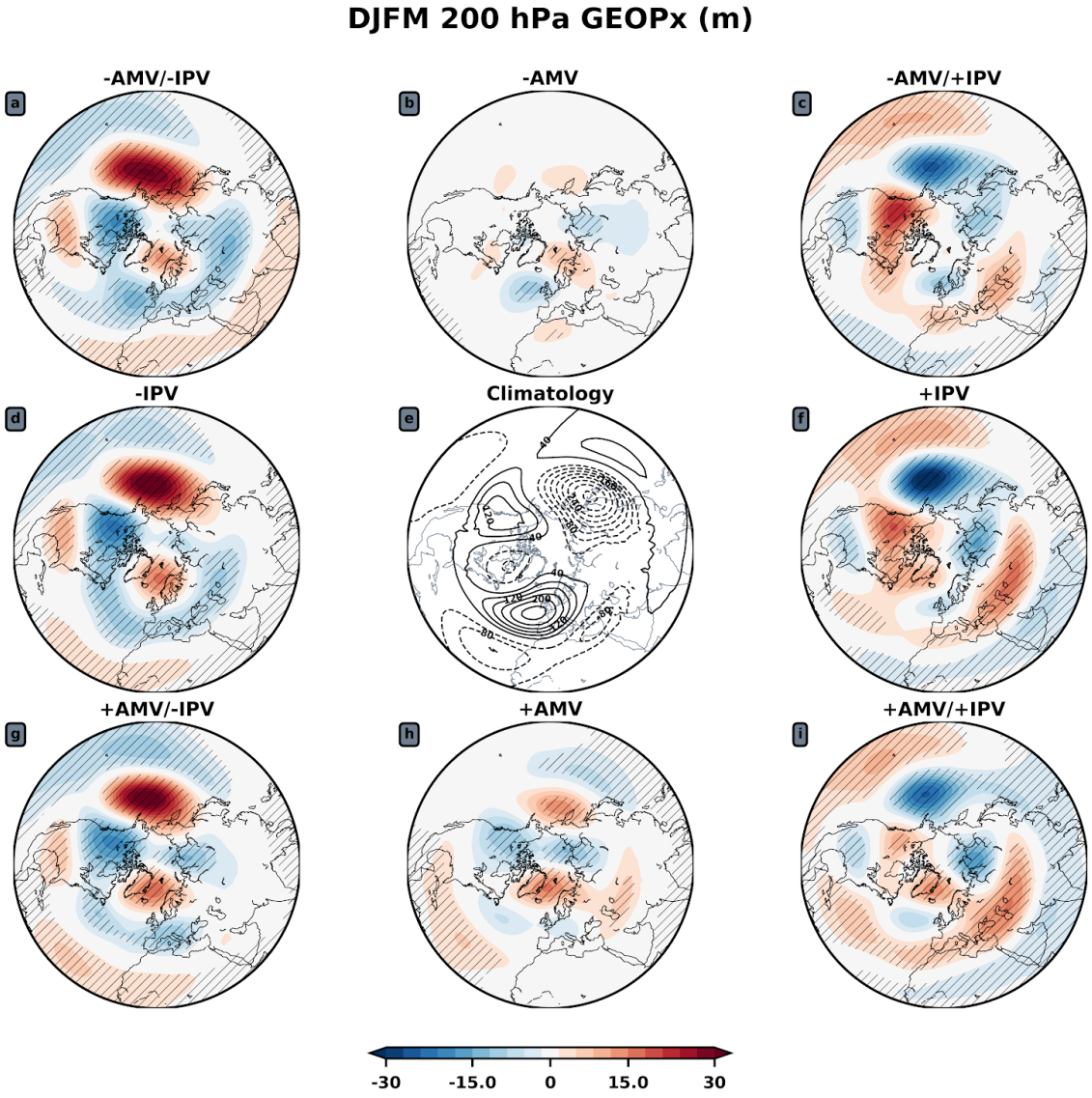

Figure 2.2: Dec. - Mar. 200 hPa eddy geopotential height anomalies. Climatological zonal means are removed to calculate the eddy component. Anomalies are calculated as the difference between each experiment and the control, denoted “climatology” (e). Hatching denotes p-values < 0.05 via a student’s t-test.

Figure 2.2 shows extended winter (DJFM) 200 hPa eddy geopotential height anomalies. The climatological stationary wave pattern reveals a characteristic wave-2 structure (Garfinkel et al. 2020) with the two strongest signals being the Aleutian Low over the North Pacific and ridging in the North Atlantic (Fig. 2.2e). Positive IPV (+IPV) forcing results in a positive Pacific North American (PNA) teleconnection pattern (Fig. 2.2c, f, i). Negative IPV (-IPV) forcing results in a negative PNA pattern (Fig. 2.2a, d, g). That is, a Rossby wavetrain propagates out of the subtropical Pacific, shown by alternating positive (anticyclonic) and negative (cyclonic) height anomalies spaced 6000 km apart that are directed poleward before curving eastward across North America, and equatorward over the tropical Atlantic (Horel and Wallace 1981). The increases and decreases of 200 hPa height correspond with increases and decreases in sea level pressure (Fig. 2.3). The Aleutian Low weakens during -IPV (Fig. 2.2d, 2.3d) and deepens during +IPV (Fig. 2.2f, 2.3f). Deepening of the Aleutian Low promotes warmer temperatures over Alaska, northwestern Canada, and the northwestern part of the United States (Wallace & Gutzler, 1981; Kren et al. 2016).

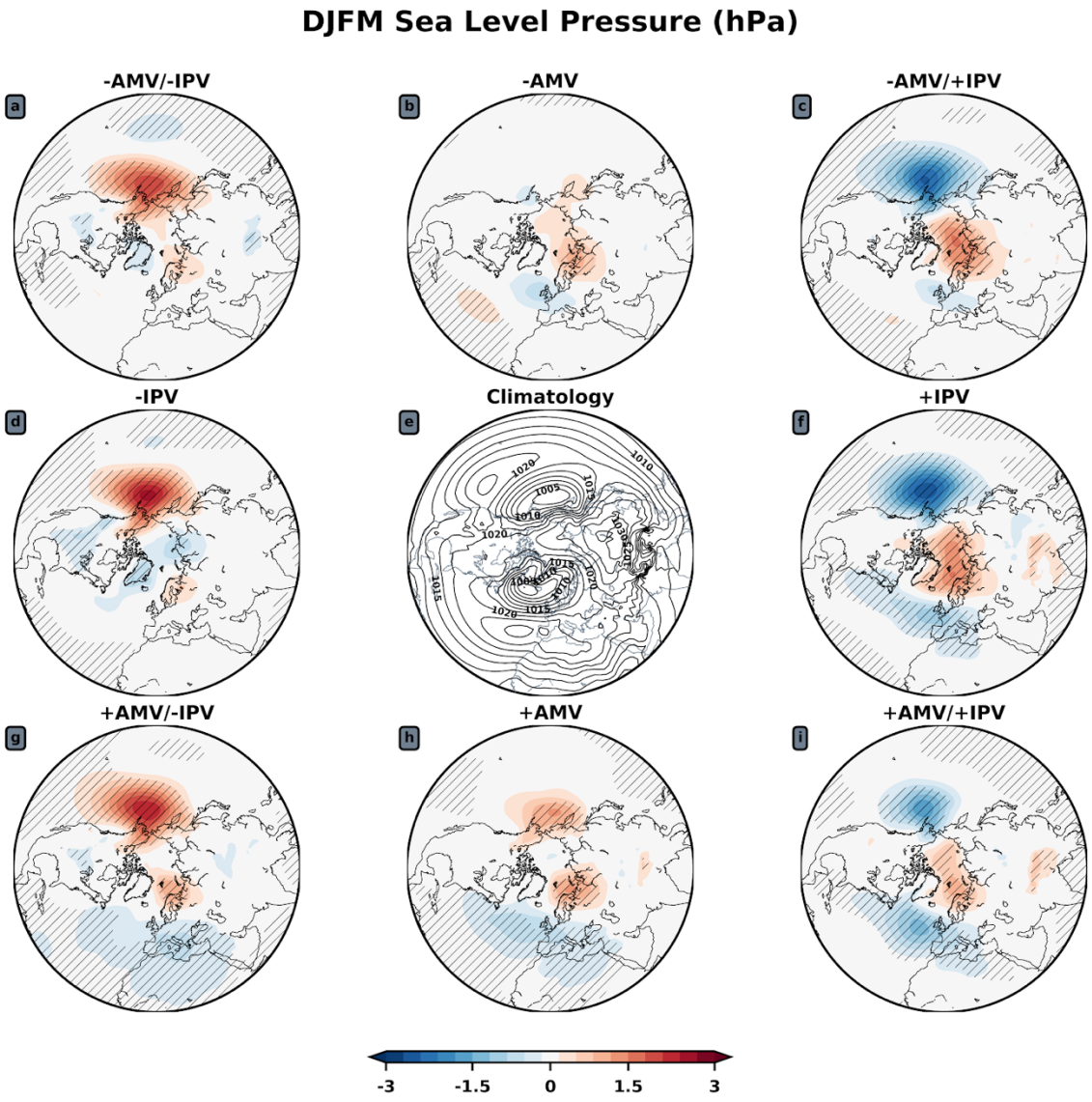

Figure 2.3: As in Figure 2.2, but for sea level pressure. The contour interval on (2.1e) is 2.5 hPa.

While the atmospheric response to -AMV is weak (Fig. 2.2b, 2.3b), the response to +AMV is a little stronger (Fig. 2.2h, 2.3h). In the North Atlantic, +AMV promotes a negative NAO like signal (consistent with WACCM experiments from Peings and Magnusdottir, 2016). In the North Pacific, the response opposes the effect of +IPV. The +AMV decreases the height in the western subtropical Pacific (Fig. 2.2h) and increases the height in the extratropical North Pacific. These two anomalies oppose the height anomalies forced by +IPV (Fig. 2.2f). When both

forcings are combined (+AIV), the North Pacific response is broadly similar to +IPV, but weaker, due to the cancellation effect of the +AMV (Fig. 2.3i). The impact of each form of IPV and AMV variability on the North Pacific is quantified in Figure 2.4, which shows the change in the PNA index induced by each forcing.

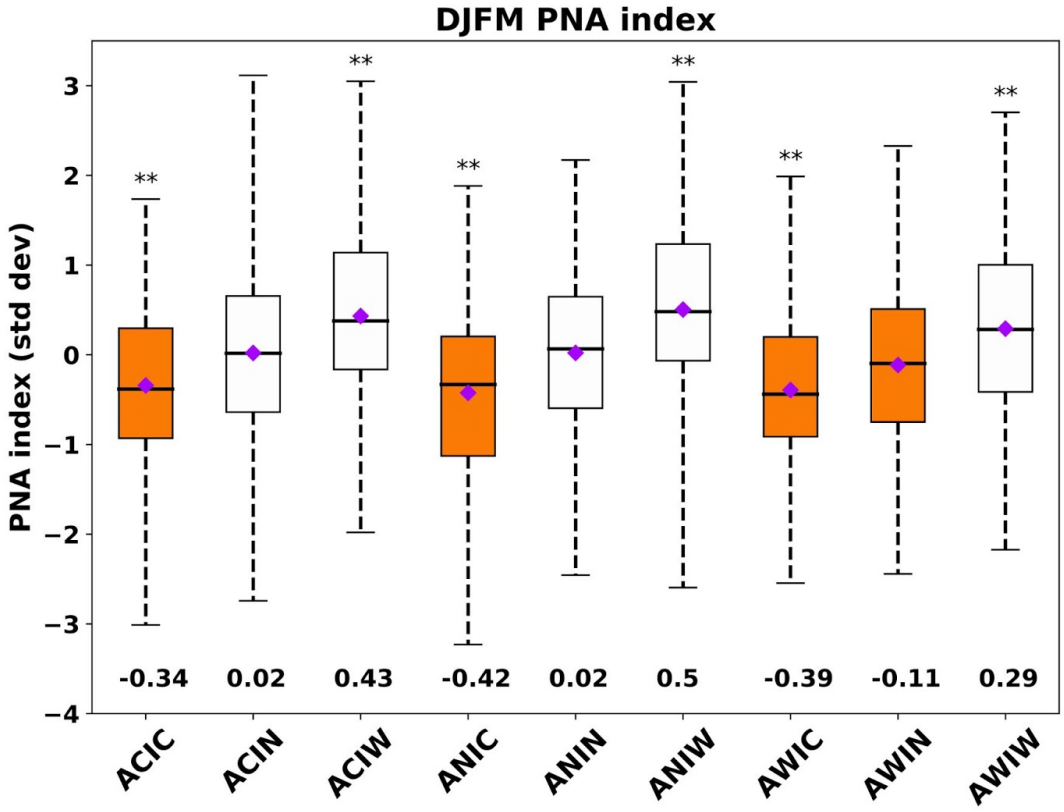

Figure 2.4: Dec. - Mar. PNA indices for each perturbation run calculated using standardized Z500 values and the formula provided by Wallace and Gutzler. On the x-axis, “A” refers to AMV, “C” to cold phase, “I” to IPV, and “W” to warm phase. So AWIC is the +AMV, -IPV experiment. Median values are indicated by each black bar across a boxplot, means are shown by purple diamonds, and printed below each boxplot. Box with negative means are shown in orange. Above each whisker, “**” refers to p-values < 0.05 with a student’s t-test.

The largest and most robust PNA responses are forced by the IPV. -IPV variability forces a negative PNA wavetrain. The pure -IPV response elicits a strong PNA pattern (mean = -0.42) with both negative (-0.34) and positive (-0.39) AMV dampening the mean values. +IPV variability forces a positive PNA response. The pure +IPV response elicits the strongest positive

PNA response (0.5), which is damped by the negative (0.43) and positive (0.29) AMV. +AMV reduces the strength of the +IPV PNA response by about 40%.

2.3.2 Modulation of the North Pacific upper troposphere by +AMV

To further investigate the competition between +IPV and +AMV in the North Pacific, Figure 2.5 shows velocity potential responses to +IPV, +AMV, and +AIV at 250 hPa. Walker Circulation variability is apparent in the control response (Fig. 2.5a). In the reanalysis record, negative velocity potential dominates the eastern hemisphere near the Maritime Continent, highlighting upward motion and convective outflow over the largest climatological heat source (Lau & Yang, 2003; Wang, 2004). In the western hemisphere, convergent flow is strongest over the east Pacific where the Pacific component of the Walker Circulation descends. Another dipole of negative and positive velocity potential exists over South America and the Atlantic, indicating the Atlantic sector Walker Circulation cell (Fig. 2.5a). The +IPV induces a response (Fig. 2.5b) resembling that forced by El Nino with decreased (increased) large-scale divergence in the tropical western (eastern) Pacific (García-Serrano et al. 2017).

+AMV induces anomalous 200 hPa divergence in the tropical Atlantic (Fig. 2.5c). It also induces convergence over the Maritime Continent, a modulation of the Walker Circulation that produces anomalous subsidence there (Fig. 2.5c). This effect is conserved during +AIV (Fig. 2.5d), when the +AMV reinforces the convergence over the Maritime Continent forced by +IPV.

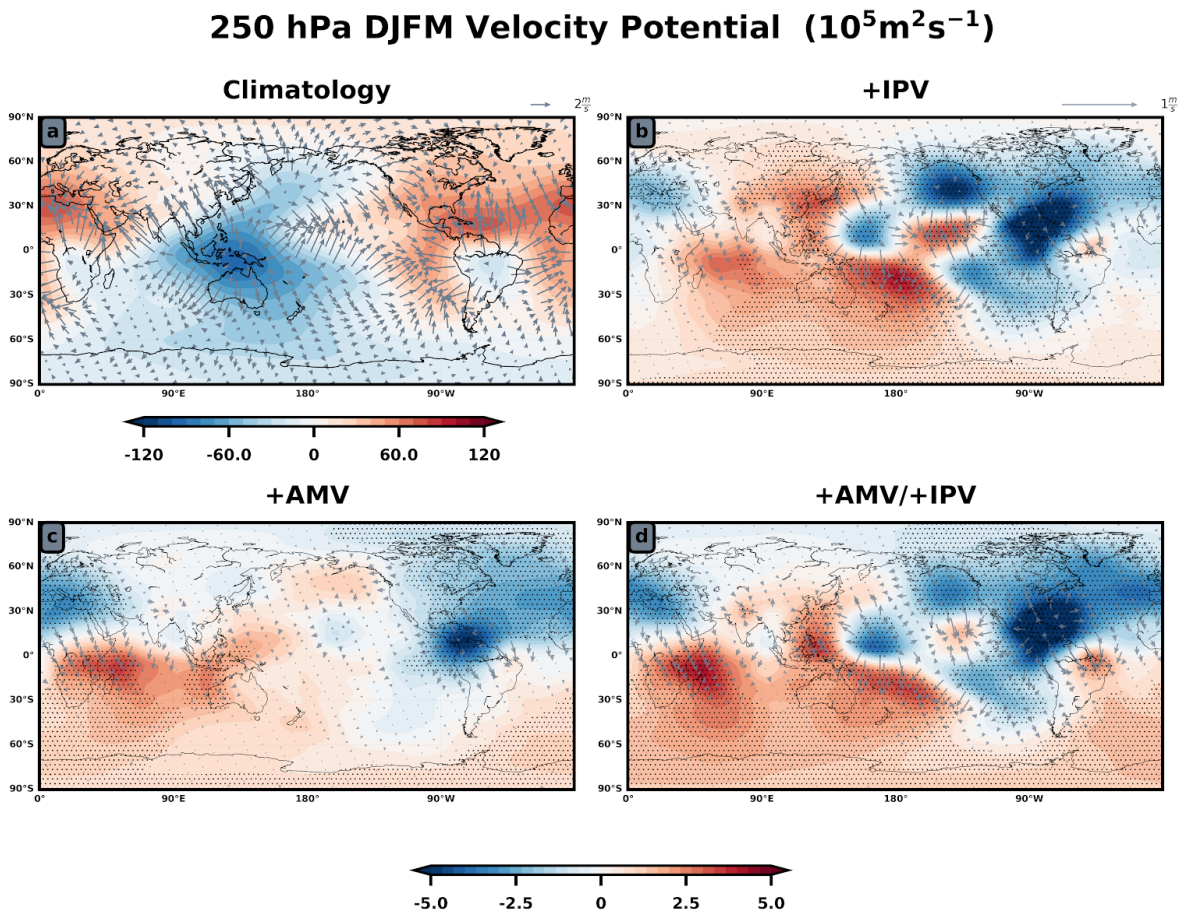

Figure 2.5: Dec. - Mar. 250 hPa velocity potential and divergent wind anomalies. Anomalies are calculated as the difference between each experiment and the control, denoted “climatology” (a). Stippling denotes p-values < 0.05 via a student’s t-test. Statistically significant divergent wind vectors are shown in gray.

The changes in the tropical circulation are clearer when looking at pressure-longitude cross-sections of omega (multiplied by -1). In line with the previous results here, the atmospheric response, even in the tropics, is dominated by the IPV (Fig. 2.6).

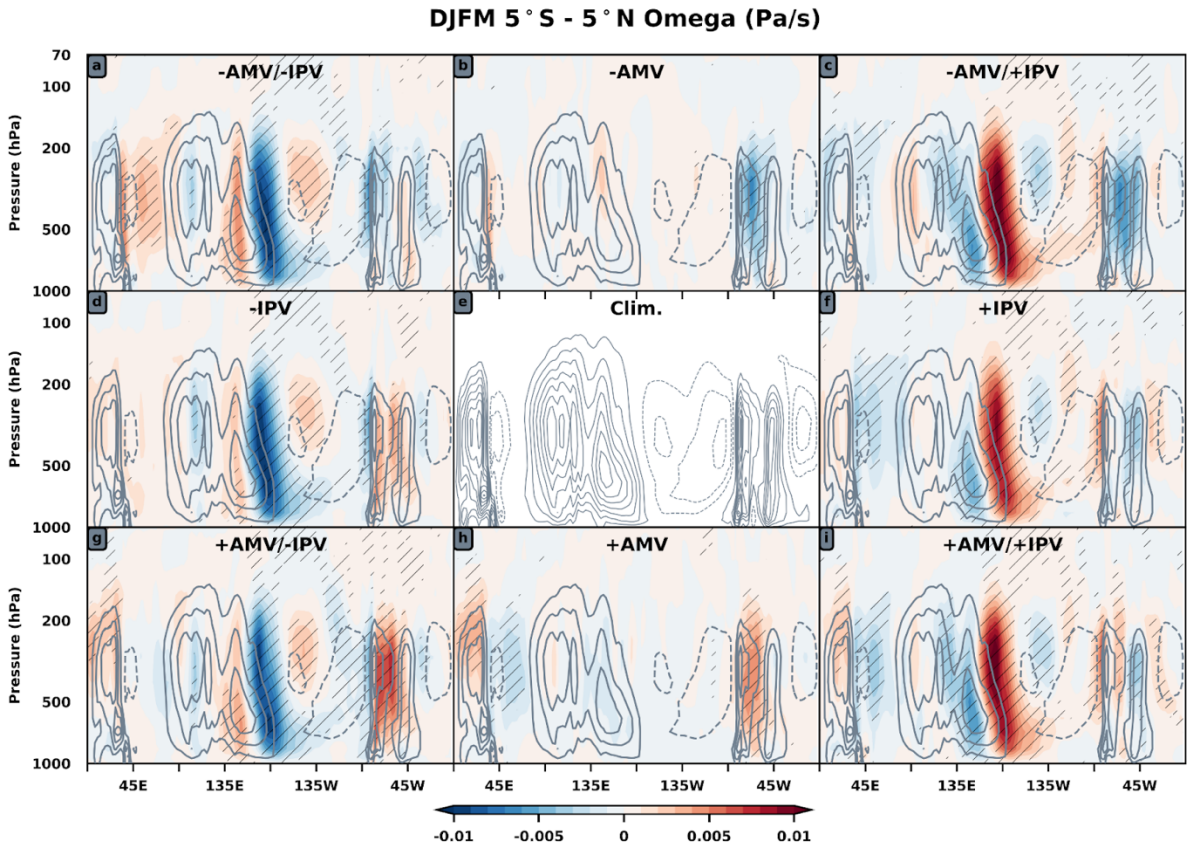

Figure 2.6: Dec. - Mar. omega (multiplied by -1) responses averaged between 5°N to 5°S. Red means ascent and blue mean descent. The climatological contours in gray use interval +/- 0.02 Pa/second with the zero contour not shown. For the climatology (f), the number of contour intervals is doubled (interval of +/- 0.01 Pa/s).

+IPV (-IPV) induces ascent (descent) over the central Pacific, descent (ascent) over the Maritime Continent, and descent (ascent) over the Atlantic sector Walker Cell (Fig. 2.6f, d). This is very similar to the response forced by ENSO (Wang, 2004). +AMV reinforces ascent over the climatological Atlantic sector Walker Cell (Fig. 2.6h) and -AMV suppresses it (Fig. 2.6b). While it is not quantified explicitly here, the four experiments in which neither of the modes are in a neutral state (Fig. 2.6a, c, g, i), appear to be linear combinations of the individual IPV and AMV responses they are made up of (Fig. 2.6b, d, f, h). During +AIV, there is more descent over the Maritime Continent region, ~ 120°E-160°E (Fig. 2.6i) than in response to +IPV alone (Fig. 2.6f). This is consistent with more upper tropospheric convergence over the Maritime Continent during +AIV (Fig. 2.5d) than in response to +IPV (Fig. 2.5b) or +AMV alone (Fig. 2.5c).

The anomalous upper tropospheric convergence induced by +AMV is not confined to the deep tropics only (Fig. 2.5c). It is found throughout the subtropical western Pacific, which is a Rossby wave source region that responds to the local horizontal vorticity gradient (Sardeshmukh & Hoskins, 1988; Watson et al., 2016; Scaife et al., 2017). By promoting anomalous convergence over the subtropical western Pacific, thereby suppressing the climatological divergence in the same region (Fig. 2.5c), the +AMV suppresses the climatological tropics-extratropics Rossby wavetrain propagating over the western Pacific. This can be seen in Figure 2.2. The subtropical climatological ridge and the Aleutian Low (Fig. 2.2e) are suppressed by the +AMV (Fig. 2.2h).

Previous studies have shown this modulation of the North Pacific atmosphere by the +AMV. Sun et al. (2017) argue that the connection between the +AMV and the North Pacific is two-fold: (1) upper tropospheric divergence over the North Atlantic is compensated for by upper tropospheric convergence in the North Pacific, subsequent subsidence and formation of a high pressure and (2) upper-tropospheric convergence in the tropical central-eastern Pacific induced by the +AMV can initiate a Rossby wavetrain propagating into the extratropics, thereby enhancing the first effect. Similarly, Davini et al., (2015) argue that anomalies associated with +AMV (specifically in the tropical Atlantic) excite a Rossby wavetrain over the Pacific that weakens the Aleutian Low in response to a poleward displacement of the Intertropical Convergence Zone (ITCZ). This decadal teleconnection bridging the tropical atmospheres of each basin also operates at the interannual timescale. Perturbations to the Walker Circulation induced by positive tropical Atlantic SST anomalies induce upper tropospheric convergence and surface wind changes over the Pacific within one season of the initial forcing (Simpkins et al., 2016). Similarly, perturbations to the Walker Circulation induced by ENSO SST lead to warming of Tropical North Atlantic SST with just a one season lag (Giannini et al. 2001; Wang 2004; García-Serrano et al. 2017).

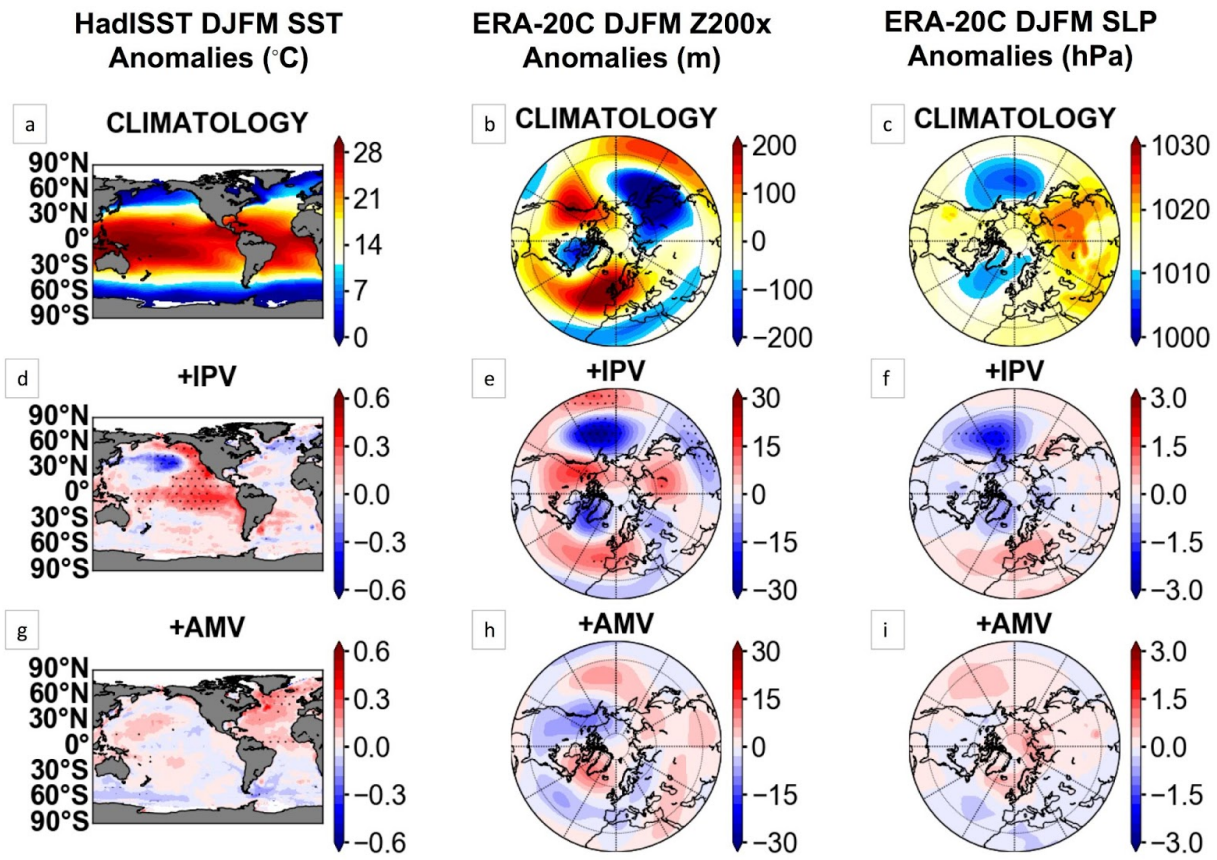

Figure 2.7: Extended winter HadISST SST 1926-2010 climatology (a), +IPV anomalies (d), and +AMV anomalies (g). Positive (warm) anomalies are red and negative (cold) anomalies are blue. The climatology (a) is shown in a different color scale. The middle column contains ERA-20C Z200x anomalies (m) for the +IPV (e), +AMV (h), and a similar climatology shown in a different color scale (b). Positive (negative) anomalies correspond to increases (decreases) in the height field. The last column contains ERA-20C sea level pressure anomalies (hPa) for the +IPV (f), +AMV (i), and a similar climatology (c). Hatching with black dots indicates statistical significance at or above 95%.

To further assess this mechanism, composites of extended winter Northern Hemisphere sea level pressure (SLP) anomalies and 200 hPa stationary wave anomalies are made using ERA-20C reanalysis data (Poli et al., 2016) provided by the European Centre for Medium-Range Weather Forecasts (Fig. 2.7). Positive IPV and AMV years are taken from Henley et al. (2015) and Trenberth & Shea, (2006) to create composites based on the 1926-2010 climatology. The Aleutian Low deepens during positive IPV at 200 hPa (Fig. 2.7e) and at the surface (Fig. 2.7f).

There is no robust atmospheric response to the +AMV (Fig. 2.7h, i). These SLP and stationary wave results are consistent in NCEP reanalysis also (not shown).

2.3.3 Planetary wave responses to IPV and AMV variability

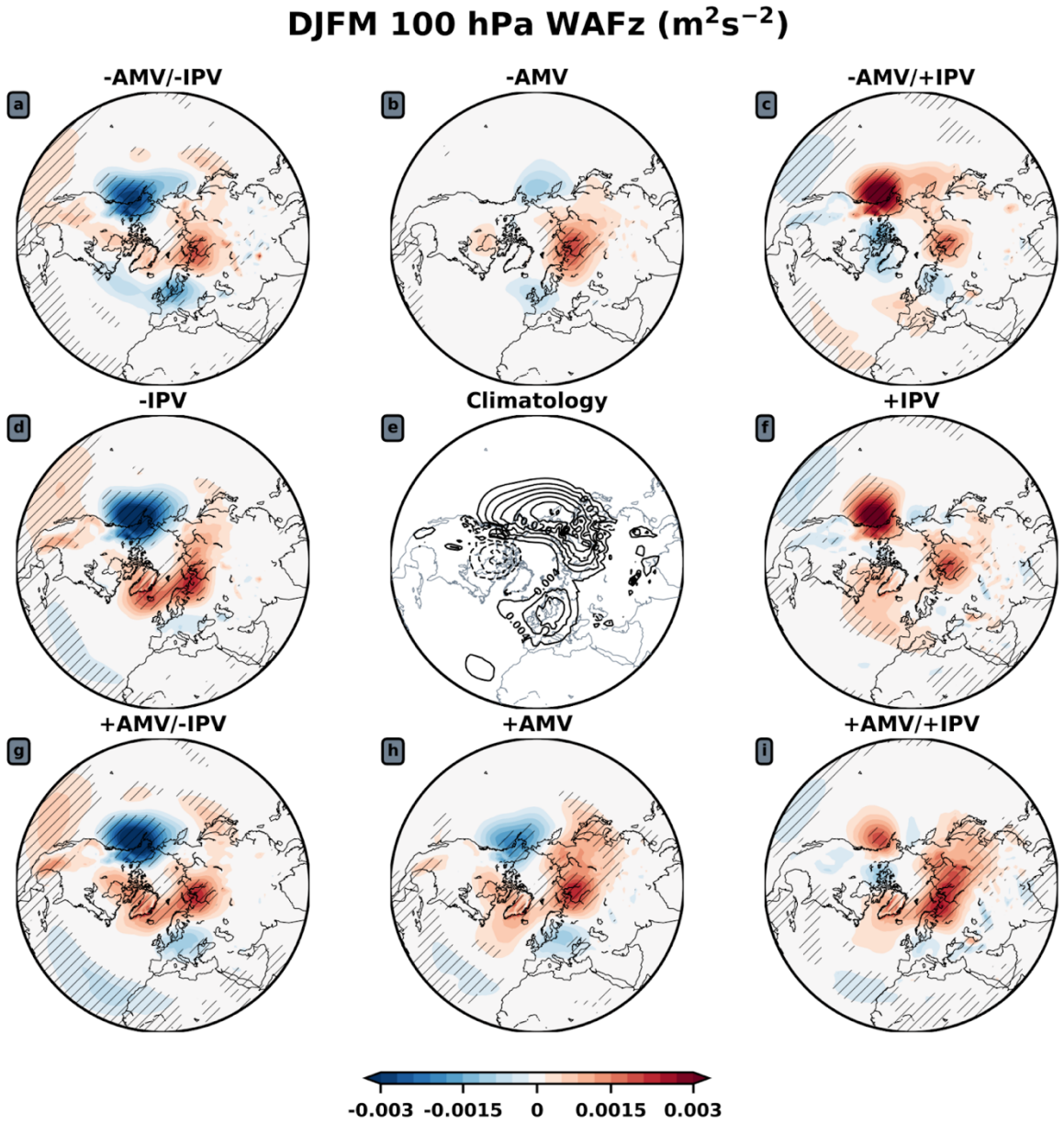

Figure 2.8: Dec. - Mar. 100 hPa vertical wave activity flux anomalies. All wavenumbers are included in the calculation. Anomalies are calculated as the difference between each experiment and the control, denoted “climatology” (e). Hatching denotes p-values < 0.05 via a student’s t-test.

Constructive (destructive) interference of the climatological stationary wave pattern (as seen in Fig. 2.2e) with anomalous forced planetary waves leads to enhanced (suppressed) upward

propagation of planetary scale wave activity from the troposphere into the stratosphere (Smith et al. 2010; Fletcher and Kushner 2011). Figure 2.2 revealed that the IPV and AMV both modulate the climatological stationary wave pattern, therefore, they both likely modulate wave activity flux (WAF) entering the polar stratosphere.

To identify the source regions of wave activity, the 100 hPa vertical wave activity flux, the Plumb flux (Plumb 1985), is shown in Figure 2.8. The Plumb flux is a three-dimensional generalization of the Eliassen Palm (EP) flux (Edmon et al. 1980). Consistent with Plumb (1985), WACCM exhibits maximum vertical wave propagation in the North Pacific/Eastern Asia and the North Atlantic/Western Europe (Fig. 2.8e). With +IPV forcing, the upward wave activity flux intensifies over the eastern North Pacific and modestly over the North Atlantic and Northern Eurasia (Fig. 2.8f). Conversely, with +AMV forcing there is reduced upward propagation across the entire North Pacific, however there is an increase over Northern Eurasia (Fig. 2.8h). The +AIV (Fig. 2.8i) results in increased upward wave propagation across Eurasia and over the eastern North Pacific, albeit the latter is reduced compared to the +IPV case.

These regions of enhanced or reduced upward WAF can be explained by the linear interference method of planetary wave amplification (Smith et al. 2010; Fletcher and Kushner 2011). Figure 2.2 showed that positive (negative) IPV deepens (increases the height of) the climatological Aleutian Low, an example of constructive (destructive) interference. The constructive interference occurring during +IPV enhances the upward WAF over the North Pacific whereas upward WAF is suppressed during -IPV because of destructive interference. Similar to -IPV, the +AMV decreases the climatological upward WAF in the North Pacific (Fig. 2.8h) by increasing the 200 hPa height field there (Fig. 2.2h), an effect that is conserved during +AIV (Fig. 2.2i), which results in reduced upward WAF over the North Pacific (Fig. 2.8h). +AMV does

compensate for reduced upward WAF in the North Pacific by increasing upward WAF over Eurasia (Fig. 2.8h).

2.3.4 Polar stratospheric response

One way to quantify the impact of these WAF anomalies on the polar stratosphere is to calculate the number of SSWs for each experiment. The algorithm of Charlton and Polvani (2007) is used: for days between November 1st and March 31st, the central date of a warming is the first day in which the zonal-mean zonal wind at 60°N and 10 hPa becomes easterly. Following identification of the central date, 20 consecutive days of westerly winds must exist before the next central date can be identified. The control experiment yields 103 SSWs in 200 years, or 0.52 events per extended winter season. This frequency is lower than previous studies, which likely results from the polar stratospheric cold bias in the model that strengthens the polar vortex (Marsh et al. 2013). The observed SSW frequency reported in Charlton & Polvani, (2007) is 0.67 events/season. Butler et al., (2017) created a similar SSW climatology using a lengthier reanalysis data set and found the SSW frequency to be 0.63 events/season. The number of SSWs for each of the perturbation experiments is listed in Table 2.

Forcing	Number of SSWs	Events per season	% Change
-AMV/-IPV	98	0.49	-5%
-AMV	110	0.55	+7%
-AMV/+IPV	114	0.57	+11%
-IPV	104	0.52	+ 1%
Control	103	0.52	N/A
+IPV	130	0.65	+ 26%
+AMV/-IPV	117	0.59	+ 14%
+AMV	118	0.59	+ 15%
+AMV/+IPV	137	0.69	+ 33%

TABLE 2.1 Number and frequency of stratospheric sudden warmings in events per extended winter season. Both number of events and frequency are calculated using daily data (Nov. – Mar.) over the entire 200-year period.

There is no substantial change in the frequency of SSWs in response to -IPV alone, or when it is combined with -AMV. However, +AMV increases the frequency of SSWs by about 15%, an effect that is conserved when it is combined with -IPV. This increase in the number of SSWs during +AMV likely results from enhanced upward wave activity flux over Eurasia (Fig. 2.8h). SSW frequency increases by about 26% due to +IPV forcing. The stratospheric response to the +IPV and +AMV is not additive as the +AIV forcing results in a more modest increase in SSWs (+ 33%) relative to +IPV. Therefore, although the +AMV dampens the response to the +IPV in the troposphere by weakening the Aleutian Low, the +AMV does not appear to dramatically change the response to +IPV in the stratosphere.

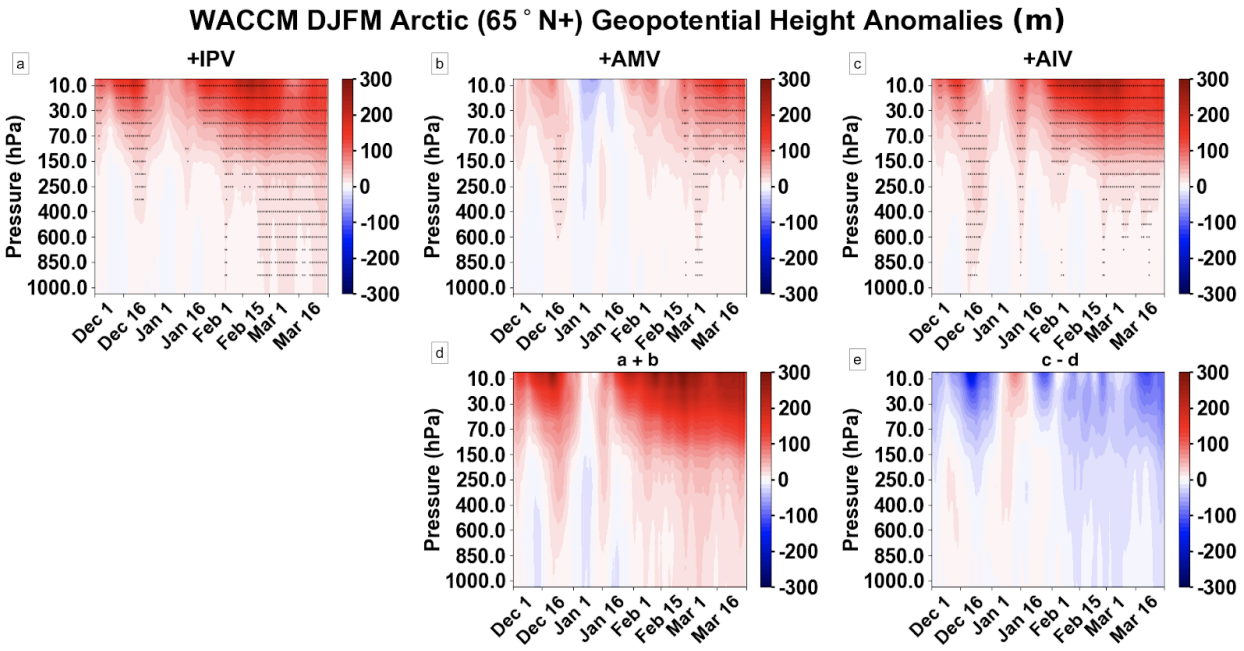

Figure 2.9: Extended winter daily geopotential height anomalies averaged over the polar cap north of 65°N. These cross sections exhibit time (days) on the x-axis and pressure levels on the y-axis. Shown are the anomalies for the (a) +IPV, (b) +AMV, and (c) +AIV perturbations. Hatching denotes anomalies statistically significant at or above 95%. Two additional composites are calculated: (d) the sum of +IPV and +AMV. (e) is the difference between the +AIV anomalies and the aforementioned linear sum (d).

To further characterize the polar stratospheric response to +IPV, +AMV, and +AIV, their daily polar cap (north of 65°N) geopotential height anomalies between 1000 hPa and 10 hPa are shown in Figure 2.9. Positive height anomalies manifest throughout the extended winter season due to the +IPV (Fig. 2.9a). This is expected as the aforementioned upward propagating planetary waves decelerate the stratospheric jet by (not shown) inducing a residual circulation (poleward and sinking motion), that is accompanied by adiabatic temperature increase below the forcing region (Dunkerton et al. 1981; Limpasuvan et al. 2004). The warming associated with these stratospheric perturbations consistently propagates downward (~400 hPa) throughout the extended winter season. However, particularly in late winter (February and March), the stratospheric anomalies propagate downward into the troposphere, a NAM like response.

Compared to the +IPV case, the Arctic atmospheric response to +AMV forcing (Fig. 2.9b) is modest with comparatively weak positive anomalies observed in mid-December and March. The early winter warming that begins ~ Dec. 8th, seen at 10 hPa, propagates downward into the troposphere terminating late in December. During late winter, the height anomalies are slightly stronger in the stratosphere, and propagate farther into the troposphere (as was the case with the +IPV as well).

The +AIV geopotential height anomalies (Fig. 2.9c) resemble the +IPV induced signal (in line with the SSW results), with slightly reinforced anomalies in the stratosphere in late winter, however with more (less) downward propagation in early (late) winter. As illustrated in Fig. 2.9d (sum of Fig. 2.9a and Fig. 2.9b) and 2.9e (difference between Fig. 2.9c and Fig. 2.9d), the response to +AMV and +IPV by themselves are not additive, since most of the response in the +AIV experiment is less than the sum of the responses to each of +AMV and +IPV. In particular, a noteworthy difference is the smaller propagation of the signal into the troposphere in late winter (Fig. 2.9e).

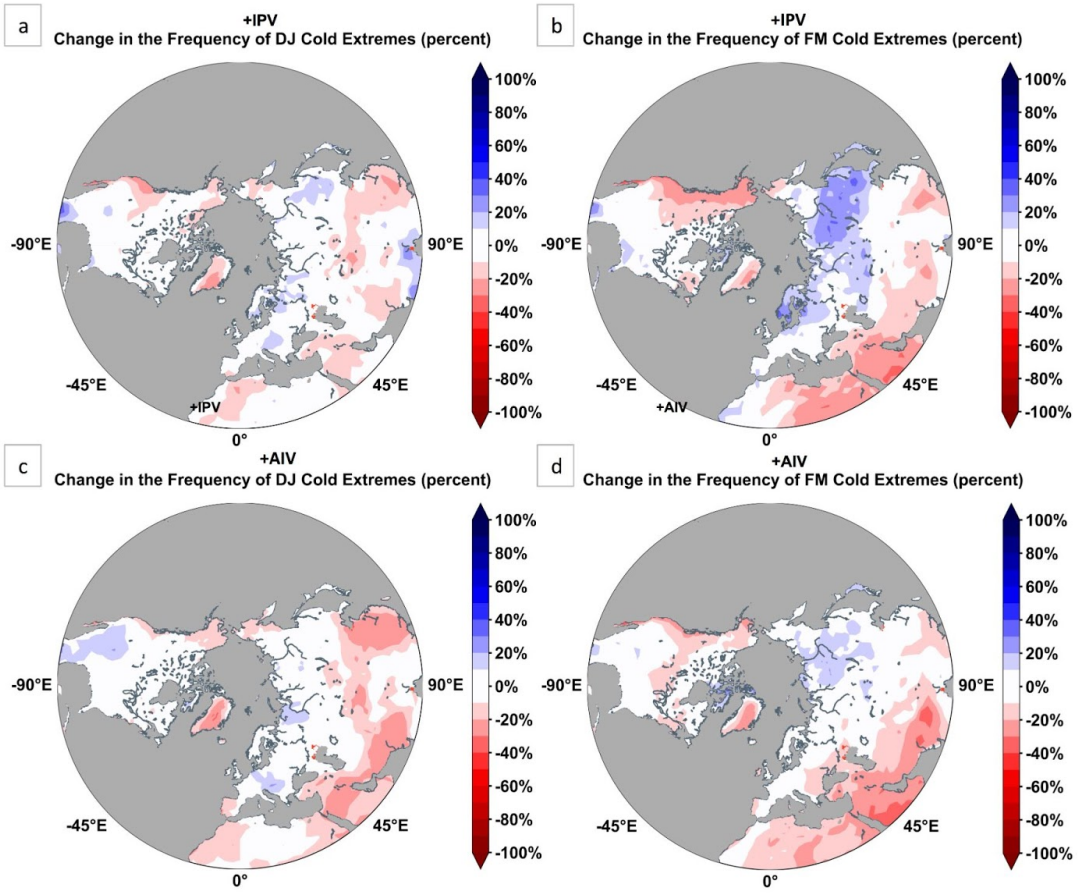

Figure 2.10: The change in frequency of cold extremes for +IPV in (a) early and (b) late winter. (c-d) The same as (a-b) except for +AIV. Increases in frequency are shaded in blue and decreases in red. Cold extremes are days during which the daily temperature falls below the climatological 10th percentile temperature value for that specific day and location.

Given the impacts of SSWs and downward propagation of NAM anomalies on the surface circulation (Baldwin and Dunkerton 1999), these results have implications for the frequency of extreme weather events at the surface. Figure 2.10 shows the changes in the frequency of DJ and FM cold extremes with +IPV and +AIV forcing. The Expert Team on Climate Change Detection Indices (ETCCDI) defines cold extremes as the percentage of days below the 10th percentile temperature for a specific location (Karl et al. 1999). The +IPV forcing decreases the frequency of cold extremes over the North American west coast, Northern Africa, and Asia, while cold extreme frequency increases over Scandinavia and Siberia (Fig. 2.10a,b). The

anomalies are more pronounced in late winter (Fig. 2.10b), consistent with late winter stratosphere-troposphere coupling induced by +IPV forcing (Fig. 2.9a). Including the warm Atlantic SST anomalies in the +AIV case leads to a striking difference in the response of cold extremes over Eurasia and North America (Fig. 2.10c,d). The increase in cold extremes over Scandinavia/Siberia is almost entirely canceled out, and the decrease in cold extremes over western North America is also reduced, especially in late winter. This is likely a consequence of reduced stratosphere-troposphere coupling with +AMV identified in Fig. 2.9.

2.4 Discussion and Conclusion

In this study, a high-top global climate model is used to assess the atmospheric response to each combination of IPV and AMV variability during winter. The wintertime tropospheric and stratospheric responses to the IPV and AMV are consistently dominated by the IPV. This is a really interesting finding because several studies suggest that AMV leads IPV by a little over a decade (Zhang and Delworth 2007; Sun et al. 2017) and that this relationship is mediated through the North Pacific (An et al. 2021). So while the atmospheric response to the IPV may be stronger, the AMV may be dominant in its own right because it may affect the phase of the IPV.

Considering the current positive AMV polarity in nature, and the expected transition of the IPV to positive phase (Meehl et al. 2016), more targeted study is done for the positive IPV, positive AMV, and concurrent positive IPV and AMV experiments. A robust feature of the atmospheric response to positive IPV is a positive PNA wavetrain leading to a deepening of the Aleutian Low. The positive AMV opposes the North Pacific atmospheric response to positive IPV and leads to a weaker response of the Aleutian Low in the experiment when both forcings are considered. This cancellation effect arises through a modulation of the Walker Circulation, which induces upper tropospheric convergence in the western Pacific. In general, the IPV forces larger

changes in the Walker Circulation than the AMV. Sun et al. (2017) and An et al. (2021) also show wavetrains originating out of the central Pacific in response to positive AMV. They express that air-sea feedbacks are important for the teleconnection, which the experimental protocol here does not capture by construction, which is a limitation of this work.

Despite reduced upward WAF over the North Pacific when the positive AMV is combined with the positive IPV, both forcings results in a warmer polar stratosphere. Positive AMV does not dramatically change the stratospheric response to positive IPV, rather it appears to exert a significant influence on the degree of stratosphere-troposphere coupling. Cold extreme temperatures become more frequent over Eurasia in response to the positive IPV during late winter, consistent with increased stratosphere-troposphere coupling and the negative NAM response. However, this increase in the frequency of cold extremes by positive IPV alone completely vanishes if the positive AMV is considered with the positive IPV.

2.5. Sensitivity to the QBO

A final consideration is how the stratospheric Quasi-Biennial Oscillation (QBO) would modify these results. When the QBO is easterly (westerly) in the lower stratosphere, the polar vortex that forms during boreal winter is weaker (stronger) than average (Holton and Tan 1980). This occurs because the QBO modifies the planetary scale wave activity flux entering the stratosphere. This suggests that the QBO could reinforce or suppress the effect of the IPV and AMV on the planetary wave activity flux, thereby generating different polar cap responses (Fig. 2.9) and potentially different surface temperature responses (Fig. 2.10).

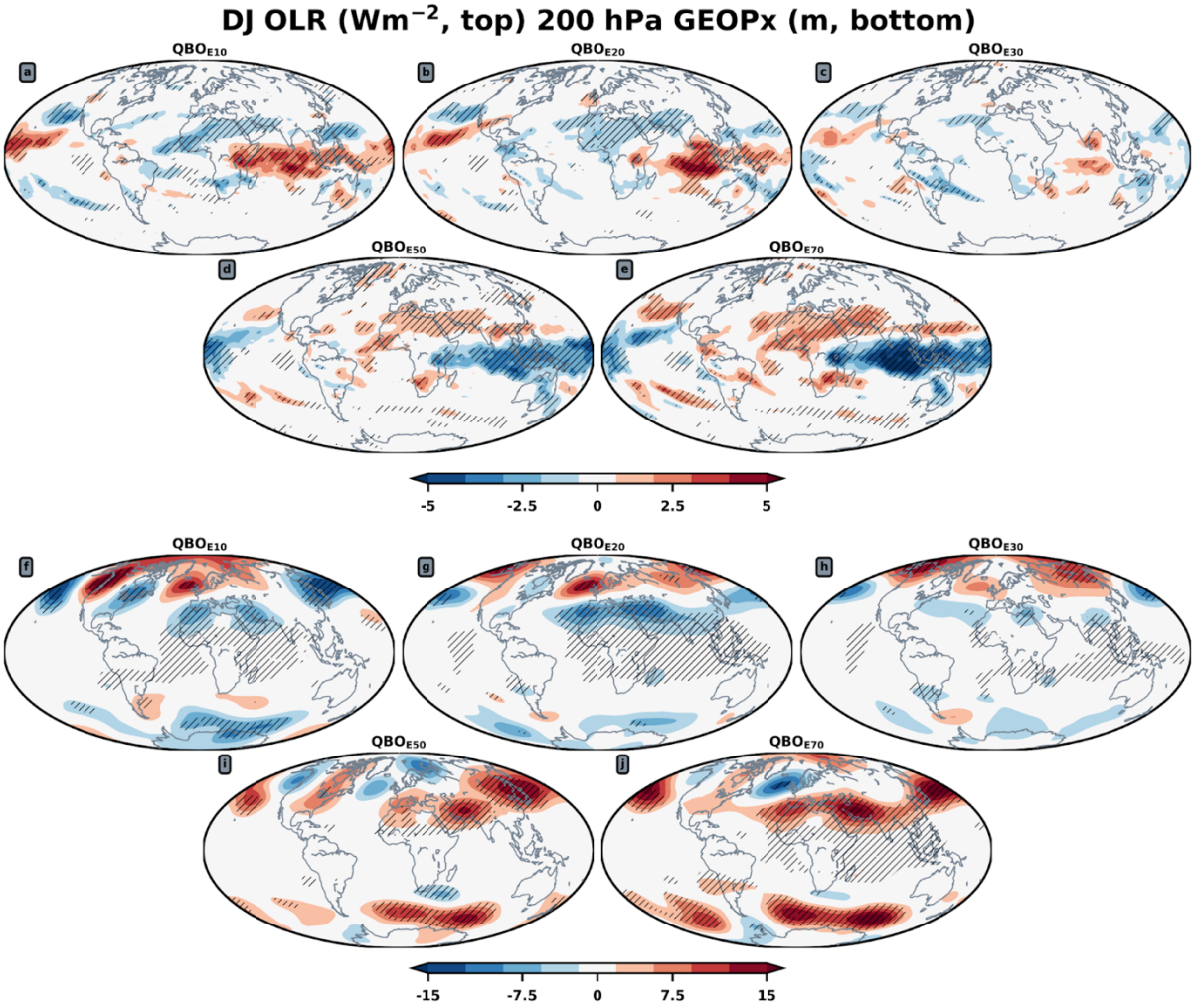

Figure 2.11: Dec. - Jan. outgoing longwave radiation (top) and 200 geopotential height (bottom) responses to the QBO in a 300 member set of 1-year timeslice experiments (described in the next chapter). The QBO is defined using the weakest 33% of winds (easterlies) at 10 hPa (a,f), 20 hPa (b,g), and so on. Response corresponding to p-values < 0.05 are hatched. The contour interval is +/- 1 W m^{-2} for the OLR and +/- 3 m for the geopotential height.

An important question to consider before splitting the results of this chapter by QBO phase is how should the QBO be defined. To illustrate this, Figure 2.11 shows the December-January outgoing longwave radiation (OLR) and 200 hPa geopotential height responses to QBO in a 300 year SC-WACCM4 experiment set with fixed climatological sea surface temperature and sea ice variability. Anomalies are calculated as deviations from the seasonal cycle when QBO easterlies are located at 10 hPa (Fig. 2.11a), 20 hPa (Fig. 2.11b), and so on.

The atmospheric responses are generally strongest when QBO easterlies are located at 10 hPa (Fig. 2.11a,f) or 70 hPa (Fig. 2.11e,j). When the QBO easterlies are at 10 hPa, the QBO westerlies are located in the lower stratosphere. This suppresses OLR (Fig. 2.11a) and produces a wavetrain in the North Pacific (Fig. 2.11f). When QBO easterlies are at 70 hPa, OLR is enhanced (Fig. 2.11e) and a weaker, but opposite sign wavetrain forms in the North Pacific (Fig. 2.11j). The weakest tropospheric responses occur when QBO easterlies are located at 30 hPa (Fig. 2.11c,h). In this case, the QBO westerlies have diminished in the lower tropical stratosphere and the QBO easterlies are too high to impact the tropospheric circulation. How the QBO is indexed matters.

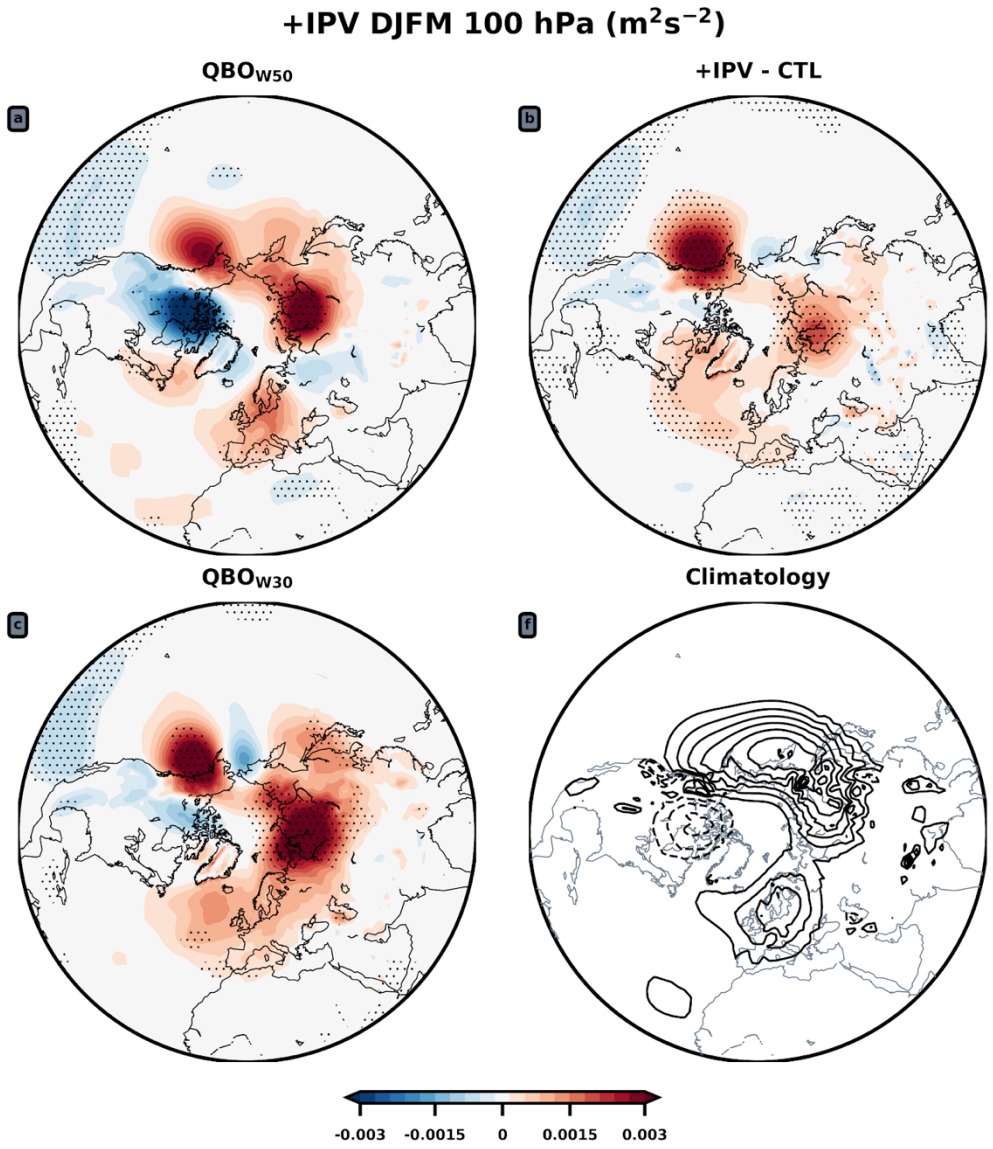

Figure 2.12: Dec. - Mar. 100 hPa vertical wave activity flux anomalies. (c) The response to +IPV forcing. The QBO index defined as the Dec.-Jan. time averaged, zonally averaged, and latitudinally averaged winds between 5°S and 5°N. The upper (lower) tercile of winds make up the westerly (easterly) winters. (a) and (c) show atmospheric responses to a westerly QBO defined at 50 hPa and 30 hPa, respectively. (b) shows the atmospheric response to positive IPV regardless of the background QBO state. (d) Climatological DJFM 100 hPa wave activity flux with +/-.004 m^2s^2 contours.

Using a single isobar QBO index means that all results will be sensitive to that background QBO state. In Fig. 2.12, the wave activity flux response forced by positive IPV (Fig. 2.12b) is subsampled for westerly QBO winters. Positive IPV alone generates upward wave activity flux

over the North Pacific and over Eurasia (Fig. 2.12b). If the QBO is westerly at 50 hPa, the North Pacific is no longer a source of upward wave activity flux and downward wave propagation is enhanced over North America (Fig. 2.12a). However, if the QBO index is simply defined using the next available isobar, 30 hPa, the results are completely different (Fig. 2.12c). The North Pacific is a source of upward wave activity flux, so is Eurasia, and there is no enhancement of downward wave propagation over North America (Fig. 2.12d).

The QBO has a clear impact on the atmospheric response to +IPV, but why and how? Many studies have benchmarked how the QBO modulates planetary scale waves (Dunkerton & Baldwin, 1991; Garfinkel et al., 2012; Lu et al. 2014; Lu et al. 2020). However, it is not clear what longitudinal sector the anomalous wave activity flux associated with the QBO comes from. As a result, it is not clear how the QBO is forcing the anomalous wave activity flux. The QBO may be acting through (1) linear interference to force planetary waves from the troposphere, (2) by forcing upward wave activity flux exclusively within the stratosphere, (3) or acting on synoptic scale eddies, which may interact with the planetary scale flow, thereby exciting the planetary waves. This lack of clarity is an impediment to winter predictability. If we better understand how the QBO preconditions the atmosphere to cause the Holton-Tan effect, maybe predictability of SSWs and Northern Annular Mode variability can advance beyond two week timescales. The QBO is one of the most important forms of low frequency variability influencing stratosphere-troposphere coupling.

Acknowledgements: I am very thankful to Cristophe Cassou for developing the SST fields that were used as forcing fields for this project. The developers of the WACCM cannot be thanked enough. This research was supported by NSF Grant AGS-1624038. We also acknowledge high-performance computing support from Yellowstone (ark:/85065/d7wd3xhc) provided by NCAR's CISL, sponsored by the NSF.

Chapter 3

Variation in the Holton-Tan effect by longitude

As appears in:

Elsbury, D., Peings, Y., & Magnusdottir, G. (2021). Variation in the Holton–Tan effect by longitude. *Quarterly Journal of the Royal Meteorological Society*, doi.org/10.1002/qj.3993

3.1. Background

Alternating easterly and westerly winds descend through the tropical stratosphere with an averaged periodicity of roughly 28-months while both longer (35 months) and shorter (22 months) periods have been observed (Bushell et al. 2020). This variability is called the Quasi-Biennial Oscillation (QBO). While the QBO is located in the tropics, it has effects on the global scale circulation (Gray et al. 2018). One of these teleconnections is the so-called Holton-Tan effect: when QBO easterlies (QBOE) are located in the lower tropical stratosphere, the polar vortex that forms during boreal winter is weaker than its climatological average (Fig. 3.1). Conversely, the circumpolar westerlies making up the polar vortex are stronger when QBO westerlies are present in the tropical lower stratosphere (QBOW). What we know about this teleconnection continues to progress (Holton and Tan 1980; Lu et al. 2020). However, how the teleconnection varies over longitude, apart from the conventional zonal mean, is less frequently shown. That is the subject of this study.

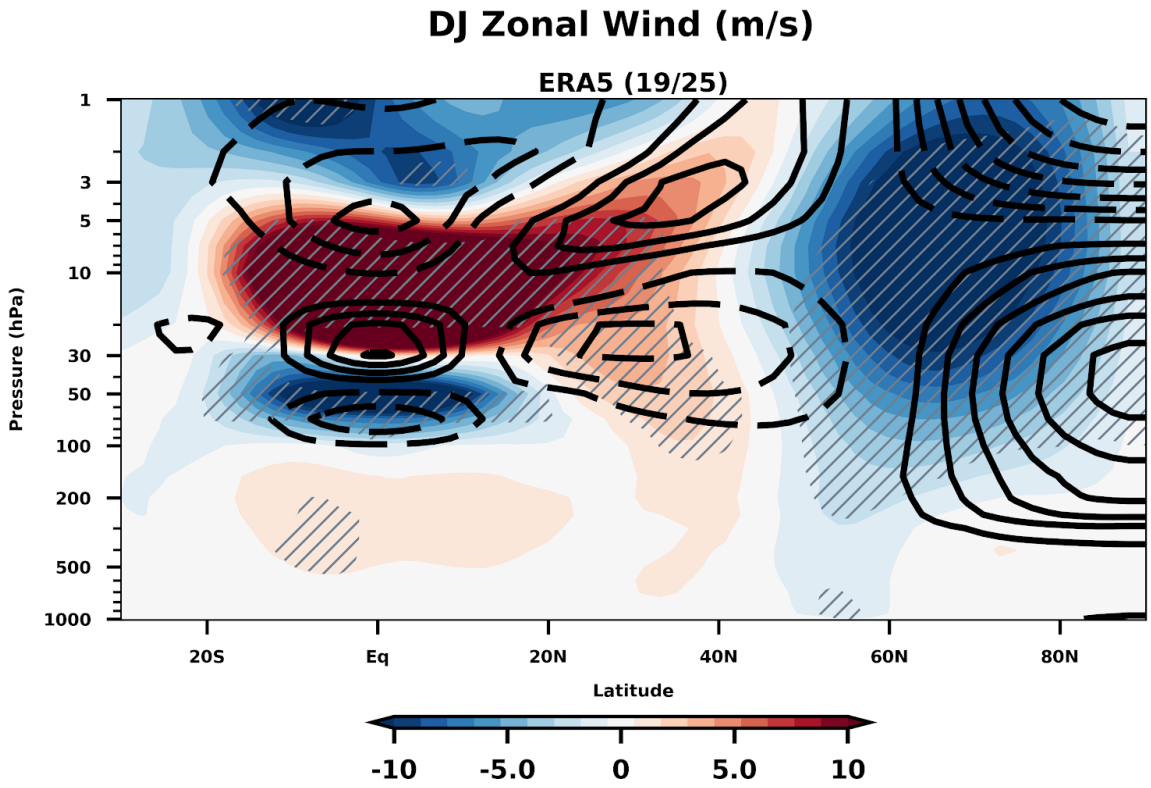

Figure 3.1: ERA5 1979-2019 Dec. - Jan. (DJ) zonal mean zonal wind anomalies are shaded. Gray hatching denotes statistical significance, p-values < 0.05 via a student's t-test, when comparing easterly QBO anomalies to westerly QBO anomalies. Warm (cool) temperature anomalies are shown in black with +/- 1 K contours. The 30 hPa phase angle index of Huang et al. (2012) is used. Anomalies are calculated as QBOE months (19) minus QBOW months (25). QBOE is defined as phases 1-4 and QBOW as phases 5-8. Years in which the Nino 3.4 index is equal to or exceeds +/- 1 sigma are excluded.

Stationary planetary scale waves propagate upward and equatorward through the stratosphere during boreal winter (Matsuno 1970). Per the classic Holton-Tan mechanism, the zero-wind line separating the QBO easterlies from the winter hemisphere westerlies confines planetary waves and their breaking into the northern hemisphere (Holton and Tan 1980; Lu et al. 2020). As more waves break in the winter stratosphere, depositing westward momentum into the flow, the polar stratosphere is more likely to warm and the polar vortex decelerates, eliciting a downward propagating NAM response, which is known to affect the North Atlantic troposphere (Andrews et al. 2019). The Holton-Tan effect is found in reanalysis data (Holton and Tan 1980, 1982; Dunkerton and Baldwin 1991; Gray et al., 2001; Lu et al., 2008; Naoe & Shibata, 2010;

(Yamashita et al., 2011; Lu et al. 2014; Anstey & Shepherd, 2014; White et al., 2015; Lu et al. 2020) and in idealized model experiments (Gray, 2003; Naito & Yoden, 2006; Yamashita et al. 2011; Garfinkel et al., 2012; Rao et al., 2020a). This explanation of the Holton-Tan effect really focuses on the role of the QBO easterlies.

However, the QBO induced mean meridional circulation (QBO-MMC) is also important for this teleconnection. For schematics and discussion of the QBO-MMC, see Plumb et al. (1982) or Collimore et al. (2003). The QBO-MMC acts as a residual mean meridional circulation that maintains the dynamically forced temperature response to the QBO against radiative relaxation (Pahlavan et al., 2021; Hitchman et al., 2021). Westerly (easterly) QBO shear coincides with tropical warming (cooling), which is generated by adiabatic descent (ascent). In the case of westerly QBO shear for instance, the *tropical* adiabatic descent is complemented by poleward divergence of the circulation, *subtropical/mid-latitude* ascent, and a return flow towards the tropics. Therefore, the QBO-MMC induces opposite temperature responses at mid-latitudes compared to the temperature responses in the tropics, which is seen in Fig. 3.1.

The QBO-MMC influences where planetary waves may propagate. Garfinkel et al. (2012) and Lu et al. (2014) showed in model experiments and reanalysis, respectively, that the QBO-MMC changes the stratospheric mean flow geometry in the middle stratosphere, confining planetary waves, which would otherwise propagate equatorward, to higher latitudes where they break. This mechanism takes the emphasis off of the lower stratospheric (50 hPa) QBO easterlies in causing the Holton-Tan effect and places it on the middle stratosphere (10 hPa) QBO-MMC. In my opinion, the Holton-Tan effect has a lower stratospheric branch, dependent on the QBO easterlies, and an upper stratospheric branch, dependent on the QBO-MMC. This chapter only focuses on the lower stratospheric branch. The upper stratospheric branch is examined in Chapter 4.

3.1.2 Why the Holton-Tan effect may vary over longitude

The QBO is able to change the strength of the polar stratospheric wind by affecting the extratropical stationary planetary scale wave pattern. Studies have emphasized that the QBO affects the extratropical stationary wave-1 pattern in particular (Garfinkel et al., 2012; Lu et al., 2014; Lu et al., 2020; Rao et al., 2020a). Having said this, the idea of the Holton-Tan effect "varying over longitude" is silly because 180° of longitude are dominated by a ridge and 180° by a trough. However, the QBO is not only affecting the wave-1 pattern, but also the wave-2 and the wave-3 patterns (Lu et al., 2020). This presents an interesting opportunity. When superimposed on top of each other, the combined wave-1, wave-2 and wave-3 responses to the QBO may exhibit a complex structure not resembling any single zonal wavenumber. If this is the case, then the amplitude of the combined wave-1, wave-2, and wave-3 signature may be very large over some longitudes, but not over others. We could say then that those longitudes that have a large amplitude stationary wave response to the QBO exhibit heightened sensitivity to the QBO. I hypothesize that the stationary wave response to the QBO is irregular, with larger amplitudes over some longitudes, but not others. Because the Holton-Tan effect depends on the variability of the stationary wave pattern, which I am proposing is irregular in form relative to a simple wave-1 structure, I hypothesize that the upward propagating stationary wave that causes the Holton-Tan effect is coming from a particular longitudinal domain.

Looking for zonal asymmetry requires a large ensemble of data to limit the influence of internal variability and extract the QBO effect. This is limiting in reanalysis when decomposing between easterly and westerly QBO years leads to about 20 years of data for each, a small sample in regards to the highly variable northern hemisphere atmospheric circulation in winter. In this study, a 1500-year set of experiments performed with the Whole Atmosphere Community

Climate Model version 4 (WACCM) is used to explore the QBO teleconnections with robustness. These questions are the starting point for this chapter:

(1) How does the QBO effect on the extratropical circulation vary over longitude? How does the QBO influence planetary waves in specific sectors: the North Atlantic (45°W to 45°E), over Siberia (45°E to 135°E), the North Pacific (135°E to 135°W), and over North America (135°W to 45°W).

(2) What is the impact of the QBO on the extratropical atmosphere versus that from polar stratospheric variability? For this, a nudging technique is used to turn off the polar stratospheric feedback to the QBO in the model (the Holton-Tan effect). This isolates a more direct atmospheric response to the QBO that is referred to as the "direct effect" in this paper, which will be contrasted with the "indirect effect," the latter being the variability of the Holton-Tan effect.

3.2 Methods

3.2.1 Diagnostic tools

The QBO is indexed at different isobars (10, 20, 30, 50, and 70 hPa) to show the dependency of the results on the QBO phase. The index is made from the cosine latitude weighted, latitudinally and longitudinally averaged, time averaged December and January (DJ) zonal winds between 5°S and 5°N at the designated isobaric surface. The Holton-Tan effect is strictly an early winter, December-January (DJ) feature (Lu et al. 2014; White et al. 2015; Lu et al. 2020). The

sequential December and January periods are averaged together and the lowest tercile of averaged wind speeds is used to define the easterly QBO indices.

The QBO is referred to by what isobar the QBO is easterly at. So QBO_{10} means easterlies are located at 10 hPa, QBO_{20} at 20 hPa and so on. Judging by the winds in the lower stratosphere, QBO_{10} is the most westerly QBO (QBOW) state and QBO_{50} is a prototypical easterly QBO state (QBOE). QBO_{10} and QBO_{20} feature a waning lower stratospheric QBOW. QBO_{30} features a nascent lower stratospheric QBOE, and QBO_{50} and QBO_{70} prominent lower stratospheric QBOE.

Hereafter, every plot will show anomalies: anomalies during an individual month or day are calculated as deviations from that month's (e.g., December *or* January) or day's climatology. A two-sided student t-test is used to calculate significance: anomalies corresponding to the easterly QBO indices (33% of the anomalies, 500 timesteps) are compared to the remaining 67% of the anomalies (1000 timesteps).

The 3D wave activity flux of Plumb (equation 5.7, 1985) is used throughout. When zonally averaged, it reduces to the Eliassen Palm flux (Edmon et al. 1980). The zonal, meridional, and vertical components are used to calculate the WAF divergence, which indicates where wave generation or dissipation is taking place (Plumb 1985). The WAF is calculated using waves 1-3 as inputs for all analyses in the chapter. The contribution of waves four and up is found to be small and is not included.

3.2.2 Model

The Atmospheric General Circulation Model (AGCM) used in this study is the Whole Atmosphere Community Climate Model (WACCM, Marsh et al. 2013) with CAM4 physics and the specified chemistry option (referred to as SC-WACCM4, Smith et al. 2014). The specified chemistry decreases the computational cost of the model while retaining comparable climatology with the standard version. This is the main motivation for using specified chemistry since in this particular study, large ensemble size is prioritized over model complexity. The model domain extends from the surface to 5.1×10^{-6} hPa, ~ 145 kilometers with 66 vertical levels and a horizontal resolution of 1.9° latitude by 2.5° longitude. SC-WACCM4 does not simulate a QBO, but it includes an option to prescribe it by nudging the equatorial winds between 22°S and 22°N, from 86 hPa to 4 hPa. The climatological 28-month QBO cycle derived from radiosonde data is imposed in the model (Matthes et al. 2010).

3.2.3 Control experiment

The control (CTL) experiment consists of a concatenation of five 300-member experiments forced with the 1979-2008 average annual cycle of present-day sea surface temperature (derived from HadISST data, Rayner et al. 2003). The external forcings (greenhouse gases, aerosols, volcanoes) are set to their 2000 value. Each ensemble member is started on April 1st and ends after the completion of May 31st of the following year. The first April and May, are discarded for spin-up, leaving one full year of experiment for each member. The five different experiments only differ by their treatment of Arctic sea ice. These experiments are part of the Polar Amplification Model Intercomparison Project (PAMIP), which aims to investigate polar-mid-latitude linkages (Smith et al. 2019). They include the following sea ice concentration (SIC)

and sea ice thickness (SIT) forcings : (1) present-day SIC (1979-2008 average annual cycle) with fixed 2m SIT ; (2) preindustrial SIC (derived from preindustrial CMIP5 control runs) with fixed 2m SIT ; (3) future SIC (derived from RCP8.5 CMIP5 runs) with fixed 2m SIT ; (4) present-day SIC with spatially varying SIT (1979-2008 average annual cycle from PIOMAS, Zhang and Rothrock 2003) ; (5) future SIC with future SIT (also derived from RCP8.5 CMIP5 runs). Details on the experimental design are given in Smith et al. (2019).

The assumption made is that if robust in our model, the Holton-Tan effect should not be too dependent on the state of Arctic sea ice. To verify this, the wave activity flux (WAF, Plumb 1985) responses to the QBO are isolated given different sea ice background states. Different sea ice forcings promote different WAF responses to the QBO. Compare the future experiment (Fig. 3.2e) with the preindustrial SIC/fixed SIT responses for instance (Fig. 3.2b). In general, the stratospheric upward WAF and WAF convergence responses in the extratropical wave-guide are similar across the experiments. Therefore, the five experiments are concatenated to obtain a valuable ensemble of 1500 year, which allows for highly robust results.

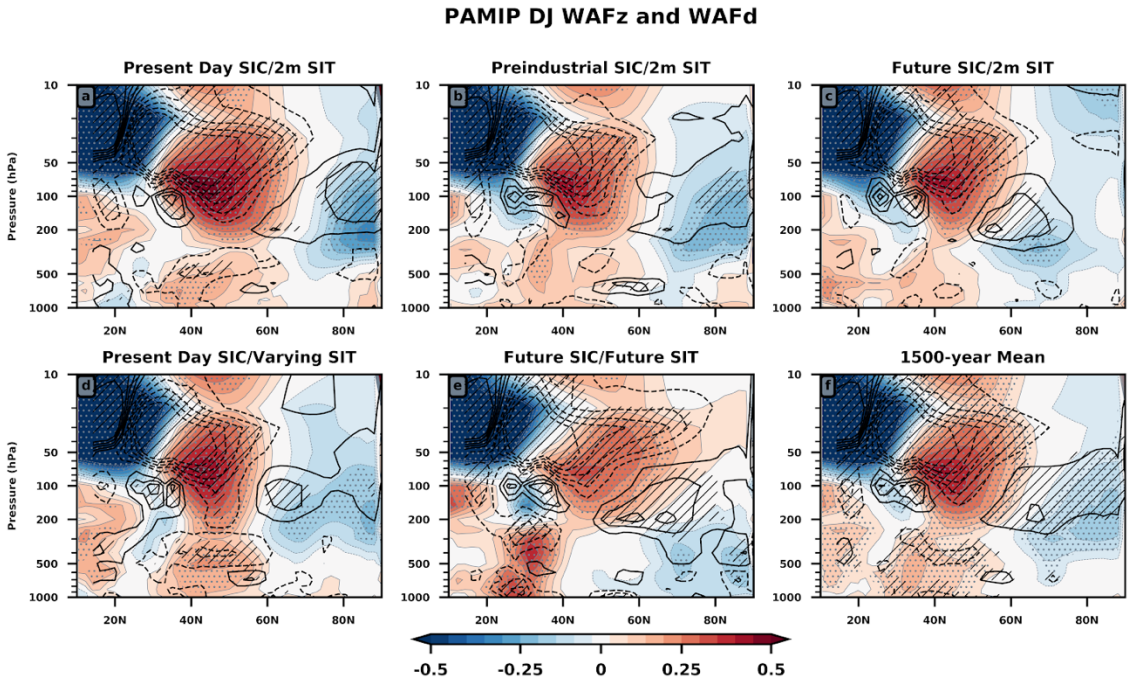

Figure 3.2: Dec. – Jan. averages of the normalized wave activity flux (WAF) responses. A QBO_{30} index is used. The vertical WAF component (WAFz) is shown in color and standardized. Significance is stippled with gray dots coinciding with p-values < 0.05 from a student's t-test. Black contours show the standardized WAF divergence (WAFd). The intervals are +/- 0.1 standard deviations. The zero contour is not shown. Significance for WAFd is calculated the same way as for WAFz, but it is hatched. Panel (f) shows the average of the 500 QBO_{30} DJ periods. Significance is calculated by comparing the 500 QBO_{30} DJ periods to the 1000 non-easterly QBO_{30} DJ periods. Composite (f) is most similar to composites included in the rest of this chapter.

Each of the ensemble members is initialized with a different month in the QBO cycle. For instance, member one is forced starting with the first month of the 28-month QBO cycle, while member two is forced starting with month two of the 28-month QBO cycle, and so on. Thus, with a 28-month cycle and 1500 ensemble members, each month of the QBO cycle is used to initialize about 50 members. This deliberate "walking down" of the QBO ensures that there will be variability in the QBO cycle among members. Note that the transient response to the QBO is diagnosed. Following Garfinkel and Hartmann 2011b, this is more pertinent to studying the response to the QBO than a multi-year response. A multi-year equilibrated response could be conflated with a response to the QBO, but also with subtropical stratospheric "memory" that could influence planetary wave propagation (Scott and Haynes 1998).

3.2.4 Climatological polar stratosphere (CPS) experiment

An additional experiment, called CPS for Climatological Polar Stratosphere, is used to isolate the tropospheric response to the QBO from the polar stratospheric response. It is forced with the 1979-2008 average annual cycle of SST/SIC and the same prescribed QBO. The polar stratospheric variability in CPS is suppressed by nudging the atmospheric circulation in the polar stratosphere towards its climatology. This prevents the propagation of waves into the polar stratosphere and reveals the tropospheric response to the QBO in the absence of the polar stratosphere response.

To implement the nudging, a reference 3-hour climatology is created from experiment (1) in the aforementioned list of five experiments. The prognostic equations for temperature, zonal wind, and meridional wind of the polar stratosphere (north of 65°N and above 200 hPa) are nudged toward the reference climatology at every 30-minute time step of the SC-WACCM4 run. The strength of the nudging, corresponding to a specific rate of Newtonian relaxation, is prescribed so that the atmosphere is fully constrained toward the target state every 2.5 hours. This allows the model experiment to exhibit some internal variability while ensuring that climatological polar stratospheric winds and temperature field between the CTL and CPS experiments are similar. A more thorough description of this nudging of the polar stratosphere towards climatology can be found in the supporting information of Peings et al. (2019).

3.2.5 Transient QBO response experiments

Three additional experiments are used to analyze the transient atmospheric response to the QBO. The control is a 100-year experiment with present day fixed SST/SIC variability and no prescribed QBO cycle. Branching is done every November 1st. Two sets of branched runs are performed, one in which the tropical stratosphere is nudged toward QBOW, and another toward QBOE. The runs last until January 31st. More details about these experiments are given when results from these experiments are discussed.

3.3 Results

3.3.1 QBO indexing scheme and Holton-Tan effect

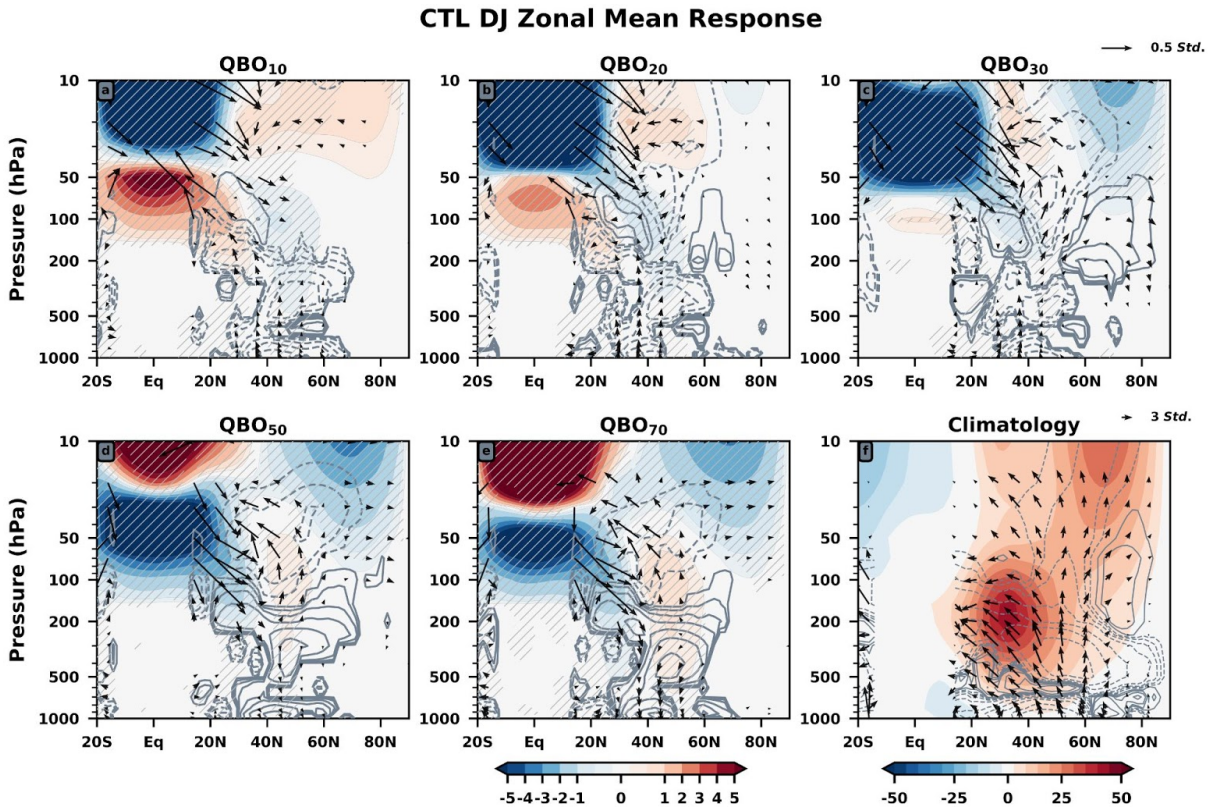

Figure 3.3: December and January (DJ) zonal mean responses to each of the five QBO indices. The isobar used to index the QBO is in the title of each composite. Zonal wind anomalies are shaded and extra contour levels are used about zero to show the tropospheric wind response: gray stippling is used to denote statistical significance. Wave activity flux (WAF) divergence is shown in black contours with intervals of +/ .001, .0025, .005, .01, .025, .05, .1, .25, .5 m/s/day. Standardized (by climatological standard deviation) vertical and meridional WAF responses are shown as vectors. Only statistically significant responses are shown for all fields other than zonal wind. Fig. 1f shows the climatological response: zonal wind is shaded, WAF divergence is shown similarly with intervals of +/ .01, .025, .05, .1, .25, .5, 1, 2.5, 5 m/s/day, and WAF vectors are instead shown as gray.

Figure 3.3 shows the zonal mean response to the QBO cycle with wave activity flux vectors and divergence overlaid on the zonal wind anomalies. Each frame in Figure 3.3 is composited using a different isobar to index the QBO (10 hPa for Fig. 3.3a, 20 hPa for Fig. 3.3b and so on).

	10 hPa	20 hPa	30 hPa	50 hPa	70 hPa
10 hPa	**990**	627	285	0	0
20 hPa	627	**990**	648	180	3
30 hPa	285	648	**990**	522	301
50 hPa	0	180	522	**990**	769
70 hPa	0	3	301	769	**990**

Table 3.1. The number of months making up the QBO index for each level between 10 hPa and 70 hPa is seen on the diagonal of this matrix. Other cells show the number of the months overlapping between different QBO indices. For example, 285 of the 990 months making up the QBO 30 hPa index overlap with the QBO 10 hPa index.

Ensemble members tend to overlap between adjacent QBO indices (Table 3.1). For instance, 627 of the 990 December and January easterly months making up the QBO_{10} index are also in the QBO_{20} index. Regardless of this overlap, composites created using different QBO indices contain unique features showing that the background atmospheric state is sensitive to which isobar is chosen to define the QBO index.

Consistent with the Holton-Tan effect, the polar vortex is weaker while QBOE occupies the lower tropical stratosphere (Figs. 3.3d,e). Conversely, the vortex is stronger (Fig. 3.3a) than the climatology when the lower stratosphere features a prominent QBOW. Since this result is based on an average of 500 DJ seasons, it corroborates that the Holton-Tan effect is a robust part of the atmospheric response to the QBO in SC-WACCM4 (as previously shown in Zhang et al. 2019).

As an additional metric to quantify how the polar cap changes by QBO phase, the number of SSWs per QBO phase is calculated using the 300-year experiment set with prescribed present-day climatological SST and SIC. The QBO is indexed using December and January. Using the same tercile indexing method, 100 members are analyzed for each QBO background state. SSWs are defined using the Charlton and Polvani (2007) definition, using U10 at 60°N from November 1st to March 31st, excluding final warmings. These results (Table 3.2) show that the vortex is most disturbed during $QBO_{30\text{-}50\text{-}70}$, during which 60, 81, and 78 SSWs occur, respectively, per 100 years. QBO_{10} and QBO_{20} feature 46 and 49 SSWs, respectively. Across all 300 years, there are 168 SSWs, a frequency of 0.56 events per season, lower than the climatological average, which is just over six events per decade (Butler et al. 2017).

	10 hPa	20 hPa	30 hPa	50 hPa	70 hPa
10 hPa	**46**	27	13	0	0
20 hPa	27	**49**	27	8	0
30 hPa	13	27	**60**	29	17
50 hPa	0	8	29	**81**	50
70 hPa	0	0	17	50	**78**

Table 3.2. The number of SSWs occurring per QBO index between 10 hPa and 70 hPa are bolded and located on the diagonal of this matrix. Other cells show the number of SSWs that overlap with an adjacent QBO index.

During QBO_{10}, in the troposphere the equatorward portion of the subtropical jet strengthens while its poleward portion weakens (Fig. 3.3a). The opposite set of anomalies is found during $QBO_{50\text{-}70}$. A speculation is that the arching of the zonal-mean zonal wind anomalies out of the subtropical stratosphere is a response to the QBO-MMC: it is thought to modify the synoptic

scale eddy momentum flux in the lower mid-latitude stratosphere (Garfinkel and Hartmann 2011a,b; Wang et al. 2018). While the tropospheric wind anomalies are small, recall that the five different sea ice forcings are used. Their unique effects on tropospheric circulation (not shown) muddy the tropospheric wind signal. Despite this, there is still a tropospheric response, suggesting that the tropospheric zonal wind response to the QBO is robust. Nonetheless, these are zonal mean composites that mask sector specific processes.

3.3.2 Modulation of planetary waves by the QBO

The QBO_{10} and QBO_{50} zonally averaged WAF response of Fig. 3.3 is shown averaged over individual sectors in Fig. 3.4, revealing distinct planetary wave responses over longitude for QBO_{10} and QBO_{50}. The 3D WAF and its corresponding 3D divergence are calculated for all grid points for all 1500-years of data. These fields are then split into four equally sized slices by longitude and averaged over longitude. This is accompanied by stereographic views of the vertical WAF at 850 hPa and 50 hPa, in Fig. 3.5 and Fig. 3.6, respectively.

The QBO uniformly suppresses equatorward propagation toward the QBO easterlies while allowing propagation toward the QBO westerlies (Fig. 3.4). This is the strongest WAF response and is consistent regardless of QBO phase or longitudinal sector.

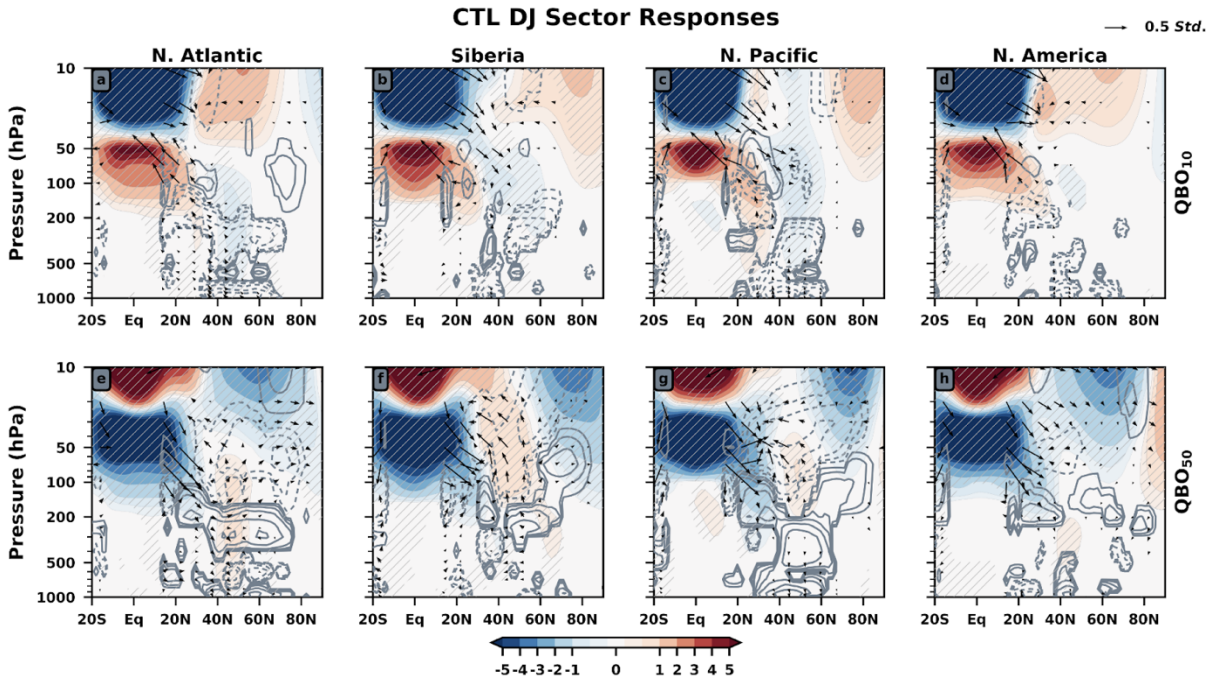

Figure 3.4: Zonally averaged anomalies of each longitudinal sector are shown with the same graphical conventions used to create Figure 1. The columns from left to right show the North Atlantic, Siberia, North Pacific, and North America responses. Each row corresponds to a different isobar used to index the QBO. The isobar is given on the right of each row.

During QBO_{10}, there is enhanced upward WAF in the troposphere between 40°N and 60°N (Fig. 3.3a). This is a reinforcement of the climatological upward WAF over the North Atlantic and North Pacific, but not the other sectors (Fig. 3.4a-d, 3.5a-c). The North Atlantic anomalous WAF points toward the QBO westerlies (Fig. 3.4a). The North Pacific anomalous WAF points upward and poleward (Fig. 3.4c), with some of it passing into the stratosphere over the North Pacific (compare Fig. 3.5a and Fig. 3.6a). In the stratosphere, the North Pacific anomalous upward WAF expands and intensifies between QBO_{10} and QBO_{20}, and then doubles in strength between QBO_{20} and QBO_{30} (Fig. 3.6a-c).

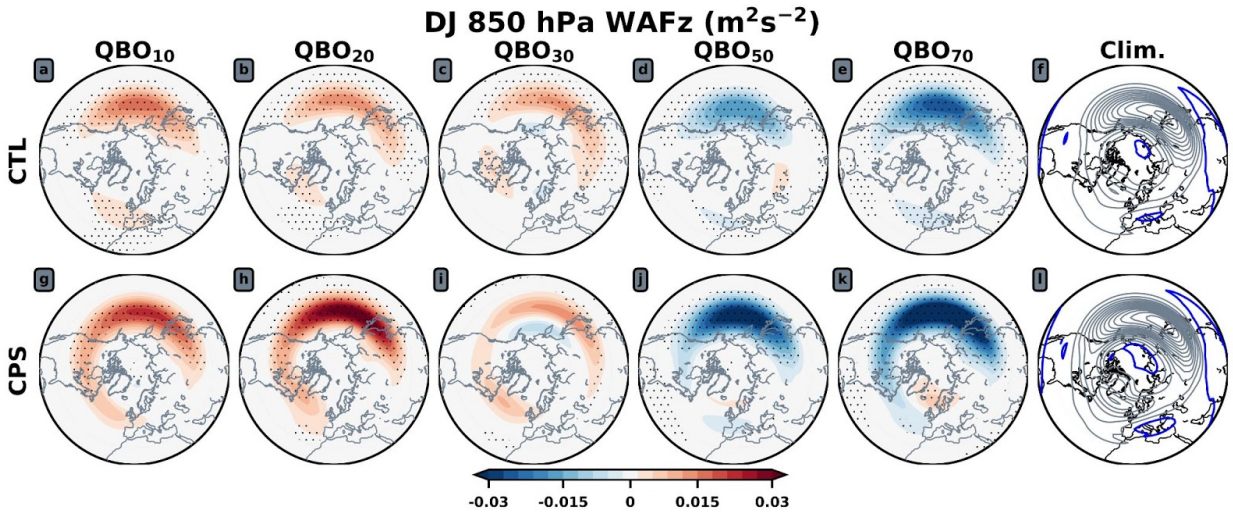

Figure 3.5: Polar stereographic views of the anomalous 850 hPa vertical WAF in the CTL (top) and in CPS (bottom). The isobar used to index the QBO is found above the composites. Stippling is used to denote statistical significance. DJ climatologies in black contours are shown on the right with intervals of +/- 0.03 m^2s^{-2}.

During QBO_{50}, the tropospheric response is opposite of that during QBO_{10} with both the climatological WAF reduced across all sectors and the climatological WAF convergence reduced at the tropopause (Fig 3.4e-h, Fig. 3.5d). In stark contrast to QBO_{10}, the anomalous upward WAF emanates from the tropopause around which there are WAF divergence anomalies. The North Atlantic anomalous WAF now propagates poleward and exhibits a "fountain-like" display as shown in White et al. (2015) (Fig. 3.4e). At 50 hPa, there is an increase in the vertical WAF over the North Pacific that shows up for every QBO phase (Fig. 3.6a-e). The anomalous stratospheric response leads to WAF convergence in the stratosphere over each sector except North America, with the largest responses observed over the North Pacific and Siberia (Fig. 3.4e-h).

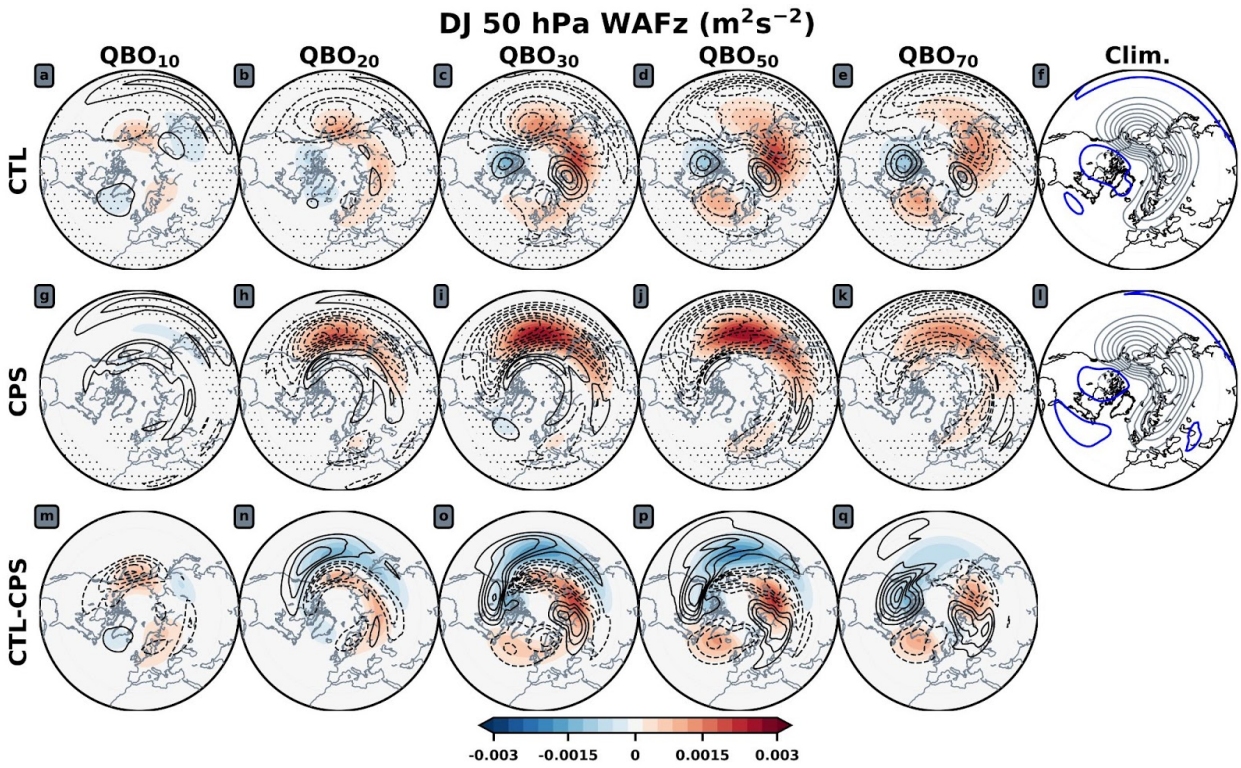

Figure 3.6: Polar stereographic views of the 50 hPa vertical WAF anomalies in the CTL (top) and in CPS (bottom). The isobar used to index the QBO is found above the composites. Stippling is used to denote statistical significance. Anomalous WAF divergence is overlaid with contour intervals of 0.0026 m/s/day with the zero-contour omitted. Only the statistically significant responses are shown. DJ climatologies in black contours are shown on the right with intervals of +/- 0.003 m^2s^{-2}. The difference between the CTL and CPS anomalies is shown in the bottom row.

In the North Atlantic, the QBO leads to increases in the upward WAF during $QBO_{50\text{-}70}$ (Fig. 3.6d,e) while the anomalous WAF is downward during $QBO_{10\text{-}20}$ (Fig. 3.6a,b). In climatology, the vertical WAF is nearly zero in the North Atlantic just south of Greenland (Fig. 3.6f) suggesting upward propagating planetary waves are generated during $QBO_{50\text{-}70}$ and downward propagating waves during QBO_{10}.

In order to better isolate the role of the QBO in generating the WAF responses, the results of the CPS experiment are analyzed. CPS includes suppressed polar stratospheric variability. In the lower troposphere, the main difference between CPS and CTL is that the CPS anomalies are

larger magnitude (Fig. 3.5, bottom row). This suggests that the polar stratospheric response to QBO in the CTL reduces the direct forcing from QBO.

In the stratosphere, the anomalous upward WAF at 50 hPa in the North Pacific vanishes during QBO_{10}, but is present in $QBO_{20\text{-}30}$ (Fig. 3.6g-i). The easterly shift of this response from the North Pacific to Siberia as the QBO phase in the lower stratosphere becomes more easterly is less pronounced relative to CTL (compare Fig. 3.6 top and middle). In fact, the dominant response in CPS is anomalous upward WAF in the North Pacific and corresponding WAF convergence there, occurring during $QBO_{20\text{-}30\text{-}50\text{-}70}$. Of all sectors, the North Pacific responses are most similar between CPS and CTL. Note how similar the WAF divergence (convergence) is between CTL and CPS during QBO_{10} (QBO_{70}) (Fig. 3.6a,g,e,k): this response arises from the QBO, not polar stratospheric variability. This is interesting as it suggests that the QBO promotes the WAF response in the North Pacific with a secondary role for polar stratospheric variability there. This North Pacific WAF is part of the "direct effect" of the QBO on the extratropical atmosphere.

On the contrary, vertical WAF anomalies over North America, the North Atlantic, and Siberia vanish in CPS. This suggests that WAF responses in these sectors are mutually dependent on the QBO and polar stratospheric variability. This is generally true regardless of QBO phase. Polar stratospheric variability can be defined as the difference between the CTL and CPS responses to the QBO (Fig. 3.6, bottom row). During QBO_{50} for instance, it accounts for anomalous downward WAF over North America, upward anomalies over the North Atlantic, and upward anomalies over Siberia (Fig. 3.6p).

CPS promotes more WAF convergence over the North Pacific than in the CTL during $QBO_{20\text{-}30\text{-}50}$. The 2.5-hour relaxation timescale in CPS should preclude any planetary wave breaking in the polar stratosphere. With the anomalous waves not allowed to break within polar latitudes,

wave breaking is enhanced in the extratropics, mainly over the North Pacific (compare Fig. 3.6 top and middle). An inference is that QBO initiates the lower stratospheric Holton-Tan effect through the North Pacific. Since the polar stratosphere cannot accept inbound waves, wave breaking is more vigorous in the mid-latitude stratosphere. Since the polar stratosphere cannot be disturbed, no downstream WAF changes may take place over North America, the North Atlantic, and Siberia. The "indirect effect," which takes place once the QBO modulates the polar stratosphere, is shut off in CPS. This hypothesized spatiotemporal evolution is analyzed in subsequent sections.

3.3.3 Tropospheric response: competition between the direct and indirect effect

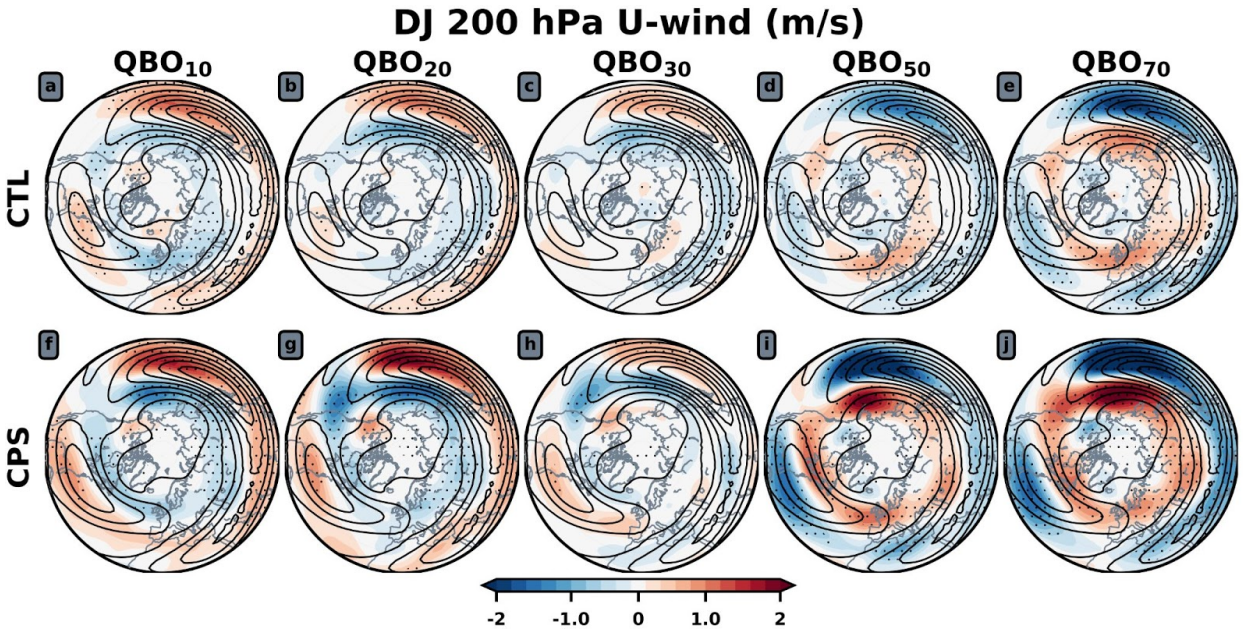

Figure 3.7: Polar stereographic views of the 200 hPa zonal wind response to the QBO in the CTL (top) and in CPS (bottom). Wind anomalies are shaded and stippling is used to denote statistical significance. The isobar used to index the QBO is found above the row 1 plot. The DJ climatological wind is superimposed in black contours with contour levels of 10, 20, 30 … m/s with no zero-contour line.

Fig. 3.7 shows the CTL and CPS 200 hPa zonal wind anomalies. $QBO_{10\text{-}20\text{-}30}$ feature equatorward shifting jets (Fig. 3.7a-c) while $QBO_{50\text{-}70}$ feature poleward shifting jets (Fig. 3.7d,e). Since CPS suppresses the polar stratospheric response to the QBO, it represents an opportunity to show the direct influence of the QBO on the extratropical zonal circulation. The CPS 200 hPa zonal wind anomalies (Fig. 3.7f-j) are stronger and more zonally symmetric about the mid-latitudes than those in the CTL (Fig. 3.7a-e). This indicates that the QBO and polar stratospheric variability compete to alter extratropical flow. This competition is most pronounced over the North Pacific (e.g., Fig. 3.7d vs. 3.7i).

To investigate the apparent competition between the direct effect of the QBO and the polar stratospheric response to it in the troposphere, the CTL and CPS temperature (shading) and zonal wind (contours) responses in the North Pacific (135°E to 135°W) are compared.

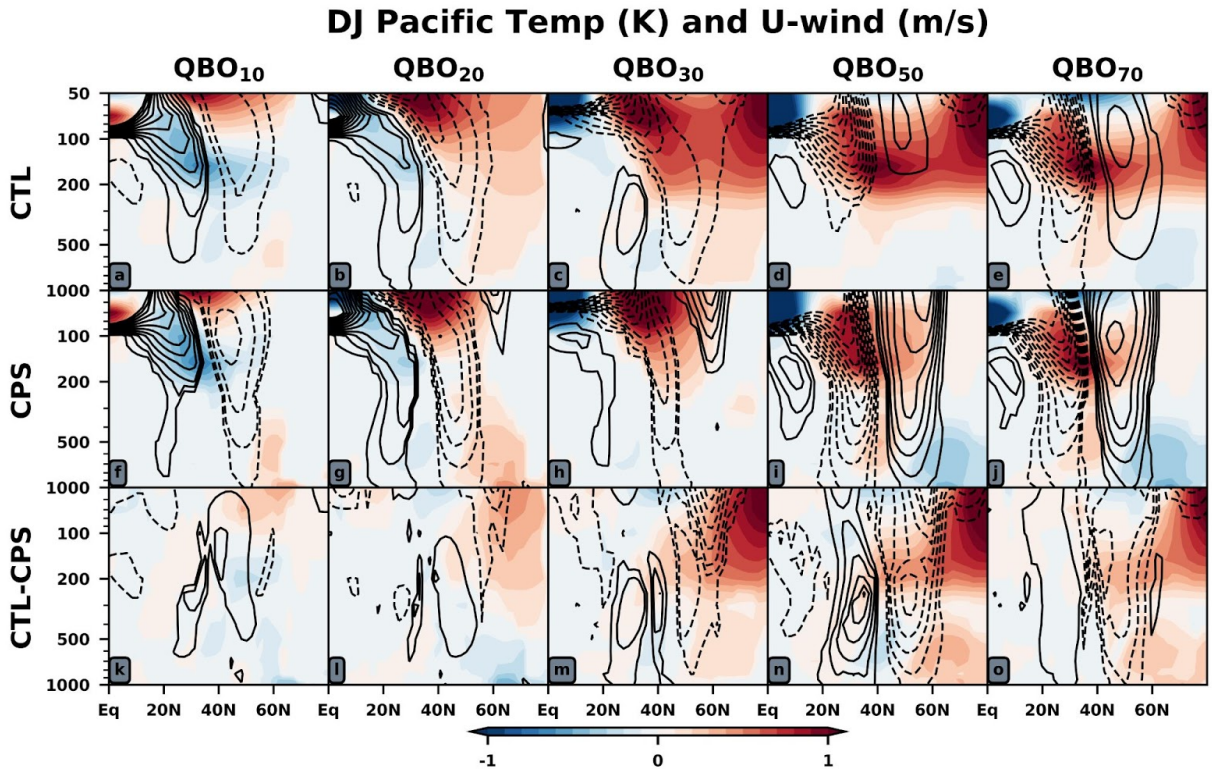

Figure 3.8: Pacific sector (135°E to 135°W) zonal mean zonal wind (black contours, 0.25 m/s interval) and temperature responses (shading) to the QBO. The first row features the CTL response, middle is for CPS, and the bottom is the difference between CTL and CPS responses to the QBO. The isobar used to index the QBO is found above these composites. Only responses corresponding to p-values < 0.05 are shown.

Tropical heating and extratropical cooling manifest near the tropopause during QBO_{10} in CTL and CPS (Fig. 3.8a,f). The tropical warming maintains thermal wind balance for the QBO westerly shear. The cooling over the extratropical tropopause is likely a response to the QBO mean meridional circulation (QBO-MMC). While studying the tropospheric response to the QBO with the same AGCM, Garfinkel and Hartmann (2011a,b) found that the QBO promotes changes in the extratropical upper tropospheric horizontal eddy momentum flux. Mean meridional circulations are known to arise in the troposphere in response to either lower stratospheric temperature anomalies or changes in the lower stratospheric horizontal eddy momentum flux (Haigh et al. 2005; Simpson et al. 2009; Simpson et al. 2012; Ait-Chaalal & Schneider, 2015). I infer that this meridional circulation is there during QBO_{10} by looking at the

weak tropospheric temperature anomalies (Fig. 3.8a): the ascending (descending) branch of this inferred circulation is visible in the mid-troposphere at 40°N (65°N). This supports zonal wind anomalies developing deeper in the troposphere, thereby communicating the initial stratospheric temperature perturbations into tropospheric zonal wind forcing. Something to consider is how the mid-latitude lower stratospheric temperature response forms. The lower stratospheric temperature anomalies likely arise in response to the QBO-MMC. But the QBO-MMC's role is not perfectly clear because it may be the case that it is modifying the lower stratospheric mean flow, and hence affecting where eddies propagate. If the eddy mean flow interaction promotes meridional redistribution of potential vorticity, this may promote cross isentropic circulations whose ascending and descending branches coincide with temperature change (as described in Haynes and McIntyre 1987). Then the eddies would actually be responsible for the mid-latitude lower stratospheric cooling during QBO_{10} (Fig. 3.8a) and warming during QBO_{50} (Fig. 3.8d). During QBO_{50} in the CTL (Fig. 3.8d), the stratospheric temperature response reverses sign compared to QBO_{10}. Cold anomalies appear in the tropical stratosphere, warming in the mid-latitude lower stratosphere and polar stratospheric warming consistent with the Holton-Tan effect. The tropospheric temperature response also reverses in sign compared to QBO_{10} (Fig. 3.8d). During QBO_{50} in the CPS (Fig. 3.8d), the temperature responses are very similar, but the polar stratospheric warming resulting from the Holton-Tan effect is absent because polar stratospheric variability is suppressed in CPS. As a result, the troposphere actually exhibits a zonal wind response. An interpretation of this result is that QBO_{50} alone promotes a poleward shift of the tropospheric jet in the North Pacific mid-latitudes. Conversely, the polar stratospheric warming resulting from the Holton-Tan effect opposes this response. The polar stratosphere's role can be approximated by subtracting the CPS QBO_{50} response from the CTL QBO_{50} response (Fig. 3.8n). In this case, the polar stratosphere promotes an equatorward shift of the tropospheric jet over the North Pacific (Fig. 3.8n).

In summary, the tropospheric zonal wind and temperature anomalies directly driven by QBOE are moderated by the indirect effect of a warmer polar stratosphere during QBOE. Although this QBO-polar stratosphere competition is consistent among all sectors in the stratosphere, the stratosphere-troposphere coupling and tropospheric response is most pronounced in the North Pacific relative to other longitudes. This enhanced tropospheric response in the North Pacific may be due to the large climatological tropospheric planetary wave flux in this sector, which is thought to facilitate enhanced stratosphere-troposphere coupling (White et al. 2019).

3.3.4 Timing of the polar vortex response: importance of the North Pacific

To better understand the spatiotemporal evolution of the extratropical response to the QBO, Fig. 3.9 shows the daily 10 hPa polar cap (60°N-90°N) geopotential height anomalies forced by the QBO. The responses are split into four longitudinal sectors: North Pacific (135°E to 135°W), North America (135°W to 45°W), North Atlantic (45°W to 45°E), Siberia (45°E and 135°E). Only the prescribed present-day SST/SIC experiment is used (300 years total). The QBO is indexed based on the December-January QBO phase only. The increases (QBOE) and decreases (QBOW) in height are consistent with the Holton-Tan effect and the largest magnitude responses occur over North America and the North Atlantic. There is a general slant of the geopotential height responses from the top left of Fig. 3.9 toward the bottom right. The QBO affects when the polar cap warms: earlier during QBOE and later during QBOW.

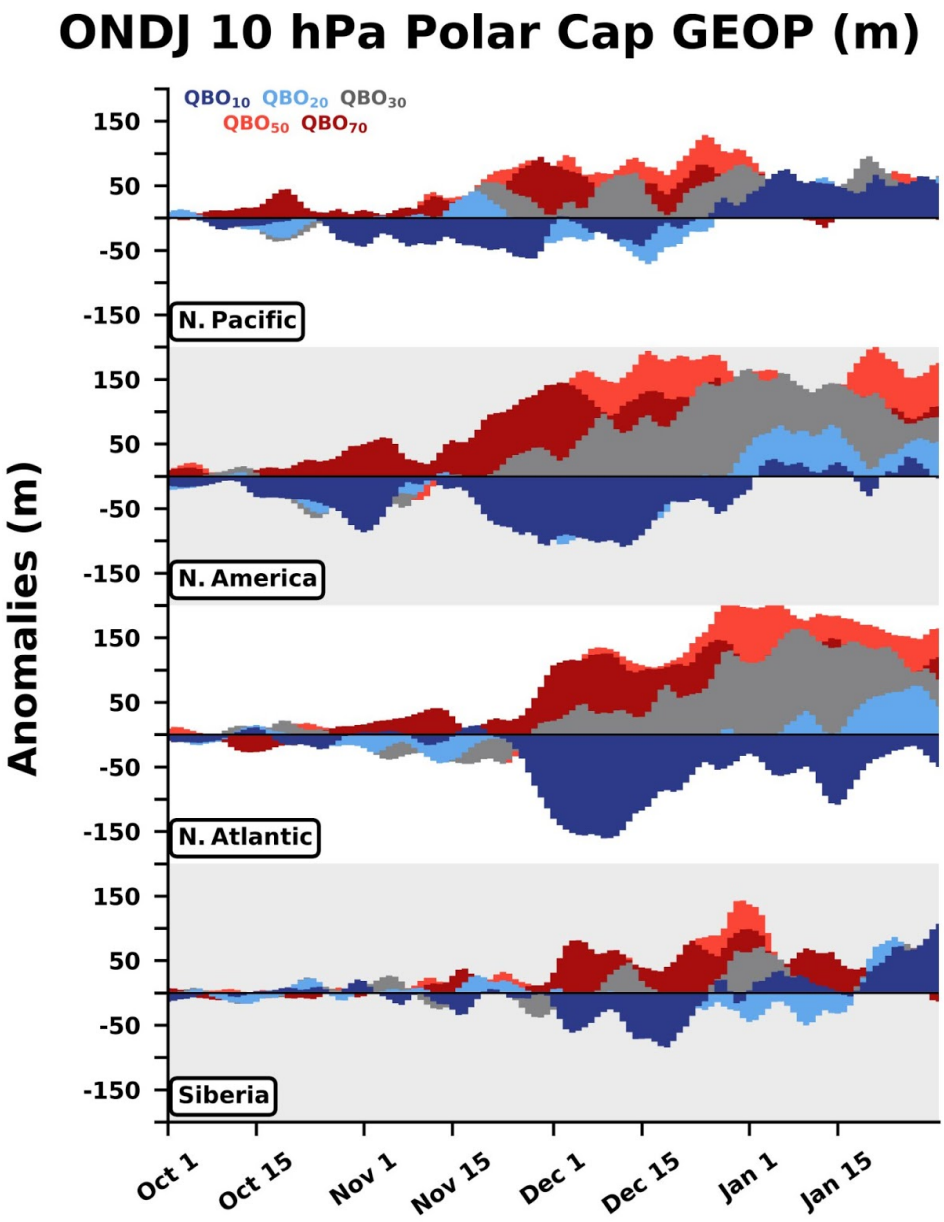

Figure 3.9: October to January (ONDJ) daily 10 hPa geopotential height anomalies (m) over the polar cap (60°N-90°N) and split amongst the four equally sized sectors: North Pacific (135°E to 135°W), North America (135°W to 45°W), North Atlantic (45°W to 45°E), and Siberia (45°E to 135°E). The five different colors used identify the isobar used to index the QBO with QBOW indices corresponding to blue and QBOE indices corresponding to red. The QBO is indexed using only December and January, however October and November are included for the analysis.

3.3.5 Stratospheric wave response

In Fig. 3.10, the 50 hPa geopotential height anomalies and 510 K potential vorticity (PV) anomalies reveal that the position of the polar cyclonic flow changes for each QBO phase. Heights decrease over North America during QBO_{10} (Fig. 3.10a) while they decrease over Eurasia as the QBO phase becomes more easterly (Fig. 3.10c). As indicated by Fig. 3.9, heights increase most over North America and over the North Atlantic during $QBO_{30\text{-}50\text{-}70}$ (Fig. 3.10c-e).

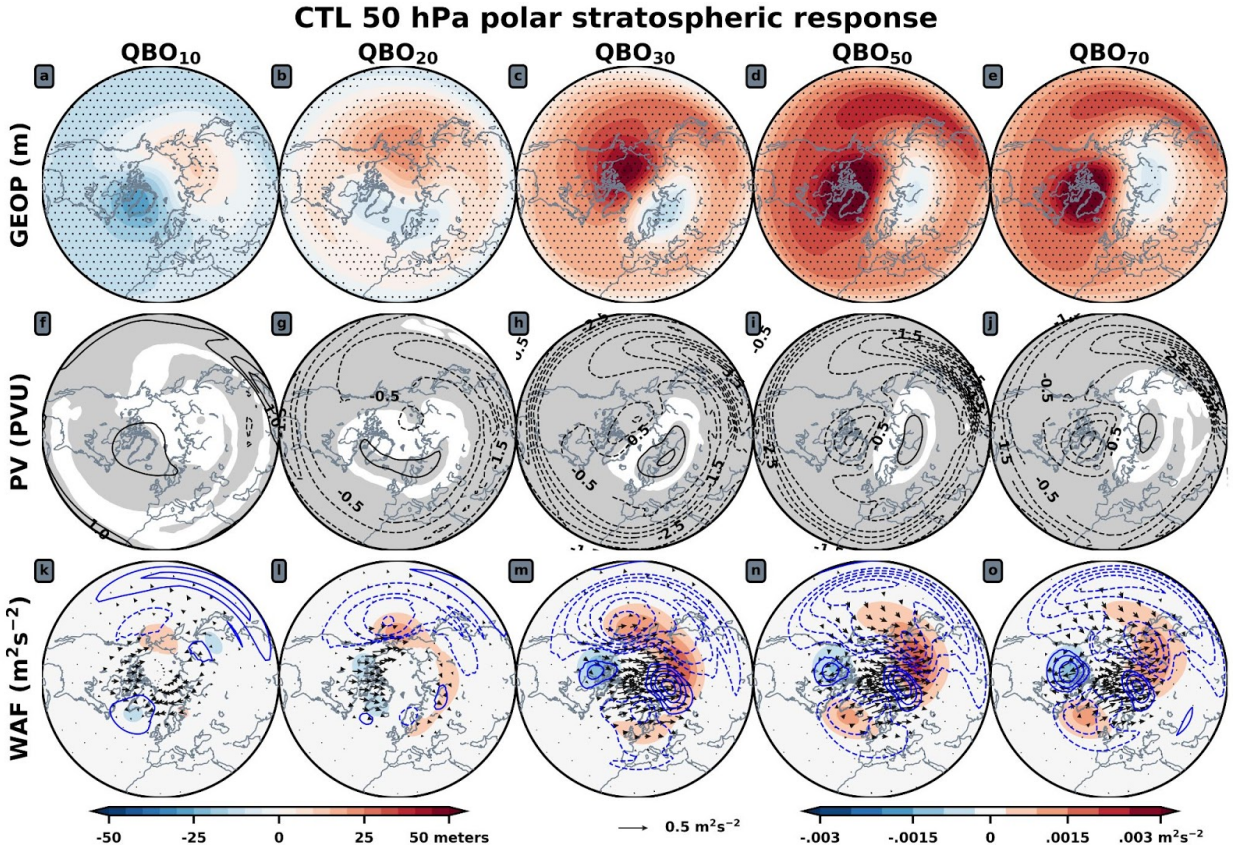

Figure 3.10: Polar stereographic views of the 50 hPa response to the QBO in the seasonal mean. Each column corresponds to a different isobar used to index the QBO. This isobar is denoted in the title of the composites in row one. Row one shows the geopotential height responses, row two the PV responses, and row three the 3D WAF responses. Geopotential height anomalies are shaded and stippling denotes statistical significance. PV anomalies are shown in contours with an interval of +/- 0.5 PVU and gray shading denotes statistical significance. For the 3D WAF, the vertical component is shaded, the meridional and zonal components are shown as vectors, and WAF divergence is shown in blue contours with intervals of +/- 0.0026 m/s/day, excluding the zero contour. Only statistically significant responses are shown.

The position of the anomalous polar trough and polar warming, which vary by QBO phase, coincide with distinct potential vorticity gradients, each supporting different planetary wave responses. The 50 hPa three-dimensional wave activity flux anomalies reveal that the anomalous wave trains propagate along positive PV gradients. During QBO_{30}, the anomalous wave propagates east towards Eurasia away from the North Atlantic (Fig. 3.10m) along the weak, but positive anomalous PV gradient (Fig. 3.10h). This is opposite of the QBO_{10} response

in which the wave propagates west toward the North Atlantic from Eurasia (Fig. 3.10k). The following features are ubiquitous among all QBO phases: there is (1) propagation of the anomalous wave toward the anomalous polar trough, and (2) prominent WAF convergence in the North Pacific.

Fig. 3.6 and now Fig. 3.10 have both shown concurrent increases in the upward flux over the North Atlantic and Siberia during $QBO_{50\text{-}70}$. A speculation is that this is associated with the position of the anomalous polar cyclonic flow, which is superimposed directly between these two anomalous upward WAF responses. This suggests that the spatiotemporal evolution of the polar cyclonic flow given a background QBO state (Fig. 3.9) is important because it preconditions the stratosphere to support planetary wave propagation. A similar inference can be made from Fig. 3.6: if polar stratospheric variability is suppressed, the WAF responses over North America, the North Atlantic, and Siberia vanish during $QBO_{50\text{-}70}$. This question is posed: does the anomalous WAF over the North Pacific precede the change in polar stratospheric flow, which ultimately drives the upward WAF over the North Atlantic and other sectors? The transient experiments are used to help answer this question.

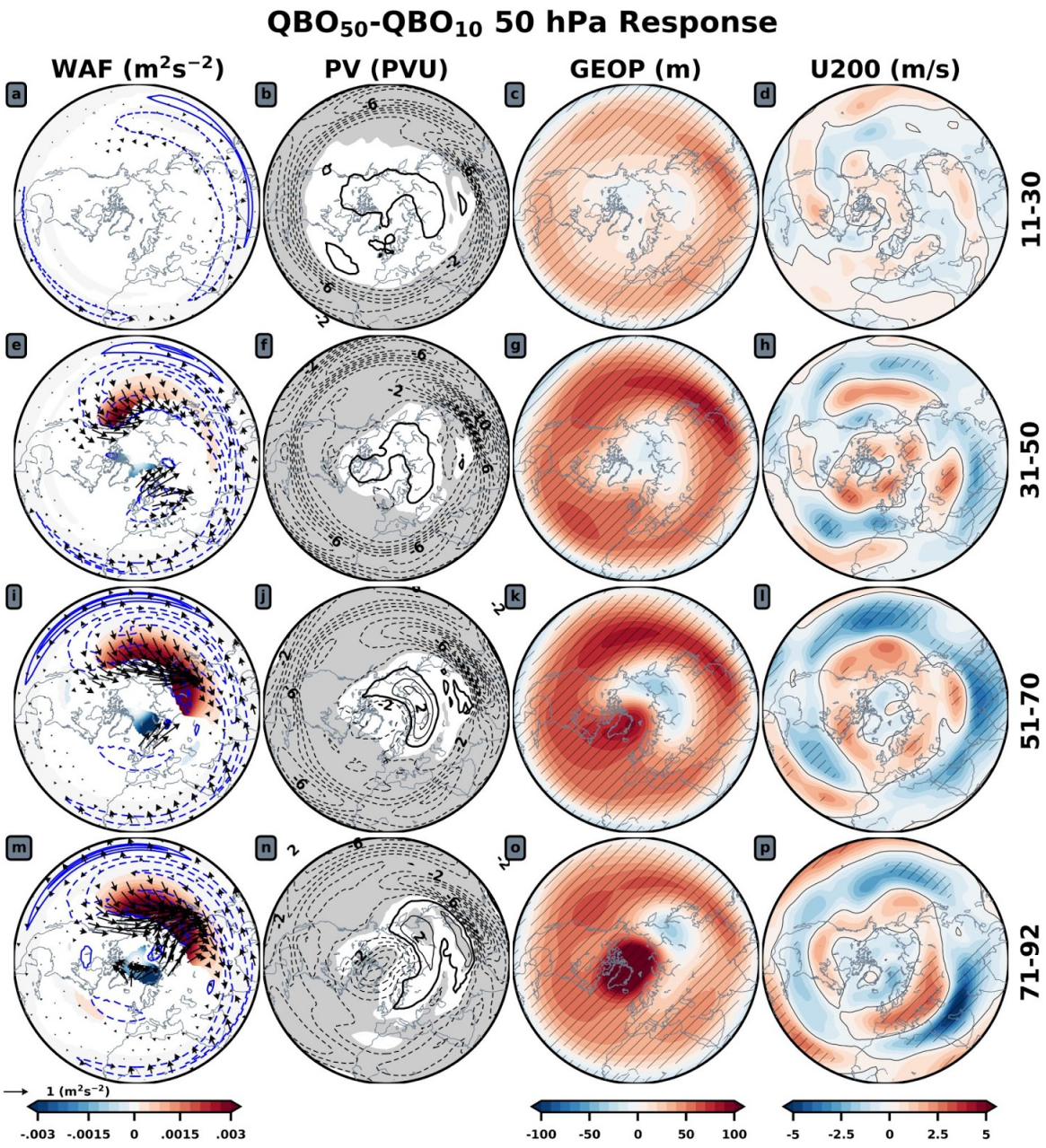

Figure 3.11: Polar stereographic views of the 50 hPa atmospheric response to turning on the QBO in the branched experiments. Anomalies are calculated as $QBO_{50} - QBO_{10}$, which highlights the response to easterly QBO. Row one shows the response over days 11-30, row two: days 31-50, row three: days 51-70, and row four: 71-92. From left to right, column one shows the 3D WAF response. The vertical component is shaded, the meridional and zonal components are shown as vectors, and WAF divergence is shown in contours with an interval of +/- 0.00864 m/s/day, excluding the zero contour. Only statistically significant responses are shown. Column two shows the 510 K PV response. The contour interval in +/- 1 PVU and gray shading denotes statistical significance. Column three shows the geopotential height response in shading and hatching denotes statistical significance. Column four shows the 200 hPa zonal wind response with hatching used to denote statistical significance.

The control transient experiment features no QBO. I branch from November 1st of the control and turn on the QBO. Note that the QBO begins descending once the nudging is activated and it takes about a month for the QBO-MMC to develop in the extratropics (not shown). The QBO is imposed so that it progresses toward the desired QBO profile by mid-December. The easterly QBO experiment exhibits the QBO_{50} profile and the westerly QBO experiment exhibits the QBO_{10} profile.

Figure 3.11 shows the 50 hPa WAF anomalies in the transient experiments with the horizontal components shown as vectors, the vertical component in shading, and the divergence of the WAF in blue contours. Anomalies are defined as the QBO_{50} minus QBO_{10} responses. In the first 50 days, enhanced upward and poleward WAF is observed in the North Pacific and over Siberia resulting in WAF convergence in those regions (Fig. 3.11a,e). This is consistent with erosion of the 510 K PV gradient over East Asia above the subtropical jet region (Fig. 3.11b,f). Vorticity and geopotential are related by a Laplacian operator, hence the negative PV anomalies coincide with increases in geopotential height (Fig. 3.11c,g). The height anomalies increase over Siberia and the North Pacific from days 11-30 to days 31-50 and then expand eastward. This follows the same spatiotemporal evolution of geopotential heights in the seasonal mean (Fig. 3.9). This continues through days 51-92 as the height anomalies increase and encroach on the polar stratosphere (Fig. 3.11k,o). Meanwhile in the upper troposphere, the jet shifts poleward once the QBO-MMC becomes established in the extratropics (Fig. 3.11, right column).

For the duration of the transient experiments, the North Pacific sector (defined as 135°E to 135°W) and the eastern most part of the Siberia sector (defined as 45°E to 135°E) dominate the mid-to-high latitude WAF response. Recalling the results of the previous section, the lower stratospheric position of the Holton-Tan effect is primarily mediated through the North Pacific

sector. In response to the earlier question posed in this section, the anomalous WAF response over the North Pacific leads the changes in the polar stratospheric flow.

At no point in the transient experiments is there anomalous upward WAF in the North Atlantic reminiscent of the signal shown in Fig. 3.6d. To better understand the North Atlantic WAF responses, I composite on the North Atlantic WAF between 60°W to the Prime Meridian and 45°N to 75°N (box shown in Fig. 3.12a). This is done using daily data from the 300-year experiment set forced with prescribed present-day climatological SST and SIC. The days with the maximum and minimum vertical WAF in the North Atlantic box are selected for each year. These are referred to as “upward” and “downward” events, respectively. Both upward and downward WAF days are distributed evenly throughout the December and January period (not shown). Fig. 3.12 shows the 510 K (30 hPa) isentropic potential vorticity anomalies and full field (anomaly + climatology) corresponding to the two types of events.

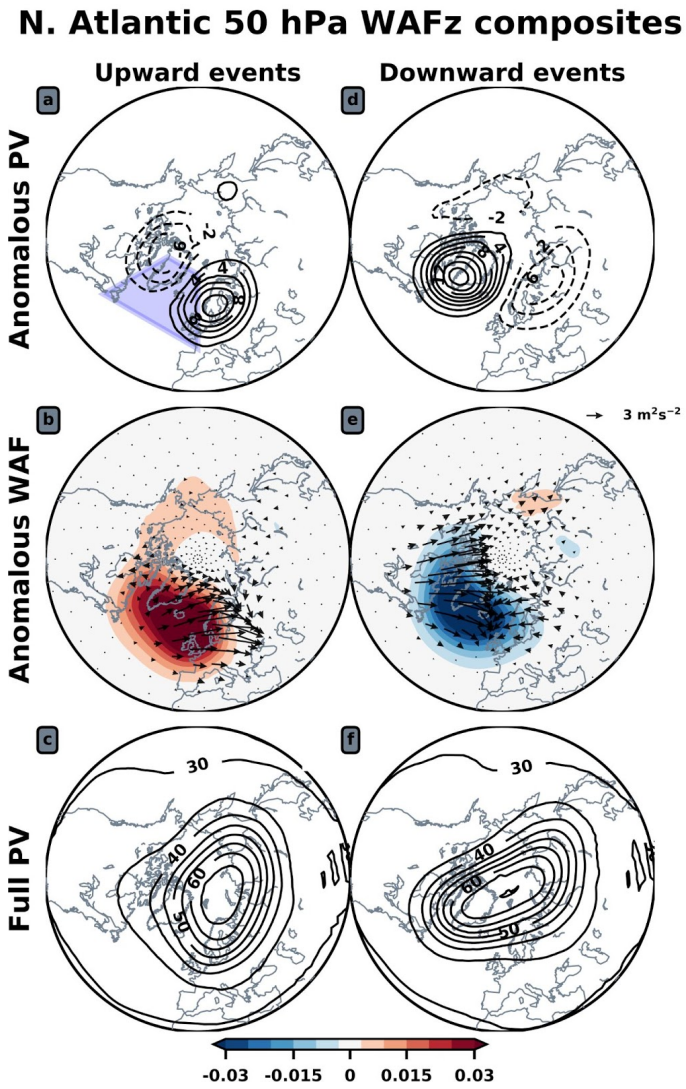

Figure 3.12: 510 K Potential vorticity (PV) and 50 hPa 3D WAF composites of “upward” and “downward” events in the North Atlantic stratosphere. Refer to text for details on how these plots are created. From left to right, column one shows responses for upward events and column two shows that for downward events. Row one shows the anomalous PV response, row two the anomalous WAF response, and row three the full PV field corresponding to these events. This is indicated to the left of column one. Composite (a) shows the domain over which the vertical WAF is averaged to create the indices for upward and downward events: 60°W to the Prime Meridian and 45°N to 75°N.

The polar vortex exhibits very different configurations for each event type. For the upward case, the polar vortex shifts toward Eurasia (Fig. 3.12c) while for the downward case, it shifts towards North America (Fig. 3.12f). In reanalysis, Zhang et al. (2019) find a shift of the polar vortex toward Eurasia during QBOE and a shift towards North America during QBOW. These results

are consistent with that study. During QBO_{10} (a QBOW background state), negative vertical WAF anomalies are found in the North Atlantic (Fig. 3.6a). Negative vertical WAF anomalies in the North Atlantic are associated with a shift of the polar vortex toward North America (Fig. 3.12f). A shift of the polar vortex toward North America is observed to occur during QBOW (Zhang et al. 2019). The opposite applies during QBOE. The position of the polar vortex, which shows modulation by the QBO in reanalysis, appears to be associated with distinct WAF responses. The anomalous horizontal wave response (Fig. 3.12b,e) always moves up the PV gradient toward the highest PV anomaly (Fig. 3.12a,d). In the transient runs, the missing ingredient for a robust upward WAF response in the North Atlantic appears to be the shift of the polar vortex toward Eurasia in the mean response.

3.3.6 Reanalysis results

Figure 3.13 is the ERA5 reanalysis equivalent of Figure 3.10. The 50 hPa geopotential height responses, the 510 K PV responses, and the 50 hPa wave activity flux responses are shown. The only difference between Fig. 3.13 and Fig. 3.10 is that the geopotential height color scale here is between +100 and -100 meters. Using data from 1979-2019, there are just ~ 13 December-January periods available for each composite.

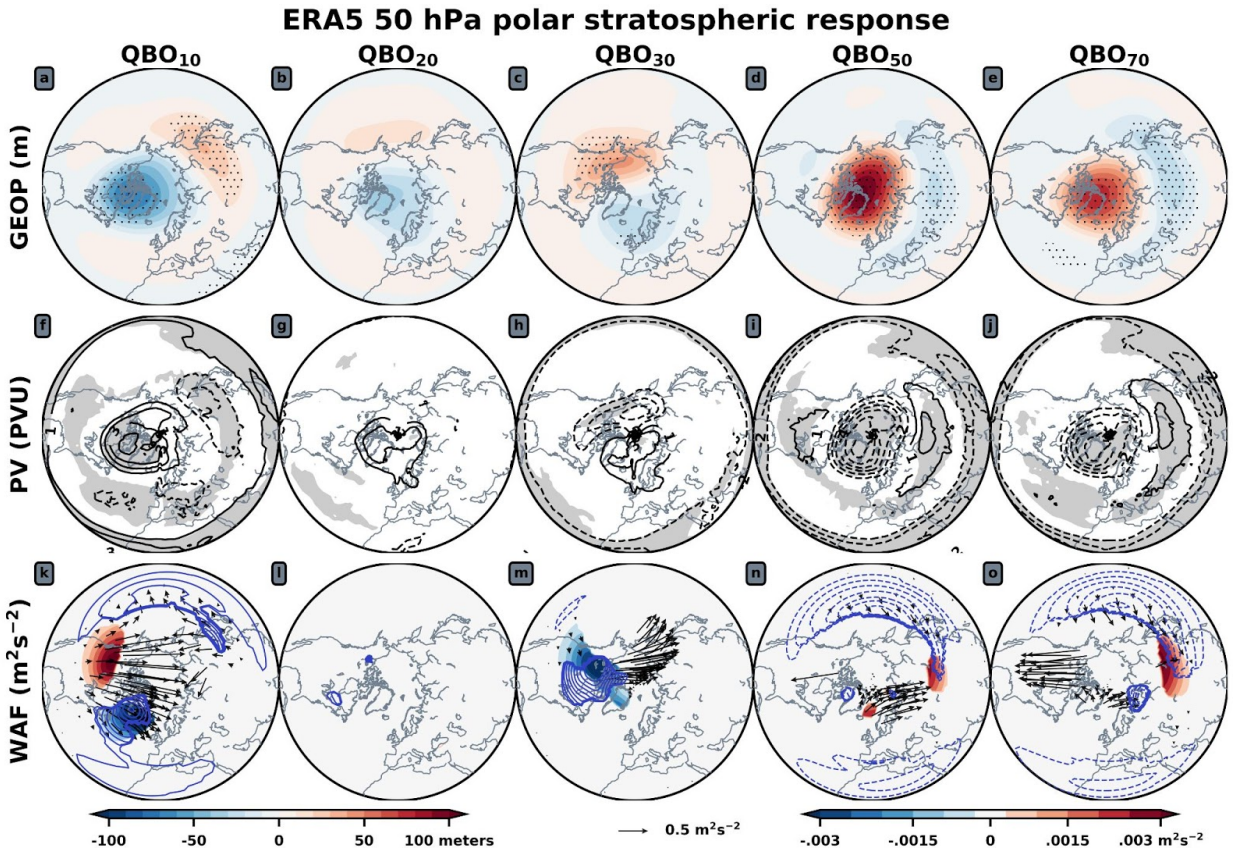

Figure 3.13: As in Figure 10, but for ERA5. The geopotential height anomaly colorscale ranges from +100 to -100 meters now to account for the stronger responses in ERA5.

The 50 hPa geopotential height responses (Fig. 3.13, first row) are generally consistent between ERA5 and SC-WACCM4 with anomalies that are roughly 3-4 times stronger in ERA5. The PV response shows that the position of the polar cyclonic flow varies with the background QBO state, similar to SC-WACCM4. The polar cyclone is reinforced closer to North America during QBO_{10} (Fig. 3.13a,f), but shifts toward Eurasia as the QBO phase in the lower stratosphere becomes more easterly (e.g., Fig. 3.13d,i). Similar to the geopotential height response, the PV response is far stronger in ERA5 relative to SC-WACCM4. QBO_{50} shows a 6 PVU degradation of the polar flow over North America versus a 2 PVU degradation for SC-WACCM4 (Fig. 3.13i vs. 3.10i). Ridging of the polar cap is more zonally symmetric about the pole in ERA5 during $QBO_{50\text{-}70}$ compared to SC-WACCM4 (Fig. 3.13d,e).

The WAF results (Fig. 3.13 third row) agree with SC-WACCM4. There is enhanced upward WAF over part of the North Pacific (but also North America) during QBO_{10} (Fig. 3.13k), which shifts easterly toward Siberia during $QBO_{50\text{-}70}$ (Fig. 3.13n,o). A key finding is that the enhancement of upward (downward) WAF in the North Atlantic during QBOE (QBOW) exists in ERA5. Using the period 1979-2017, these vertical WAF results are reproduced in National Centers for Environment (NCEP)-National Center for Atmospheric Research (NCAR) reanalysis dataset (Kalnay et al. 1996) (not shown). Given that plenty of internal variability is available to convolute these results and that each composite is made from only 13 seasons in ERA5 as opposed to 500 seasons in SC-WACCM4, these reanalysis findings also indicate that the QBO has an important impact in the North Atlantic. Further, across all sectors, both the ERA5 and NCEP WAF anomalies are roughly two to three times larger than the response in the 1500-year CTL. A final key finding is that WAF divergence responses over the North Pacific during all QBO phases are consistent with SC-WACCM4, again indicating an important role for this longitudinal sector in the teleconnection between the QBO and polar stratosphere (Fig. 3.13l-o).

3.4. Conclusions and Discussion

Coming back to the key questions identified in introduction, here is a summary of the findings:

(1) How does the QBO effect vary over longitude?

The Holton-Tan effect is a robust part of the December to January atmospheric response to the QBO in 1500 years of SC-WACCM4 data. This teleconnection varies over longitude and the results consistently show that the North Pacific portion of the atmosphere is more sensitive to the QBO than other longitudes. As suggested by the CPS experiment, which suppresses the

feedback from the polar stratosphere, the upward wave activity flux anomalies in the lower stratospheric North Pacific represent a direct response to the QBO, while wave activity flux anomalies over North America and the North Atlantic sector are a consequence of the polar stratospheric response to the QBO. Moreover, the transient experiments in which a QBO is imposed in a free running atmosphere devoid of a QBO shows that wave absorption takes place in the mid-to-high latitude North Pacific lower stratosphere before the QBO influences any other longitudes.

It is not clear why the North Pacific is more tightly coupled with QBO variability compared to other longitudes. It may result from the nearby mountain ranges, the Himalayas or Tibetan Plateau, which have pronounced impacts on the extratropical flow (White et al. 2017). It may result from the sharp land-sea contrast in temperature (Garfinkel et al. 2020). Another consideration is the QBO itself. The QBO is not zonally symmetric. The temperature fluctuations associated with the QBO and its MMC vary over longitude. The amplitude of temperature fluctuations is largest over convective areas, notably the Maritime Continent (Tegtmeier et al. 2020). A speculation of mine is that the QBO-MMC, whose latitudinal extent may be sensitive to the intrinsic qualities of the QBO (Haynes 1998), is zonally asymmetric, extending farther into the North Pacific compared to other longitudes.

The SC-WACCM4 results suggest that the QBO shifts the polar vortex toward North America during QBOW and toward Eurasia during QBOE. This is consistent with Zhang et al. (2019) who find this result in WACCM as well as reanalysis. A shift of the polar vortex toward Eurasia is consistent with an upward stationary wave activity flux in the North Atlantic. Conversely, a shift of the polar vortex toward North America is associated with downward wave propagation in the North Atlantic. In this regard, lower stratospheric wave activity flux anomalies in the North

Atlantic do not drive the polar vortex response, although they play a role in amplifying the response.

(2) What is the impact of the QBO on the extratropical atmosphere versus that from polar stratospheric variability?

The CPS experiment reveals that there is a competing effect between the midlatitude jet response to QBOE (poleward shift) and the response of the polar stratosphere to QBOE (equatorward shift). If this result is reproduced by subsequent studies, this teleconnection is a new example of stratosphere-troposphere coupling. This competition is most pronounced over the North Pacific for reasons I am not sure of. This has implications for seasonal forecasting because it implies that the influence of the QBO on the troposphere may vary from one year to another depending on the state of the polar stratosphere and how it evolves in response to the QBO. This result also has implications for model evaluations of the QBO because if models exhibit different sensitivity of the polar stratosphere to the QBO, these differences will likely be reflected in the model tropospheric response to the QBO. Recently, Richter et al. (2020) has shown that many CMIP6 models, which spontaneously generate the QBO, underestimate the QBO's amplitude in the lower stratosphere. This coupled with the variation in how the models represent the Holton-Tan effect (Rao et al. 2020a) implies that there will be spread in the modeled tropospheric responses to the QBO. This is assessed in the next chapter.

3.5. Limitations of this study

A limitation of this study is that it only focuses on the lower stratosphere. The wave absorption occurring over the lower stratospheric North Pacific and North Atlantic during QBOE should coincide with poleward residual circulations whose descending branches adiabatically warm the

polar stratosphere. In this way, part of the Holton-Tan effect is mediated through the lower stratosphere.

However, the dominant branch of the Holton-Tan effect is the middle stratospheric branch. At 10 hPa, around 30 kilometers altitude, the wave absorption and subsequent adiabatic warming of the polar stratosphere in response to QBOE is far larger than in the lower stratosphere (Garfinkel et al. 2012; Lu et al. 2014; White et al. 2015; Rao et al. 2020a; Lu et al. 2020). It is not clear how the upper stratospheric branch of the Holton-Tan effect varies over longitude.

Acknowledgements: Thank you Gudrun and Yannick for being patient with me during this entire project. It took two years and was difficult. Our collective efforts here produced some interesting results. The research group and I are very grateful to the folks who developed and maintain the AGCM we use here. Two anonymous reviewers improved the quality of this project tremendously. This research was supported by DOE Grant DE-SC0019407, NSF Grant AGS-1624038, and a NSF GRF under Grant DGE-1839285. We also very much appreciate high-performance computing support from Cheyenne provided by NCAR's CISL, sponsored by the NSF.

Chapter 4

Underestimation of the Holton-Tan effect by the CMIP6 models

4.1 Introduction

The Quasi-Biennial Oscillation (QBO) influences the global circulation through a suite of teleconnections (Gray et al. 2018). It modulates tropical convection (Son et al. 2017), upper tropospheric mid-latitude flow (Wang et al. 2018; Hitchman et al. 2021), and polar stratospheric flow in the southern (Yamashita et al. 2018) and northern hemispheres (Holton and Tan 1980; Lu et al. 2020). Each teleconnection is sensitive to the QBO's structure, its meridional extent (Hansen et al. 2013), the configuration of its easterly and westerly jets (Garfinkel et al. 2012; Gray et al. 2018), its vertical extent (Andrews et al. 2019), and how deep it reaches into the lower stratosphere (Collimore et al. 2003). Now with the Coupled Model Intercomparison Project 6 (CMIP6) models spontaneously generating the QBO, there is variability in how the models represent its structure (Richter et al. 2020). This suggests that there is variability in how the models represent the QBO teleconnections (Rao et al. 2020a,b). This study focuses on one of these teleconnections, the boreal winter polar stratospheric response to the QBO, the Holton-Tan effect (HTE, Holton and Tan 1980). There are two goals: (1) to better understand why the CMIP6 models underestimate the HTE (Fig. 1) while (2) also learning how the middle stratospheric, 850 Kelvin, branch of the teleconnection varies over longitude.

When QBO westerlies are in the middle stratosphere (10 hPa) and QBO easterlies in the lower stratosphere (50 hPa), the polar vortex is weaker than in climatology. This configuration of the QBO, denoted QBO_{E50}, influences where planetary wave breaking occurs in the stratosphere

(Hitchman and Husesmann 2009; Lu et al. 2020). QBO easterlies concentrate planetary waves and their breaking into the northern hemisphere (Holton and Tan 1980; Lu et al. 2020). This teleconnection is also simulated by models, including the 1500-year dataset used in the previous chapter.

The QBO induced mean meridional circulation (QBO-MMC) is also important for the Holton-Tan effect, especially the middle stratospheric (850 Kelvin, 10 hPa, 30 kilometers) branch of the Holton-Tan effect. The QBO-MMC acts as a residual mean meridional circulation that maintains the dynamically forced temperature response to the QBO against radiative relaxation (Plumb and Bell 1982; Pahlavan et al. 2021; Hitchman et al. 2021). Westerly (easterly) QBO shear coincides with tropical warming (cooling), which is generated by adiabatic descent (ascent). At subtropical to mid-latitudes, the QBO-MMC induces vertical motion in the opposite direction of that in the tropics, yielding opposite temperature responses (Fig. 1q). The QBO-MMC changes the mid-latitude middle stratospheric mean flow geometry, forcing more poleward refraction of planetary waves (Garfinkel et al. 2012; Lu et al. 2014), which would otherwise propagate equatorward. This weakens the polar vortex.

It is not clear how this process varies over longitude. I hypothesize that it does because the QBO demonstrates zonally asymmetric teleconnections elsewhere. It has unique impacts on the North Pacific and North Atlantic jets (Wang et al. 2018). Further, the previous chapter shows that the QBO preferentially communicates with the mid-latitude North Pacific lower stratosphere by inducing more planetary wave absorption there relative to other longitudes. However, the previous chapter does not address how and if the Holton-Tan effect may be zonally asymmetric in the middle stratosphere.

4.2 Methods

The HTE is analyzed over the 1850-2014 period using the same historical CMIP6 models as used by Richter et al. (2020) to facilitate comparison between the extratropical responses (this study) and the QBO qualities in each model (their study). The CMIP6 responses to the QBO are compared to 1979-2019 ERA5 reanalysis (Hersbach et al. 2020).

Four experiments with the specified chemistry version of the Whole Atmosphere Community Climate Model (SC-WACCM4, Smith et al. 2014) use a prescribed QBO and are therefore useful for comparing with the CMIP6 models.

The model domain is the surface up to 145 kilometers over 66 vertical levels with horizontal resolution of 1.9° latitude, 2.5° longitude. To simulate the QBO, the tropical stratospheric winds from 86 hPa-4 hPa and 22°S-22°N are relaxed toward a climatological 28-month QBO cycle derived from radiosondes (Hansen et al. 2013). These are the same experiments used in the previous chapter. They are described briefly here.

The first of the experiments, referred to as PAMIP-WCSC, is a 1500-year experiment with a repeating annual cycle of sea surface temperature (SST) corresponding to present-day climate and a suite of different Arctic sea ice forcings (potential influence of Arctic sea ice conditions on the QBO teleconnections). The second experiment, CPS-WCSC, is a 300-year experiment forced in the same way as PAMIP-WCSC except the polar stratospheric variability poleward of 60°N is relaxed toward a climatological polar stratospheric state allowing us to diagnose the influence of the QBO on the atmosphere in the absence of a polar stratospheric response to the QBO. The third experiment allows us to diagnose the transient atmospheric response to

imposing the QBO. A 100-year control experiment devoid of the prescribed QBO is run and restarts are saved for each November 1st. We branch from November 1st and then impose the QBO_{E50} profile. The QBO propagates downward and the runs last until January 31st. An additional SC-WACCM4 experiment set is used in this chapter. The fourth experiment, AMIP-WCSC, is a 370-year dataset made up of 10 ensemble members, run from 1978 to 2016, forced by the observed chronology of SST and sea ice variability.

Throughout the chapter, anomalies are calculated as deviations from the seasonal cycle. These anomalies are then subsampled by QBO phase. The QBO_{E50} index can be defined using westerlies at 10 hPa or easterlies at 50 hPa. Both yield similar results. However, the latter captures non-QBO variability for some models. Therefore, the QBO_{E50} index is defined as the December-January (DJ) time averaged, longitudinally averaged, and latitudinally averaged winds between 5°S and 5°N at 10 hPa that exceed 2.5 m/s. Further, similar results are obtained using the phase angle 30 hPa QBO index of Huang et al. (2012). This index allows for more control in picking the vertical structure of the QBO we are interested in, e.g., easterlies at 50 hPa. Results are consistent for all three QBO indices. Here I will show results using the QBO_{E50} index.

4.3 Results

4.3.1 Zonal mean zonal wind

Figure 4.1 shows zonal mean zonal wind anomalies for all 18 datasets. The models both overestimate (4.1b, g, j, o, p) and underestimate (all others) the peak 10 hPa QBO westerlies relative to ERA5 (shown by Richter et al. 2020). The QBO westerlies extend upward and poleward between 20°N-40°N in ERA5, but they are confined equatorward in CMIP6 models. Each CMIP6 QBO is narrow relative to ERA5 (10 hPa QBO widths printed above plots).

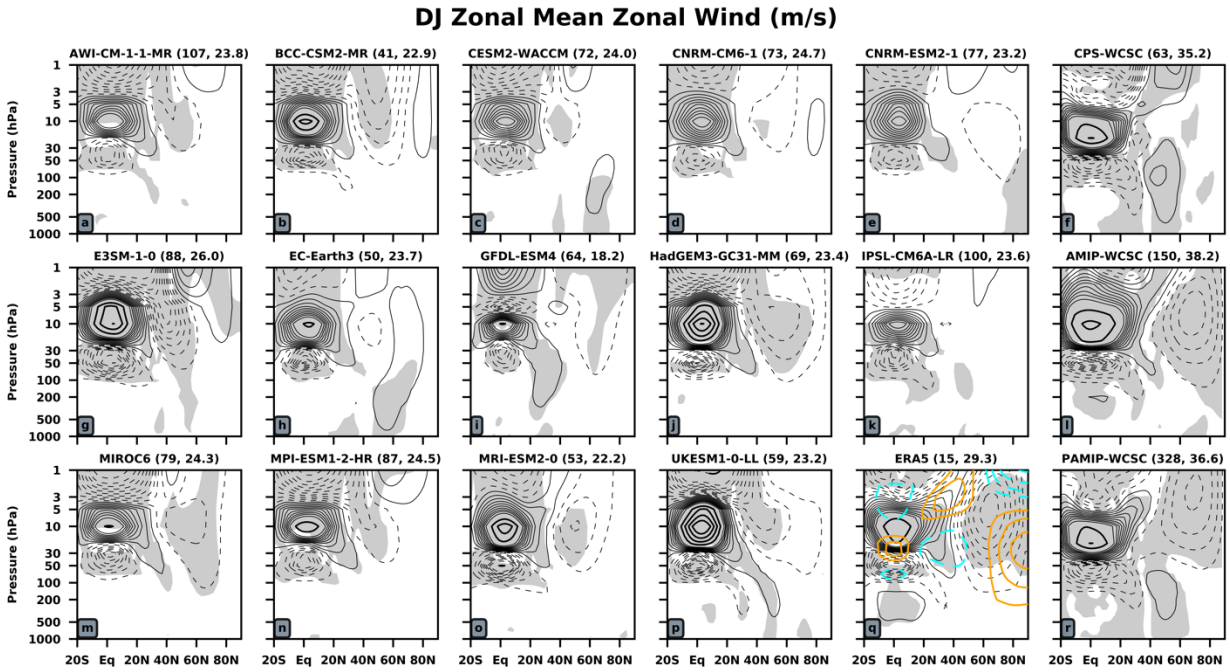

Figure 4.1: DJ zonal mean zonal wind anomalies. Thin contours show anomalies between +/- 8.5 m/s with intervals of +/- 1m/s. Thick contours correspond to +10, 15, 20 … m/s. Gray shading denotes statistical significance, p-values < 0.05 via a student's t-test, when comparing QBO_{E50} anomalies to all other anomalies. To the right of model titles is the number of DJ periods averaged together to make each composite and the 10 hPa latitudinal width of the QBO. Widths are calculated by applying the "half-maximum" method of Richter et al. (2020) and Bushell et al. (2020) to the anomalous 10 hPa response from each plot. Warm (cool) temperature anomalies are shown on Fig. 4.1q with +/- 1 K contours.

The 50 hPa peak QBO easterlies match ERA5 in four cases (4.1g, j, o, p) and are underestimated otherwise. Each unique QBO coincides with unique tropical stratospheric temperature perturbations (not shown), which the QBO-MMC must maintain against radiative relaxation. Therefore, the QBO-MMC differs in each model. Prescribing the QBO ensures that it has sufficient lower stratospheric amplitude. The QBO, in the absence of a HTE, pushes the tropospheric jet poleward (CPS-WCSC, Fig. 4.1f). This is moderated by an equatorward jet shift in AMIP-WCSC and PAMIP-WCSC (Fig. 4.1l,r) due to a warm polar stratosphere caused by the HTE (Chapter 4). These experiments with prescribed QBOs show that when a realistic QBO exists in the model, teleconnections more closely resemble observations, notably the HTE.

When the Holton-Tan effect is not simulated by a model, this cuts off a stratosphere-troposphere coupling pathway.

While some models simulate a weakening of the polar stratospheric winds (BCC-CSM2-MR, HadGEM3-GC31-MM, MIROC6, UKESM1-0-LL), each model underestimates the HTE relative to ERA5 (Fig. 4.1q) and the prescribed QBO runs (Fig 4.1l, r). AWI-CM-1-1-MR, E3SM-1-0, MPI-ESM1-2-HR, and MRI-ESM2-0 each have extratropical easterly anomalies, but they are not at polar latitudes. Underestimation of the HTE occurs with all three QBO indices. This should hinder stratospheric interaction with the tropospheric jet.

4.3.2 Zonally asymmetric middle stratospheric teleconnection

Before assessing the representation of the middle stratospheric HTE, the middle stratospheric position of the teleconnection needs to be shown in a zonally asymmetric sense. Figure 4.2 shows potential vorticity (PV) on the 850 Kelvin isentropic surface (approximately 10hPa) associated with QBO_{E50} in ERA5. The standard deviation of the field shows that PV varies between 20 and 50 PVU from 30°N to 30°S with larger variability in the North Atlantic mid-latitudes than in the North Pacific (Fig. 4.2b). The largest variations occur at polar latitudes, especially over the North Pacific.

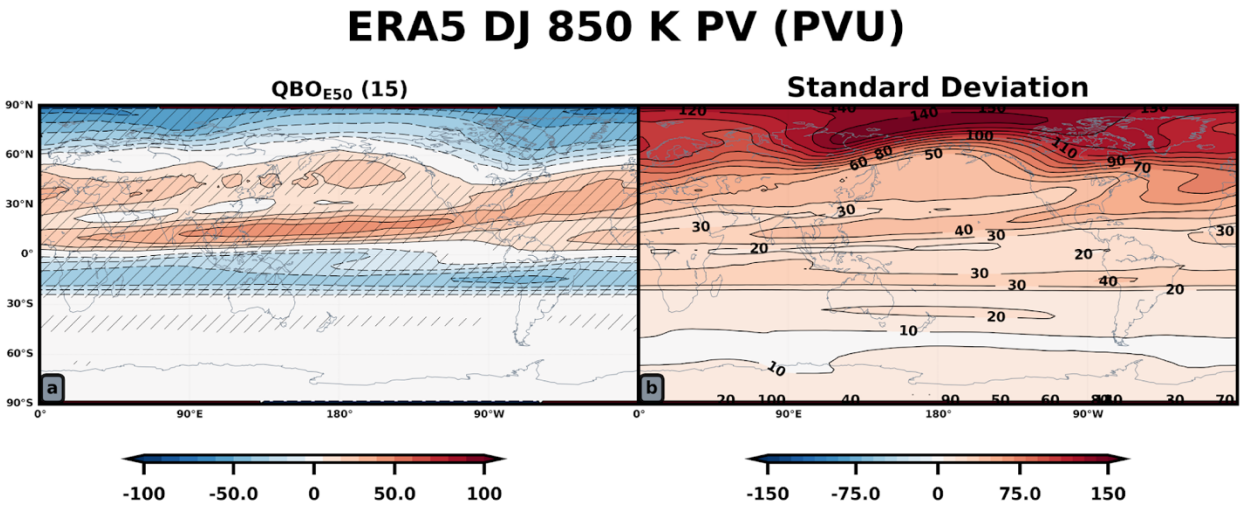

Figure 4.2: ERA5 DJ 850 Kelvin PV anomalies. Anomalies are deviations from the seasonal cycle for QBO_{E50} indices. Hatching denotes statistical significance, p-values < 0.05 via a student' t-test, when comparing QBO_{E50} anomalies to all other anomalies. The contour interval in line and shading for all panels is +/- 10 PVU. Fifteen DJ seasons are used to make the composite (a). Panel (b) shows the standard deviation of the field with contour intervals 10, 20, 30… PVU.

Relative to the standard deviation, the QBO_{E50} dominates the tropical and subtropical 850 K PV variability (Fig. 4.2a). At polar latitudes, the polar vortex is most disturbed over the North Atlantic where low PV anomalies peak at -60 PVU, about 50% of the |standard deviation| there. Fig. 4.2a mirrors the DJ 850 K first empirical orthogonal function, which accounts for 36% of the variance (Fig. 4.3a).

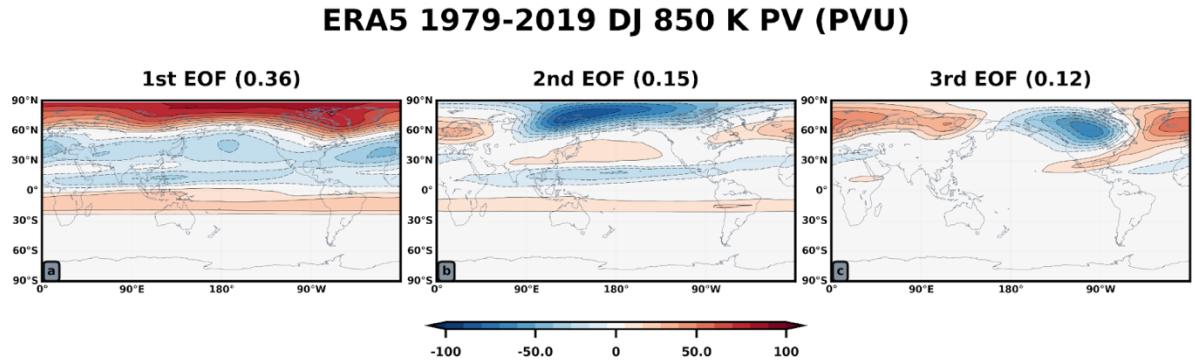

Figure 4.3: The first three empirical orthogonal functions of the ERA5 850 Kelvin potential vorticity are shown. The variance accounted for by each principal component is printed in the title of each frame.

Two bands of anomalous PV span the tropics, negative in the southern hemisphere, positive in the northern hemisphere (Fig. 4.2a). I think this is the signature of the QBO-MMC. Shown by Hitchman and Huesmann (2009), the QBO-MMC converges toward the base of the QBO westerlies, “pinching” together the PV contours: high PV from the northern hemisphere and low PV from the southern hemisphere are concentrated nearer the tropics. The negative PV anomaly in the southern hemisphere shows some zonal asymmetry while the northern hemisphere positive PV band shows strong variation over longitude.

Since internal variability may convolute these PV results, I look for these signatures in dedicated perturbation experiments. Figure 4.4 shows the evolution of the PV field once a downward propagating QBO_{E50} profile is imposed in the control experiment devoid of a QBO. Anomalies are calculated as the difference between the transient runs and control runs from which the transient experiments are branched.

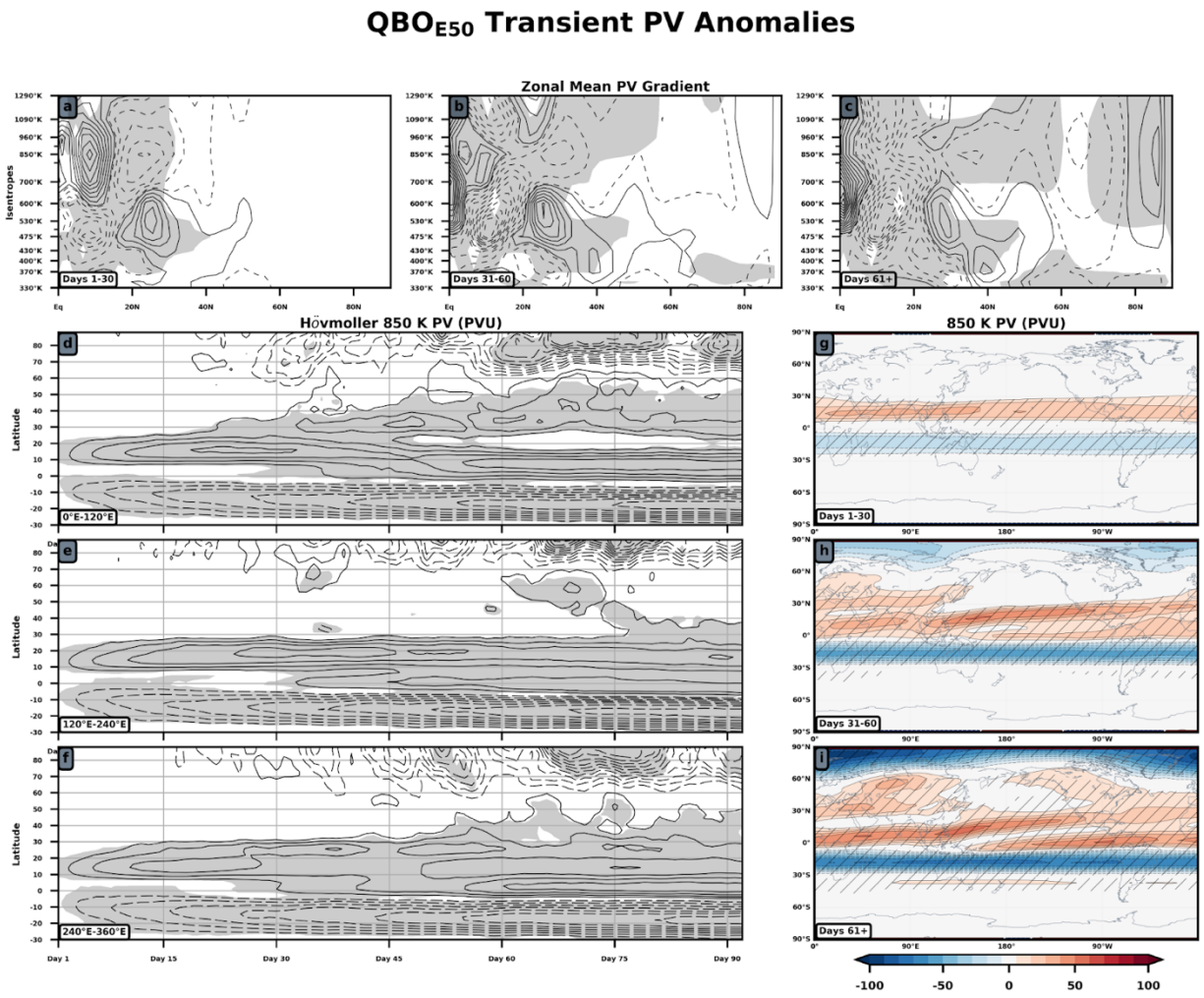

Figure 4.4: Anomalies after imposing a QBO_{E50} profile in the transient runs. (a-c): Zonal mean meridional PV gradient for successive 30-day periods after branching: dashed-negative (solid-positive) contours begin at negative (positive) $1x10^{-7}$ $K{\cdot}m{\cdot}kg^{-1}{\cdot}s^{-1}$ and decrease (increase) by negative (positive) $5x10^{-7}$ $K{\cdot}m{\cdot}kg^{-1}{\cdot}s^{-1}$ intervals. The responses at each isentrope are multiplied by $(\theta/350)^{-9/2}$ to account for logarithmic change in PV with height. (d-f): Latitude-time Hövmollers of 850 Kelvin PV (+/- 10 PVU) averaged over 0°E-120°E (d), 120°E-240°E (e), and (f) 240°E-360°E. Gray shading denotes statistical significance in (a-f), p-values < 0.05 via a student's t-test, when comparing QBO_{E50} and control responses. (g-h) Maps of 850 K PV (+/- 10 PVU) anomalies with hatching denoting statistical significance.

Figs. 4.4a-c shows change in the meridional gradient of the zonal mean PV, P_ϕ, once the QBO_{E50} is imposed. Negative anomalies mean that the PV gradient is decreased and linear wave propagation into the region is less likely while the opposite holds true for regions with positive anomalies. During days 1-30, QBOW is located around 850 K and QBOE around 530 K. Planetary waves may propagate through the 850 K westerlies, but not the 530 K easterlies

(Fig. 4.4a). P_ϕ weakens in the middle stratosphere between 30°N-50°N during days 31-60 indicating reduced likelihood for equatorward propagation (Fig. 4.4b). Beyond day 61, the polar stratospheric gradient weakens and this signal propagates downward (Fig. 4.4c). How does the spatiotemporal evolution of PV look on a horizontal surface, if we do not take a zonal average?

During the first 30 days at 850 K, the QBO-MMC spins up (Figs. 4.4g). The two anomalous PV bands indicate equatorward motion of the QBO-MMC from both hemispheres and the signal is almost zonally symmetric with more pooling of high PV near Asia (Fig. 4.4g). During the next 30 days, the positive PV anomalies become more zonally asymmetric, tilting out of the tropics toward the east (Fig. 4.4h). The evolution of the anomalous negative PV gradient poleward seen in the zonal mean occurs over Eurasia between 30°N and 50°N (Fig. 4.4h). Pooling of high PV over these continents is consistent with dilution of high PV over the pole during the last 32 days of the experiments (Fig. 4.4i).

Latitude-time Hövmollers more clearly show the importance of the Eurasia sector for coupling the QBO with the polar vortex (Figs. 4.4d-f). Equatorward (poleward) intrusion of high (low) PV occurs between 0°E-120°E during days 30-45 (Fig. 4.4d). Importantly, this change in PV over these longitudes (Fig. 4.4d) leads the other sectors (Fig. 4.4e-f). Fig. 4.4 shows that the HTE begins in the middle stratosphere (Fig. 4.4a-c), particularly over Eurasia (Fig. 4.4d,h).

While the PV intrusion is broadly located over Africa, Europe, and Asia, subsequent results will show that the PV response over mid-latitude Asia is most important for the HTE. Therefore, this regional PV response is hereafter referred to as the “PV intrusion” or “Asia P_ϕ.”

4.3.3 Middle stratosphere in the CMIP6 models

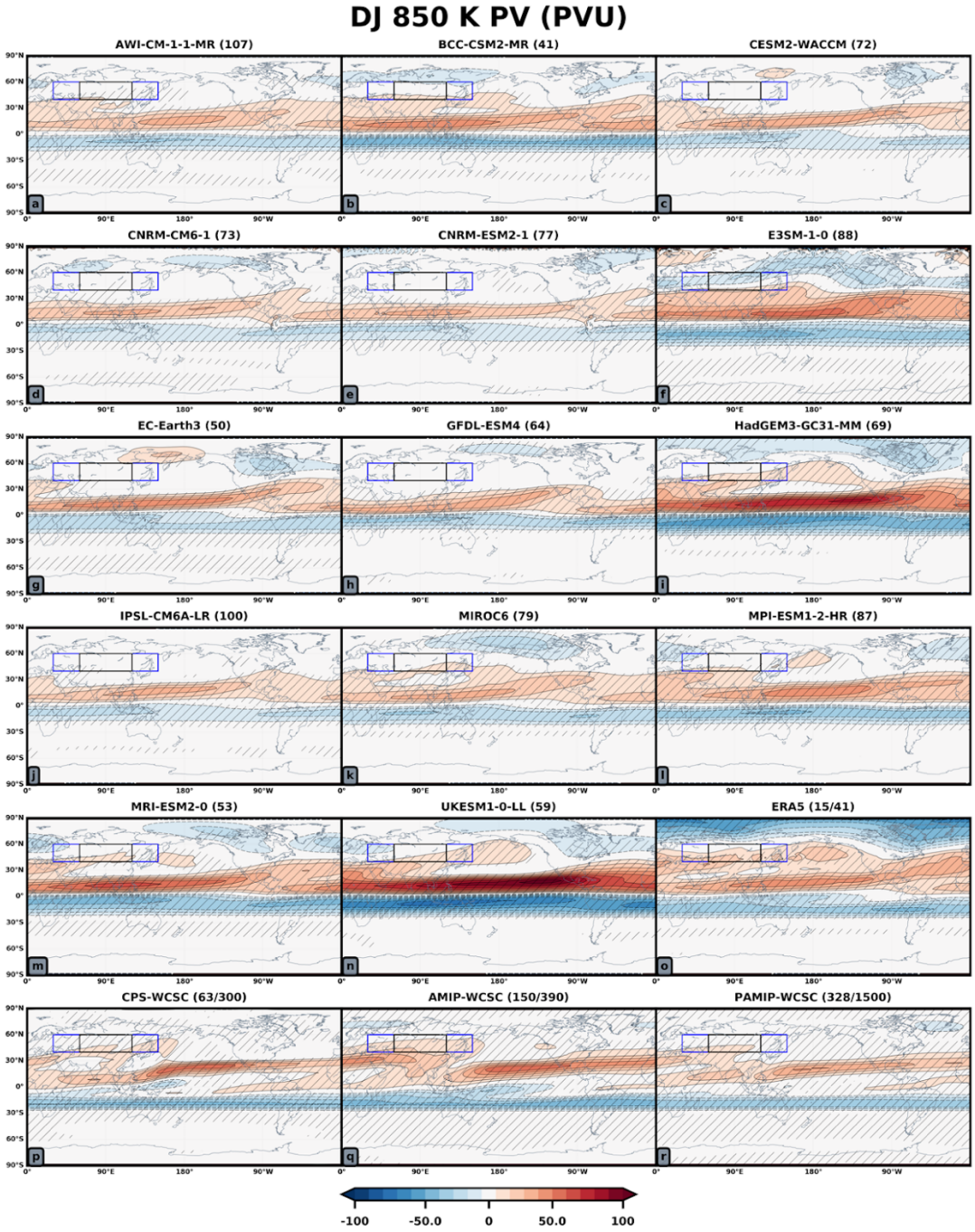

Figure 4.5: DJ 850 K PV anomalies for the 18 datasets. Contour intervals are +/- 10 m/s. Hatching denotes statistical significance, p-values < 0.05 via a student's t-test, when comparing QBO_{E50} anomalies to all other anomalies. Black and blue rectangles denote where the anomalous $_{P}$ is highly correlated with polar cap warming (Table 4.1).

Figure 4.5 shows 850 K PV anomalies for each model. From Fig. 4.1, the models that exhibit extratropical easterlies at polar latitudes (BCC-CSM2-MR, HadGEM3-GC31-MM, MIROC6, UKESM1-0-LL) or mid-latitudes (AWI-CM-1-1-MR, E3SM-1-0, MPI-ESM1-2-HR, MRI-ESM2-0) exhibit intrusion of high PV over mid-latitude Asia. Models with weaker HTEs (CESM2-WACCM, CNRM-CM6-1, CNRM-ESM2-1, EC-Earth3, GFDL-ESM4, IPSL-CM6A-LR) exhibit no pooling of PV over Asia. The CMIP6 PV intrusions are equatorward of the intrusions in ERA5 or SC-WACCM4, suggesting why the CMIP6 extratropical easterly anomalies are ubiquitously equatorward of the polar stratosphere in Fig. 4.1. Note that every dataset's QBO is zonally asymmetric with stronger flow around Indonesia or the Indian Ocean, which may explain the location of the PV intrusion (Fig. 4.6).

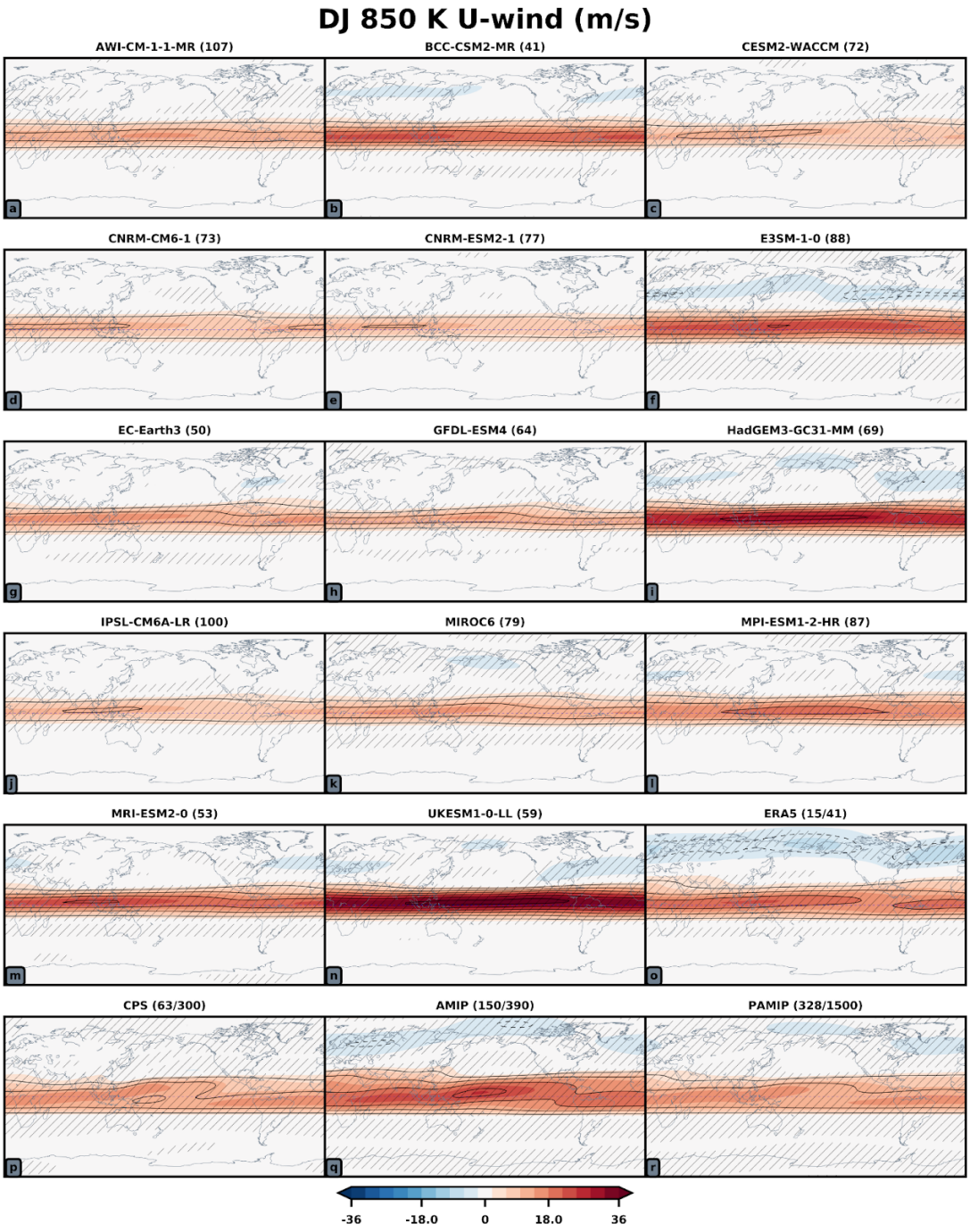

Figure 4.6: December and January time averaged 850 K zonal wind anomalies (m/s) for each of the 18 datasets. Lined contour intervals are +/- 6 m/s excluding the 0 m/s contour. Shaded contours are +/- 3.6 m/s. Hatching denotes statistical significance, p-values < 0.05 via a student's t-test, when comparing QBO_{E50} anomalies to all other anomalies. The QBO_{W10} index is defined as the temporally, zonally, and cosine weighted meridionally averaged 5°S-5°N 10 hPa DJ zonal wind exceeding (less than) 2.5 m/s. The number of DJ periods used to create each composite is printed next to each model title.

Enhanced PV over Asia indicates anomalous cyclonic flow there. Stronger westerlies on its equatorward flank should strengthen P_ϕ and reduce wave breaking. Stronger easterlies on its poleward flank should weaken P_ϕ and reduce wave propagation. Indeed, studies using reanalysis (Fig. 3b of Lu et al. 2014) and model experiments (Garfinkel et al. 2012) show that QBO_{E50} suppresses climatological equatorward planetary wave propagation at 850 K between 30°N and 50°N in favor of anomalous poleward propagation. These PV results corroborate those studies. However, a new finding is that this process occurs over Asia.

Longitude (all 40N to 60N)	Correlation (Temp 10)
0E:60E	**-0.54**
30E:90E	**-0.73**
60E:120E	**-0.82**
90E:150E	**-0.71**
120E:180E	**-0.52**
150E:210E	-0.40
180E:240E	-0.46
210E:270E	-0.44
240E:300E	-0.46
270E:330E	-0.54
300E:360E	-0.53
330E:30E	-0.50

Table 4.1: Pearson correlation coefficients between the 10 hPa polar cap (cosine weighted latitudinal average poleward of 60°N) temperature anomalies of each model and the corresponding anomalous longitudinally averaged meridional potential vorticity (PV) gradient between 40°N and 60°N. Each row of Table 1 corresponds to a different 60° longitudinal domain.Bolded correlations correspond to p-values < 0.05 when comparing QBO_{E50} anomalies to all other anomalies. Calculations are for all CMIP6 models and ERA5 reanalysis.

Fig. 4.7 suggests that the PV intrusion is associated with the HTE. It establishes the relation between the anomalous polar cap temperatures at 10 hPa and P_ϕ averaged between 40°N and

60°N over various 60° longitude windows (Table 4.1). Various 60° longitude windows are used to see over what longitudes P_ϕ is most strongly associated with the polar cap temperature anomalies. Correlations exceed 0.7 from 30°E-150°E and peak at 0.82 from 60°E-120°E (Table 4.1). This is where the PV intrusion is located (enclosed by rectangles in Fig. 4.5). Fig. 4.7a depicts the relationship between Asia P_ϕ and polar cap temperatures. The more negative Asia P_ϕ is, the warmer the polar cap is (Fig. 4.7a).

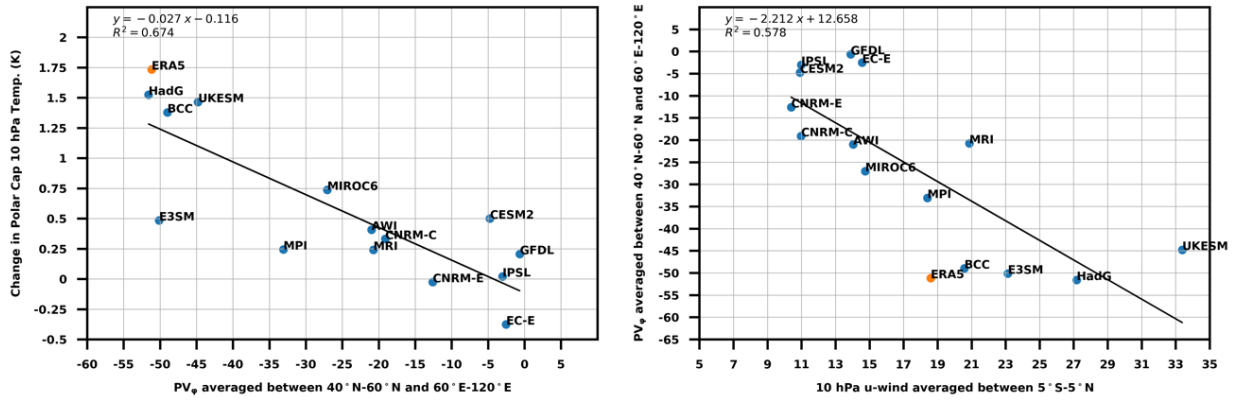

Figure 4.7: Left: The anomalous meridional PV gradient over Asia is compared to the anomalous 10 hPa polar cap (60°N+) temperature. P_ϕ is not divided by the radius of Earth when calculating it. Right: The anomalous 10 hPa QBO, longitudinally averaged and cosine weighted latitudinally averaged zonal winds between 5°S-5°N, of Figure 1 are compared to $_P$ over Asia.

Asia P_ϕ is a direct response to the QBO – it does not result from the HTE. Indeed, the PV intrusion exists in the CPS 850 K response, which reveals the impact of the QBO in the absence of a polar stratospheric response (Fig. 4.5r). Furthermore, imposing the QBO in the transient experiments promoted the PV intrusion (Fig. 4.4). Regression between the 10 hPa QBO westerly velocity and Asia P_ϕ shows that stronger QBO winds equate to more negative Asia P_ϕ (Fig. 4.7b). Citing the strong relationship between Asia P_ϕ and polar cap temperatures, underestimation of the 10 hPa QBO amplitudes is *partly* suppressing the HTE.

4.4 Discussion

4.4.1 Importance of the QBO-MMC

Stronger QBOs have larger effects on the extratropical circulation. Of the 14 CMIP6 models, the eight with strongest 10 hPa QBO westerlies are BCC-CSM2-MR, HadGEM3-GC31-MM, MIROC6, UKESM1-0-LL, AWI-CM-1-1-MR, E3SM-1-0, MPI-ESM1-2-HR, and MRI-ESM2-0 (Fig. 4.7b, compare with Fig. 2b of Richter et al. 2020). The first four models feature some weakening of the polar vortex while the latter four exhibit anomalous easterlies equatorward of the polar vortex. The models with the weakest 10 hPa QBO westerlies exhibit much weaker easterlies everywhere in the stratosphere (Fig. 4.1c, d, e, h, i, k).

Figs. 4.5 and 4.7b show that models with stronger 10 hPa QBO amplitudes feature stronger PV intrusions over Asia. Garfinkel and Hartmann (2011, Fig. 6) show that stronger QBOs have stronger QBO-MMCs, which have larger effects on the extratropical circulation. A speculation then is that the PV intrusion is the extratropical signature of the QBO-MMC. By underestimating this feature, which confines planetary waves to higher latitudes (Lu et al. 2014), the models underestimate the HTE.

4.4.2 Limitations of this argument

Underestimating the 10 hPa QBO amplitudes is not the only factor hindering the HTEs. For instance, HadGEM3-GC31-MM and UKESM1-0-LL both overestimate the 10 hPa QBO winds and still underestimate the weakening of the polar vortex relative to ERA5 (Fig. 4.1j,p).

Figure 4.1 shows that the QBOs are too narrow. Latitudinal extents of the Fig. 4.1 QBO responses are calculated at 10 hPa using the "half-maximum" method of Richter et al. (2020) and Bushell et al. (2020); see the model titles in Fig. 4.1. Regression between these extents and Asia P_ϕ shows little correlation (Fig. 4.8). Regardless, Hansen et al. (2013) have already shown that narrow QBOs coincide with a reduced HTE.

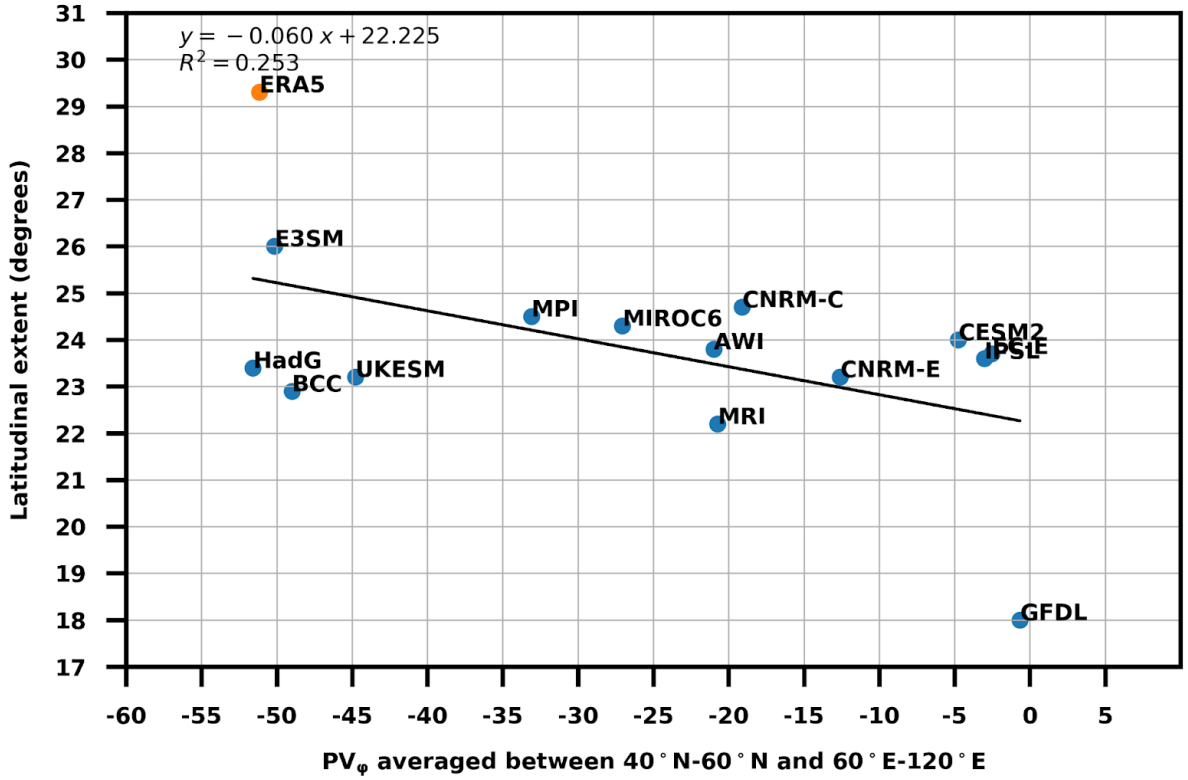

Figure 4.8: The anomalous zonally averaged meridional potential vorticity (PV) gradient between 40°N and 60°N and 60°E and 120°E is compared to the 10 hPa latitudinal width of the anomalous zonal wind anomalies in of Figure 1 in the chapter. All averaging over time is during December and January (DJ). The latitudinal width is calculated using similar methods to Richter et al. (2020) and Bushell et al. (2020). The peak value of the QBO westerlies between 5°S-5°N is identified. This is the maximum. Half of the maximum defines the northern and southern hemisphere bounds of the QBO. To cleanly identify the latitudinal width to a tenth of a degree latitude, the 10 hPa transect is linearly interpolated from 96 latitude points per dataset to 1800. Transient reversals of the QBO phase that last for 1~4 months are removed from the 10 hPa zonal wind timeseries as is done in the previously mentioned papers.

4.5 Conclusions

The HTE is analyzed in the CMIP6 historical experiments studied by Richter et al. 2020. The CMIP6 models consistently underestimate the amplitude of the HTE during December and January relative to ERA5. This conclusion is robust to three different QBO indices.

The underestimation of the HTE coincides with underestimation of the 10 hPa QBO amplitudes. The desired impact that the models are not representing is the intrusion of high PV anomalies over Asia. This signal is highly anticorrelated with polar stratospheric warming taking place during QBO_{E50}. The transient experiments in which the QBO is imposed in a live running atmosphere devoid of a QBO, and CPS, which includes no polar stratospheric variability, both suggest that the QBO promotes the intrusion of high PV air over Asia *by itself*. Further, the presence of this signal in the CMIP6 models that simulate HTE, the 1500-year SC-WACCM4 experiment set, and ERA5 suggest this is an important feature for the teleconnection in nature.

Why does the PV intrusion occur over Asia? The QBO has a stronger amplitude over that sector, but other factors may play a role too. For instance, orographic gravity wave drag over the Tibetan Plateau has a nonnegligible influence on the stratospheric mean flow (Xu et al. 2017). This will have to be investigated in future work.

As noted by Richter et al. (2020), the CMIP6 QBOs have weak amplitudes in the lower stratosphere. Further, Fig. 4.1 shows that all of the models underestimate the Holton-Tan effect. A consequence of this is that the models generally do not simulate any tropospheric response to the QBO (Fig. 4.1). Therefore, stratosphere-troposphere coupling is underestimated by the CMIP6 models.

High performance computing support is generously provided by the National Center for Atmospheric Research, sponsored by the National Science Foundation (NSF). doi:10.5065/D6RX99HX. CMIP6 data is archived very nicely and provided by the Earth System Grid Federation (https://esgf-node.llnl.gov/search/cmip6/). Thank you to various modeling agencies who have run the experiments, processed the data, and made it publicly available. ERA5 reanalysis may be accessed with Copernicus

(https://cds.climate.copernicus.eu/cdsapp#!/dataset/10.24381/cds.bd0915c6?tab=overview). doi:10.24381/cds.bd0915c6. This study is supported by the NSF, Division of Atmospheric Geospace Sciences, AGS-1624038; Division of Graduate Education, DGE-1839285, and the Department of Energy, Office of Biological Environment Research, DE-SC0019407.

Chapter 5

5.1 Summary of the research

Stratosphere-troposphere coupling is affected by low-frequency internal climate variability. The purpose of this dissertation has been to (1) assess what teleconnections are forced by the IPV, AMV, and the QBO and to assess (2) how these teleconnections enhance or suppress stratosphere-troposphere coupling.

In Chapter 2, IPV and AMV are both found to force Rossby wavetrains over the mid-latitudes during wintertime. Positive IPV coincides with a positive PNA wavetrain that propagates out of the Pacific subtropics, into the North Pacific, before curving east and south across North America. En route, this wavetrain reinforces part of the climatological wave-2 structure over the North Pacific, the Aleutian Low. This constructive interference between a forced wave and the climatological wave structure enhances the upward propagating planetary scale wave activity flux entering the stratosphere. All of this reverses during negative IPV, when increases in height over the North Pacific weaken the Aleutian Low.

Generally, the wintertime atmospheric response to the IPV is larger than the response to AMV regardless of how IPV and AMV are combined. However, positive AMV promotes ridging over the North Pacific via an interbasin teleconnection through the Walker Circulation. This dampens the tropics-extratropics Rossby wavetrain propagating into the North Pacific. As a result, when positive IPV and positive AMV are combined, the deepening of the Aleutian Low is weaker than if positive IPV alone is allowed to deepen the Aleutian Low. Therefore, less upward wave activity flux enters the stratosphere from the North Pacific when positive IPV and positive AMV

are considered together, but positive AMV partly compensates for this by enhancing upward WAF over Eurasia. Combining the positive AMV with the IPV does not really change the strength of the polar stratospheric warming that follows from enhanced planetary wave absorption in the stratosphere. Rather, the positive AMV diminishes the downward propagating Northern Annular Mode (NAM) response. During late winter with positive IPV, the NAM response propagates downward from the stratosphere to the troposphere, coinciding with an increase in frequency of the cold extreme days over Eurasia. When the positive AMV is considered together with the positive IPV, this downward coupling via the NAM is reduced, and the change in the frequency of cold extremes over Eurasia vanishes.

In Chapter 3, the atmospheric response to the QBO is considered. The QBO has an established teleconnection with the North Atlantic (Andrews et al. 2019; Anstey et al., 2021). There is also evidence from reanalysis data (Wang et al. 2018) that the QBO has a teleconnection with the North Pacific upper troposphere. In the model experiments used, when polar stratospheric variability is suppressed, the “direct effect” of QBOE is to push the North Pacific jet-stream poleward. However, when polar stratospheric variability is considered, this response vanishes because the polar stratospheric warming that occurs during QBOE pushes the North Pacific jet-stream equatorward. This is a new teleconnection, which needs more vetting. There is also consistent evidence that the QBO is coupled with the North Pacific lower stratosphere more than other longitudes. Wave absorption begins over the North Pacific as soon as QBOE is imposed in a free running atmosphere previously devoid of a QBO. This wave absorption precedes the polar stratospheric response to QBOE. Once the polar stratosphere responds to the QBO, its variability is important because movement of the polar vortex coincides with different planetary wave responses. During QBOE, the polar vortex shifts toward Eurasia and there is enhanced upward wave activity flux over the North Atlantic. During QBOW, the polar vortex shifts towards North America and there is downward wave coupling over the North

Atlantic. Kretschmer et al. (2018) also found a preference for downward wave coupling during QBOW. However, Matthias and Kretschmer (2020) show that the frequency of downward wave coupling is about once per winter, implying that downward wave coupling is independent of QBO phase. While the QBO may be associated with downward wave coupling (Lubis et al. 2016), its role is still unclear.

Chapter 4 builds on Chapter 3 by looking for zonal asymmetry in the *middle* stratosphere (10 hPa) as opposed to the lower stratosphere (50 hPa). This time, 14 CMIP6 models are used in addition to a few sensitivity experiments with prescribed QBOs. Each CMIP6 model has a unique QBO. Therefore, the associated teleconnections are unique. The QBO flattens the meridional potential vorticity (PV) gradient over Asia at 10 hPa. Models that simulate this behavior include the Holton-Tan effect while those that do not, miss the Holton-Tan effect. The anomalous PV gradient over Asia is highly correlated with polar cap warming during QBOE. The models that include the change in the PV gradient over Asia generally have stronger QBOs. Many CMIP6 models exhibit no tropospheric response to the QBO. This is partially related to the models not simulating the Holton-Tan effect, but likely results from the CMIP6 QBOs having weak tropical lower stratospheric amplitudes (Richter et al. 2020).

5.2 Ongoing research

5.2.1 The poleward shift of the North Pacific jet during QBOE

Studies using reanalysis have shown a poleward shift of the North Pacific jet-stream in response to QBOE during Fall (Inoue et al. 2011; 2013) and during midwinter (Garfinkel and Hartmann 2011a,b; Wang et al. 2018). Moreover, a poleward shift of the jet has been found in

studies analyzing the zonally averaged tropospheric response to QBOE (White et al. 2015; Hitchman et al. 2021). However, the mechanism explaining the poleward shift of the jet is not understood. In Chapter 3, I assert that the poleward shift of the jet is a response to the QMO-MMC. However, no hard evidence is provided. Haynes et al. (2021) clarify that the QBO-MMC alone cannot cause a poleward shift of the tropospheric jet. They note that the *coupled interaction of extratropical waves with the QBO-MMC* may explain the jet response. More recently, Anstey et al. (2021) find no evidence of a poleward jet shift in the North Pacific when analyzing reanalysis or a multi-model ensemble with models that spontaneously generate the QBO.

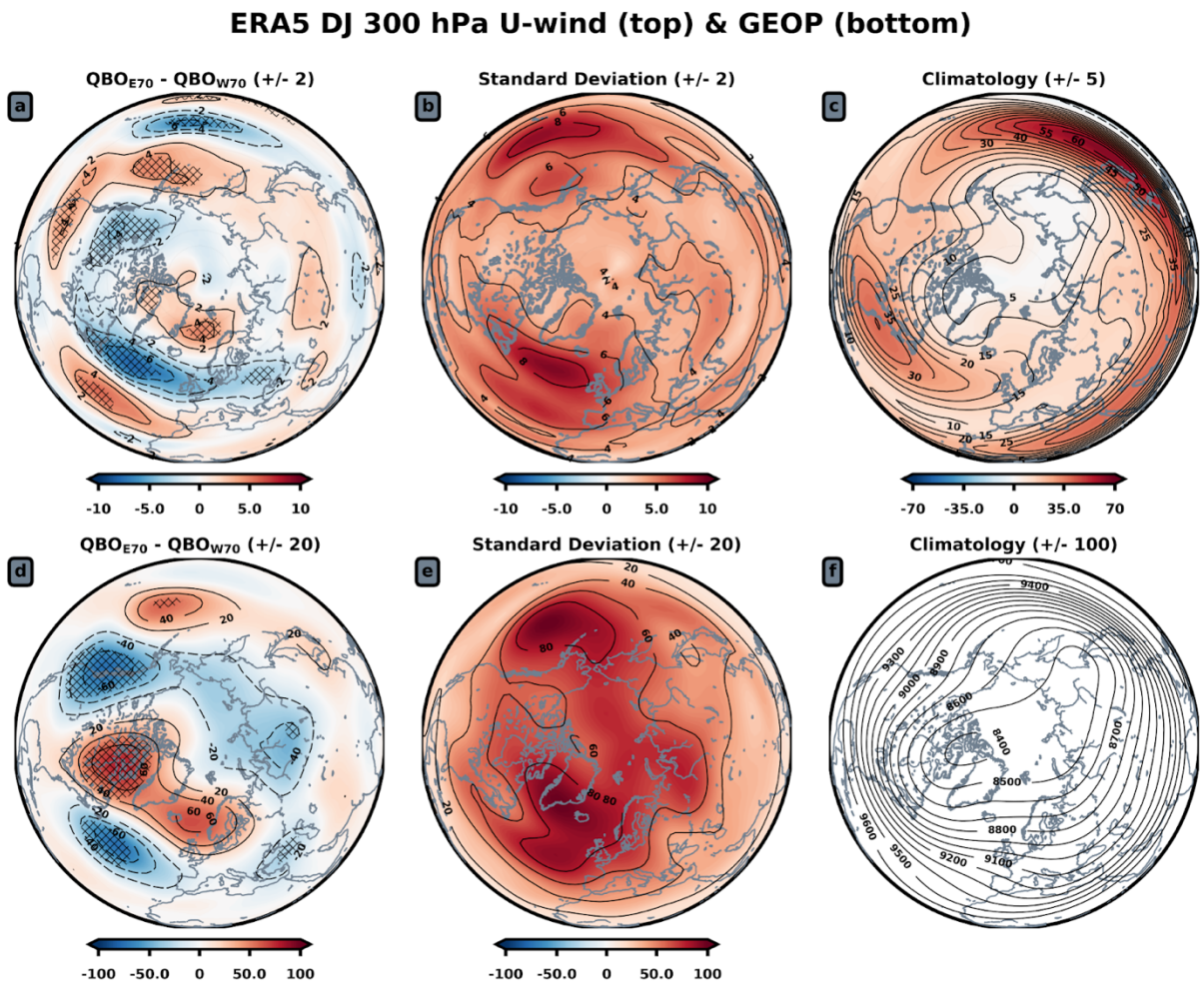

Figure 5.1: ERA5 Dec. - Jan. (DJ) 300 hPa zonal wind (top) and 300 hPa geopotential height responses to the QBO. Plots are shown in color, and the lined contour interval is indicated above each plot. The QBO is defined using its easterly phase at 70 hPa - this level is found to maximize the North Pacific response. All ENSO years in which the Nino 3.4 index exceeds +/- 1 sigma are excluded. Hatching indicates p-values < 0.05 with a student's t-test on panels (a) and (d).

Figure 5.1 shows the ERA5 300 hPa wind response to lower stratospheric easterly QBO (QBOE). The QBO is indexed at 70 hPa. This isobar is found to maximize the North Pacific response while weakening the North Atlantic sector response. Conversely, indexing the QBO at 50 hPa strengthens the North Atlantic response while weakening the North Pacific sector response (not shown).

There is a poleward shift of the jet in the North Pacific during DJ (Fig. 5.1a). It may be better to say there is an extension of the jet towards North America (Fig. 5.1a). Further, there is an increase in height over the North Pacific (Fig. 5.1d), which has been found by a few studies analyzing the response to the QBO in GCMs (Garfinkel and Hartmann 2011b, Rao et al. 2020b). There is also a negative NAO response (Fig. 5.1d). There seems to be more of a consensus in the literature that the NAO response is a robust teleconnection forced by the QBO (Andrews et al. 2019; Anstey et al. 2021). Relative to the standard deviation and climatological wind strength over each basin (Fig. 5.1b,c), the North Atlantic 300 hPa wind response is larger than the response in the North Pacific (Fig. 5.1a).

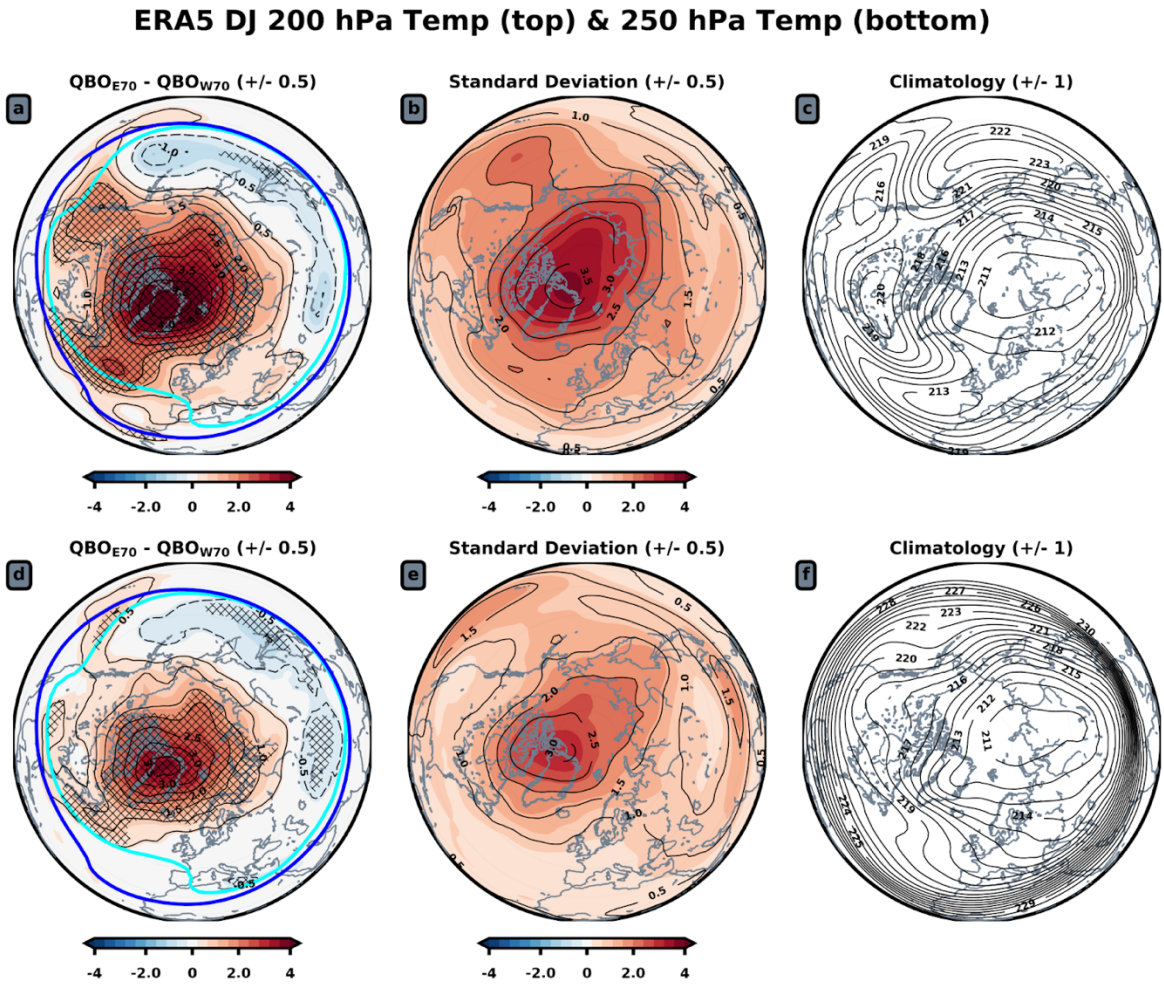

Figure 5.2: As in Fig. 5.1, but for 200 hPa temperature (top) and 250 hPa temperature (bottom). As an indication of the tropopause, the climatological 200 hPa 2-PVU line is shown in royal blue and the climatological 250 hPa 2-PVU line is shown in cyan on panels (a) and (d).

To get an idea of how the QBO may be forcing these upper tropospheric wind responses, Figure 5.2 shows the lower stratospheric temperature responses to the QBO. At 200 hPa (top) and 250 hPa (bottom), the largest temperature change is the polar stratospheric warming centered over Greenland. This is the result of the Holton-Tan effect. At 200 hPa, two “knobs” of anomalous warming are found away from the pole (Fig. 5.2a). The stronger one is found over the North Atlantic (2.5 Kelvin) and a secondary response is found over northwestern Canada (1.5 Kelvin). Using the climatological 200 hPa 2-PVU line as an indicator of the tropopause, both

the North Atlantic and North Pacific lower stratospheric warmings are pressed against the nearby tropopause (Fig. 5.2a). At 250 hPa, the North Atlantic warming is still pressed against the climatological tropopause while the northwestern Canada warming has either shifted longitudinally or diminished completely (Fig. 5.2d). Over the North Pacific at 250 hPa, anomalous warming straddles the tropopause, being found in the troposphere and stratosphere (Fig. 5.2d).

The lower stratospheric temperature is important to consider because when it fluctuates, the tropospheric wind field does too. This is shown by Haigh et al. (2005) and Simpson et al. (2009), who impose lower stratospheric warming in GCMs and find latitudinal shifting of the tropospheric jet. In particular, the change in the zonally averaged upper tropospheric horizontal eddy momentum flux induced by the lower stratospheric warming is compensated for by mean meridional circulations in the troposphere. I hypothesize that the QBO is influencing the tropospheric circulation over the North Pacific and the North Atlantic by modifying the lower stratospheric temperature.

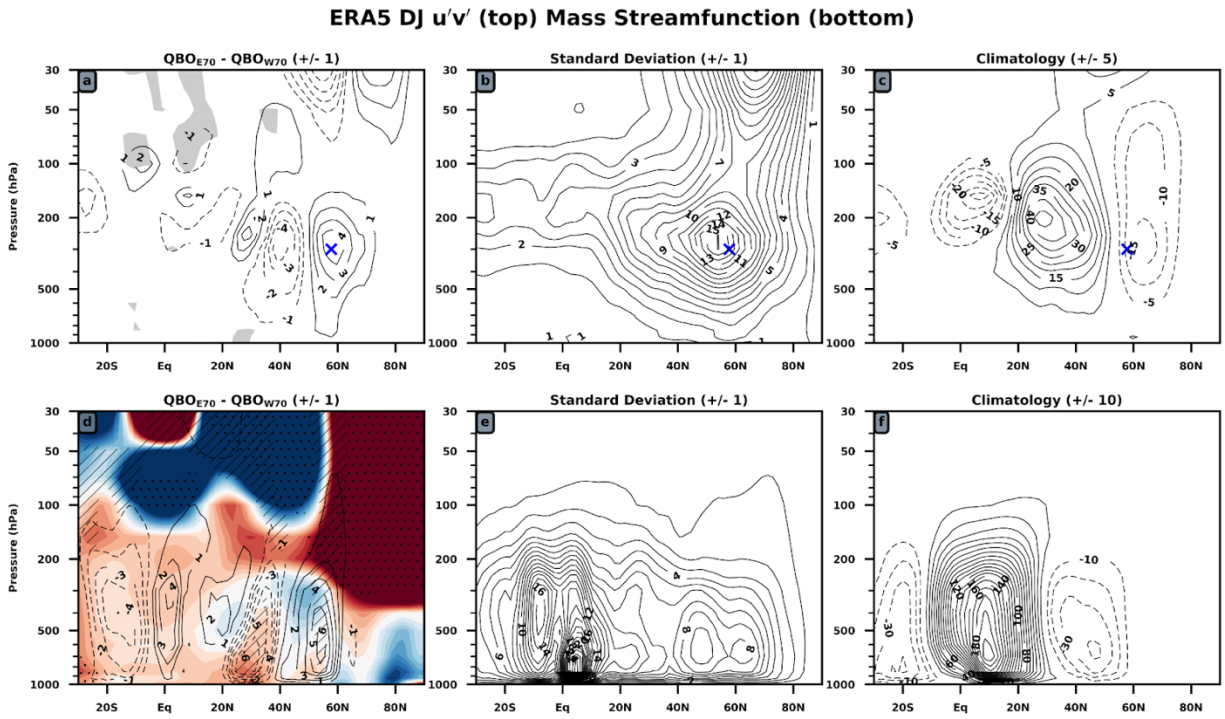

Figure 5.3: Horizontal eddy momentum flux (m^2s^2) responses are shown in row 1 and mean meridional mass streamfunction (10^9 kg/s) responses are shown in row 2. As in Figs. 5.1 and 5.2, the response to the QBO is shown in column 1, the standard deviation in column 2, and the climatologies in column 3. Contour intervals are noted in each plot's title. Statistical significance is shown by gray fill in panel (a) and is hatched in panel (d). Temperature responses are shaded on panel (d) with an arbitrary colorscale of +/- 0.5 Kelvin and significance is stippled for this field.

To begin evaluating if the lower stratospheric temperature changes induced by the QBO may promote the tropospheric wind responses shown in Fig. 5.1, Fig. 5.3 shows the horizontal eddy momentum flux (HEMF) response and the mean meridional mass streamfunction response to the QBO. The lack of significance in Fig. 3a is striking, indicating that most of the HEMF response may originate due to chance. This is unfortunate because the positive anomaly marked by a blue "X" at 300 hPa and 58°N is a 39.2% change relative to climatology (compare Fig. 5.3a with 5.3c). However, Fig. 5.5d shows that when this response is taken out of the zonal average, it does not occur by chance - it is located over northwestern Canada.

In a steady state, when taking a zonal average, there is generally descent below an area of positive HEMF and ascent directly below a region with negative HEMF (Simpson et al. 2009). In the upper troposphere, there is a northward flow where the latitudinal gradient of the HEMF is positive. Conversely, there is a southward flow where the gradient is negative. This is shown in Fig. 5.3c and 5.3f in which the climatological HEMF coincides with the position of the Hadley and Ferrel Cells. While the zonally averaged HEMF response to QBO is not robust (Fig. 5.3a), the mean meridional mass streamfunction responses to the QBO is (Fig. 5.3d). The pair of extratropical tropospheric meridional cells generally coincide with the HEMF responses above them (Fig. 5.3d). A non-statistically significant cooling forms between 40°N and 50°N at 300 hPa, where the robust anomalous mean meridional mass streamfunction response generates ascent (Fig. 5.3d).

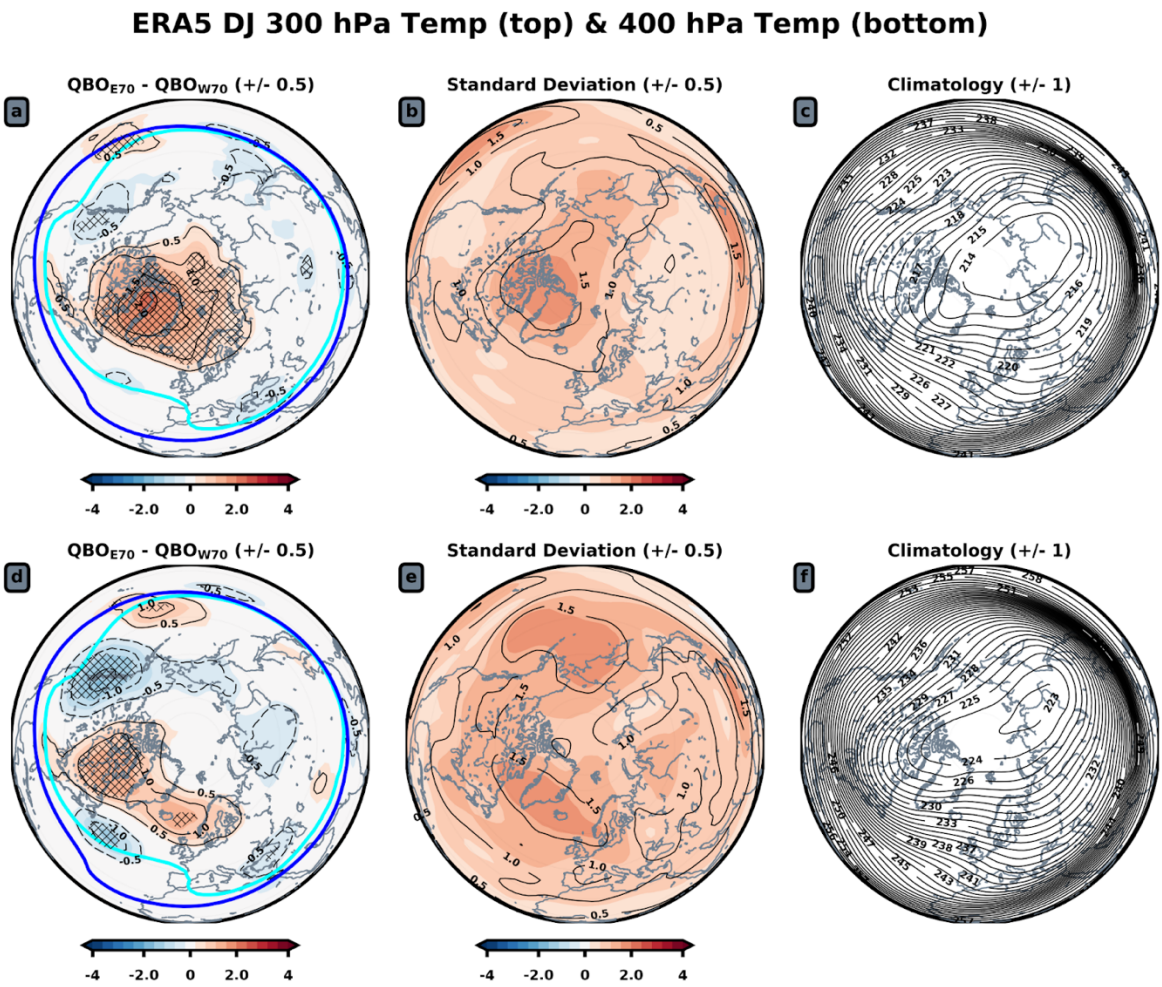

Fig. 5.4: As in Fig. 5.2, but for 300 hPa (top) and 400 hPa (bottom).

To further investigate that upper tropospheric cooling, Figs. 5.4a and 5.4d show the 300 hPa and 400 hPa temperature responses, respectively. The strongest indication of cooling in any region is over western North America and the North Pacific. Conversely, the North Atlantic sector response is dominated by an anomalous increase in temperature.

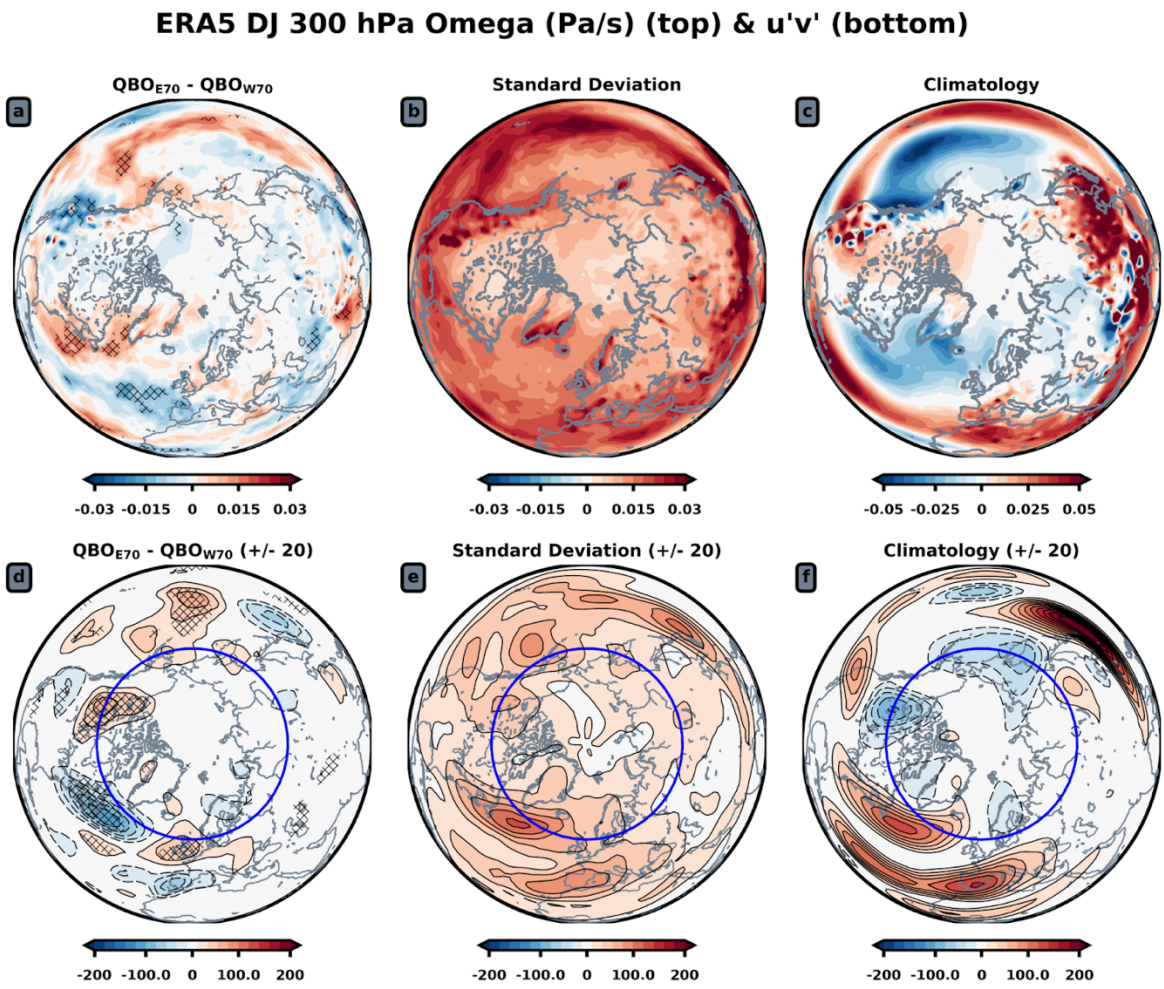

Figure 5.5: 300 hPa omega responses (top) and horizontal eddy momentum flux (m^2s^2) responses are shown (bottom). For omega, blue coincides with ascent and red coincides with descent. For panels (a) and (d), hatching denotes statistical significance. The blue line is at 58°N, to illustrate where that large positive horizontal eddy momentum flux anomaly from Fig. 5.3a is - it appears to be over northwestern Canada.

Fig. 5.5a shows that the QBO generates anomalous ascent, negative omega, over western North America and the North Pacific, precisely where that anomalous cooling is in Fig. 5.4a and 5.4d. I want to argue that the anomalous dipole of HEMF over western North America forces adiabatic ascent over the western United States, but I am not sure. I would be naively applying the zonally *averaged findings* of Haigh et al. (2005) and Simpson et al. (2009) to a non-zonally averaged case. Over the western North pacific, there is a pair of responses, the aforementioned ascent, and anomalous descent west of it (Fig. 5.5a). Similarly, there is a pair of responses over

the North Atlantic, ascent near Europe and anomalous descent west of it (Fig. 5.5a). These are very consistent with the geopotential height responses of Fig. 5.1d. However, it is difficult to tell whether or not these changes in vertical motion result from the changes in HEMF in the upper troposphere or something else.

5.2.2 Conclusions

It is not understood how the QBO modulates the position of the jet-stream in the North Pacific and North Atlantic sectors. There seems to be more of a consensus that the North Atlantic response is mediated through the Holton-Tan effect, the so-called “polar-route” of QBO influence on the troposphere (Gray et al. 2018). While a QBO effect on the North Pacific jet has been found in reanalysis (Inoue et al. 2011; 2013; Wang et al. 2018) and model experiments (Garfinkel et al. 2011a,b; Rao et al. 2020b; Elsbury et al. 2021), it most recently has *not* been found by an ensemble of model experiments and reanalysis (Anstey et al. 2021).

Evidence of a QBO teleconnection with the North Pacific is found here. However, the mechanism is still not clear. I hypothesize that the QBO modulates the lower stratospheric temperature to force the tropospheric zonal wind response. Further, I suspect that this teleconnection only is present during early winter because the Holton-Tan effect is strictly an early phenomenon (Lu et al. 2020). During late winter, a lower stratospheric easterly QBO coincides with a cooler polar vortex (Lu et al. 2020).

Pursuing this teleconnection is important because there is interest in leveraging the QBO for subseasonal to seasonal forecasting (e.g., Garfinkel et al. 2018). The next step to continue this research is to use a GCM, or several, to evaluate if the models include a poleward shift of the North Pacific jet during QBOE. I am currently using the CMIP6 models for this purpose. If the

models do not include the teleconnection, I will begin looking for which models are closest to simulating the observed response to the QBO and if any attributes of the QBO are correlated with the presence of the teleconnection.

Bibliography

Abatzoglou, J. T., & Magnusdottir, G. (2006). Planetary Wave Breaking and Nonlinear Reflection: Seasonal Cycle and Interannual Variability. In *Journal of Climate* (Vol. 19, Issue 23, pp. 6139–6152). https://doi.org/10.1175/jcli3968.1

Ait-Chaalal, F., & Schneider, T. (2015). Why Eddy Momentum Fluxes are Concentrated in the Upper Troposphere. *Journal of the Atmospheric Sciences*, *72*(4), 1585–1604.

Andrews, M. B., Knight, J. R., Scaife, A. A., Lu, Y., Wu, T., Gray, L. J., & Schenzinger, V. (2019). Observed and Simulated Teleconnections Between the Stratospheric Quasi-Biennial Oscillation and Northern Hemisphere Winter Atmospheric Circulation. In *Journal of Geophysical Research: Atmospheres* (Vol. 124, Issue 3, pp. 1219–1232). https://doi.org/10.1029/2018jd029368

Anstey, J. A., & Shepherd, T. G. (2014). High-latitude influence of the quasi-biennial oscillation. In *Quarterly Journal of the Royal Meteorological Society* (Vol. 140, Issue 678, pp. 1–21). https://doi.org/10.1002/qj.2132

Anstey, J. A., Simpson, I. R., Richter, J. H., Naoe, H., Taguchi, M., Serva, F., Gray, L. J., Butchart, N., Hamilton, K., Osprey, S., Bellprat, O., Braesicke, P., Bushell, A. C., Cagnazzo, C., Chen, C., Chun, H., Garcia, R. R., Holt, L., Kawatani, Y., … Yukimoto, S. (2021). Teleconnections of the quasi-biennial oscillation in a multi-model ensemble of QBO -resolving models. *Quarterly Journal of the Royal Meteorological Society*, *qj.4048*. https://doi.org/10.1002/qj.4048

An, X., Wu, B., Zhou, T., & Liu, B. (2021). Atlantic multidecadal oscillation drives interdecadal Pacific variability via tropical atmospheric bridge. *Journal of Climate*, *-1*(aop), 1–46.

Baldwin, M. P., Ayarzagüena, B., Birner, T., Butchart, N., Butler, A. H., Charlton-Perez, A. J., Domeisen, D. I. V., Garfinkel, C. I., Garny, H., Gerber, E. P., Hegglin, M. I., Langematz, U., & Pedatella, N. M. (2021). Sudden stratospheric warmings. *Reviews of Geophysics* , *59*(1). https://doi.org/10.1029/2020rg000708

Baldwin, M. P., & Dunkerton, T. J. (1999). Propagation of the Arctic Oscillation from the stratosphere to the troposphere. In *Journal of Geophysical Research: Atmospheres* (Vol. 104, Issue D24, pp. 30937–30946). https://doi.org/10.1029/1999jd900445

Baldwin, M. P., Gray, L. J., Dunkerton, T. J., Hamilton, K., Haynes, P. H., Randel, W. J., Holton, J. R., Alexander, M. J., Hirota, I., Horinouchi, T., Jones, D. B. A., Kinnersley, J. S., Marquardt, C., Sato, K., & Takahashi, M. (2001). The quasi-biennial oscillation. In *Reviews of Geophysics* (Vol. 39, Issue 2, pp. 179–229). https://doi.org/10.1029/1999rg000073

Barnes, E. A., & Hartmann, D. L. (2012). Detection of Rossby wave breaking and its response to shifts of the midlatitude jet with climate change. In *Journal of Geophysical Research: Atmospheres* (Vol. 117, Issue D9). https://doi.org/10.1029/2012jd017469

Barton, C. A., & McCormack, J. P. (2019). Optimization of Gravity Wave Source Parameters for Improved Seasonal Prediction of the Quasi-Biennial Oscillation. *Journal of the*. https://journals.ametsoc.org/view/journals/atsc/76/9/jas-d-19-0077.1.xml

Birner, T., & Albers, J. R. (2017). Sudden Stratospheric Warmings and Anomalous Upward Wave Activity Flux. In *SOLA* (Vol. 13A, Issue Special_Edition, pp. 8–12). https://doi.org/10.2151/sola.13a-002

Boer, G. J., Smith, D. M., Cassou, C., Doblas-Reyes, F., Danabasoglu, G., Kirtman, B., Kushnir, Y., Kimoto, M., Meehl, G. A., Msadek, R., Mueller, W. A., Taylor, K. E., Zwiers, F., Rixen, M., Ruprich-Robert, Y., & Eade, R. (2016). The Decadal Climate Prediction Project (DCPP) contribution to CMIP6. In *Geoscientific Model Development* (Vol. 9, Issue 10, pp. 3751–3777). https://doi.org/10.5194/gmd-9-3751-2016

Boljka, L., & Birner, T. (2020). Tropopause-level planetary wave source and its role in two-way troposphere–stratosphere coupling. In *Weather and Climate Dynamics* (Vol. 1, Issue 2, pp. 555–575). https://doi.org/10.5194/wcd-1-555-2020

Booth, B. B. B., Dunstone, N. J., Halloran, P. R., Andrews, T., & Bellouin, N. (2012). Aerosols implicated as a prime driver of twentieth-century North Atlantic climate variability. *Nature*, *484*(7393), 228–232.

Bushell, A. C., Anstey, J. A., Butchart, N., Kawatani, Y., Osprey, S. M., Richter, J. H., Serva, F., Braesicke, P., Cagnazzo, C., -C. Chen, C., -Y. Chun, H., Garcia, R. R., Gray, L. J., Hamilton, K., Kerzenmacher, T., -H. Kim, Y., Lott, F., McLandress, C., Naoe, H., … Yukimoto, S. (2020). Evaluation of the Quasi-Biennial Oscillation in global climate models for the SPARC QBO-initiative. In *Quarterly Journal of the Royal Meteorological Society*. https://doi.org/10.1002/qj.3765

Butchart, N., Cionni, I., Eyring, V., Shepherd, T. G., Waugh, D. W., Akiyoshi, H., Austin, J., Brühl, C., Chipperfield, M. P., Cordero, E., Dameris, M., Deckert, R., Dhomse, S., Frith, S. M., Garcia, R. R., Gettelman, A., Giorgetta, M. A., Kinnison, D. E., Li, F., … Tian, W. (2010). Chemistry–Climate Model Simulations of Twenty-First Century Stratospheric Climate and Circulation Changes. *Journal of Climate*, *23*(20), 5349–5374.

Butler, A., Charlton-Perez, A., Domeisen, D. I. V., Garfinkel, C., Gerber, E. P., Hitchcock, P., Karpechko, A. Y., Maycock, A. C., Sigmond, M., Simpson, I., & Son, S.-W. (2019). Chapter 11 - Sub-seasonal Predictability and the Stratosphere. In A. W. Robertson & F. Vitart (Eds.), *Sub-Seasonal to Seasonal Prediction* (pp. 223–241). Elsevier.

Butler, A. H., Sjoberg, J. P., Seidel, D. J., & Rosenlof, K. H. (2017). A sudden stratospheric warming compendium. In *Earth System Science Data* (Vol. 9, Issue 1, pp. 63–76). https://doi.org/10.5194/essd-9-63-2017

Cámara, A. de la, de la Cámara, A., Albers, J. R., Birner, T., Garcia, R. R., Hitchcock, P., Kinnison, D. E., & Smith, A. K. (2017). Sensitivity of Sudden Stratospheric Warmings to Previous Stratospheric Conditions. In *Journal of the Atmospheric Sciences* (Vol. 74, Issue 9, pp. 2857–2877). https://doi.org/10.1175/jas-d-17-0136.1

Cámara, A. de la, de la Cámara, A., Birner, T., & Albers, J. R. (2019). Are Sudden Stratospheric Warmings Preceded by Anomalous Tropospheric Wave Activity? In *Journal of Climate* (Vol. 32, Issue 21, pp. 7173–7189). https://doi.org/10.1175/jcli-d-19-0269.1

Cane, M. A., Clement, A. C., Murphy, L. N., & Bellomo, K. (2017). Low-Pass Filtering, Heat Flux, and Atlantic Multidecadal Variability. In *Journal of Climate* (Vol. 30, Issue 18, pp. 7529–7553). https://doi.org/10.1175/jcli-d-16-0810.1

Cassou, C., Kushnir, Y., Hawkins, E., Pirani, A., Kucharski, F., Kang, I.-S., & Caltabiano, N. (2018). Decadal Climate Variability and Predictability: Challenges and Opportunities. In *Bulletin of the American Meteorological Society* (Vol. 99, Issue 3, pp. 479–490). https://doi.org/10.1175/bams-d-16-0286.1

Charlton, A. J., O'Neill, A., Lahoz, W. A., Massacand, A. C., & Berrisford, P. (2005). The impact of the stratosphere on the troposphere during the southern hemisphere stratospheric sudden warming, September 2002. In *Quarterly Journal of the Royal Meteorological Society* (Vol. 131, Issue 609, pp. 2171–2190). https://doi.org/10.1256/qj.04.43

Charlton, A. J., & Polvani, L. M. (2007). A New Look at Stratospheric Sudden Warmings. Part I: Climatology and Modeling Benchmarks. In *Journal of Climate* (Vol. 20, Issue 3, pp. 449–469). https://doi.org/10.1175/jcli3996.1

Chen, P., & Robinson, W. A. (1992). Propagation of Planetary Waves between the Troposphere and Stratosphere. In *Journal of the Atmospheric Sciences* (Vol. 49, Issue 24, pp. 2533–2545). https://doi.org/10.1175/1520-0469(1992)049<2533:popwbt>2.0.co;2

Choi, J., & Son, S. (2019). Stratospheric initial condition for skillful surface prediction in the ECMWF model. *Geophysical Research Letters*, *46*(21), 12556–12564.

Christiansen, B. (2001). Downward propagation of zonal mean zonal wind anomalies from the stratosphere to the troposphere: Model and reanalysis. In *Journal of Geophysical Research: Atmospheres* (Vol. 106, Issue D21, pp. 27307–27322). https://doi.org/10.1029/2000jd000214

Clement, A., Bellomo, K., Murphy, L. N., Cane, M. A., Mauritsen, T., Rädel, G., & Stevens, B. (2015). The Atlantic Multidecadal Oscillation without a role for ocean circulation. *Science*, *350*(6258), 320–324.

Collimore, C. C., Martin, D. W., Hitchman, M. H., Huesmann, A., & Waliser, D. E. (2003). On The Relationship between the QBO and Tropical Deep Convection. In *Journal of Climate* (Vol. 16, Issue 15, pp. 2552–2568). https://doi.org/10.1175/1520-0442(2003)016<2552:otrbtq>2.0.co;2

Coy, L., Eckermann, S., & Hoppel, K. (2009). Planetary Wave Breaking and Tropospheric Forcing as Seen in the Stratospheric Sudden Warming of 2006. In *Journal of the Atmospheric Sciences* (Vol. 66, Issue 2, pp. 495–507). https://doi.org/10.1175/2008jas2784.1

Coy, L., & Pawson, S. (2015). The Major Stratospheric Sudden Warming of January 2013: Analyses and Forecasts in the GEOS-5 Data Assimilation System. In *Monthly Weather Review* (Vol. 143, Issue 2, pp. 491–510). https://doi.org/10.1175/mwr-d-14-00023.1

Danabasoglu, G., Yeager, S. G., Kim, W. M., Behrens, E., Bentsen, M., Bi, D., Biastoch, A., Bleck, R., Böning, C., Bozec, A., Canuto, V. M., Cassou, C., Chassignet, E., Coward, A. C., Danilov, S., Diansky, N., Drange, H., Farneti, R., Fernandez, E., … Yashayaev, I. (2016). North Atlantic simulations in Coordinated Ocean-ice Reference Experiments phase II (CORE-II). Part II: Inter-annual to decadal variability. In *Ocean Modelling* (Vol. 97, pp. 65–90). https://doi.org/10.1016/j.ocemod.2015.11.007

Davini, P., von Hardenberg, J., & Corti, S. (2015). Tropical origin for the impacts of the Atlantic Multidecadal Variability on the Euro-Atlantic climate. *Environmental Research Letters: ERL [Web Site]*, *10*(9), 094010.

Delworth, T. L., Zeng, F., Zhang, L., Zhang, R., Vecchi, G. A., & Yang, X. (2017). The Central Role of Ocean Dynamics in Connecting the North Atlantic Oscillation to the Extratropical Component of the Atlantic Multidecadal Oscillation. In *Journal of Climate* (Vol. 30, Issue 10, pp. 3789–3805). https://doi.org/10.1175/jcli-d-16-0358.1

Delworth, T., Manabe, S., & Stouffer, R. J. (1993). Interdecadal Variations of the Thermohaline Circulation in a Coupled Ocean-Atmosphere Model. In *Journal of Climate* (Vol. 6, Issue 11, pp. 1993–2011). https://doi.org/10.1175/1520-0442(1993)006<1993:ivottc>2.0.co;2

Dimdore-Miles, O., Gray, L., & Osprey, S. (n.d.). *Origins of Multi-decadal Variability in Sudden Stratospheric Warmings*. https://doi.org/10.5194/egusphere-egu21-1509

Domeisen, D. I. V., Butler, A. H., Charlton-Perez, A. J., Ayarzagüena, B., Baldwin, M. P., Dunn-Sigouin, E., Furtado, J. C., Garfinkel, C. I., Hitchcock, P., Karpechko, A. Y., Kim, H., Knight, J., Lang, A. L., Lim, E., Marshall, A., Roff, G., Schwartz, C., Simpson, I. R., Son, S., & Taguchi, M. (2020). The Role of the Stratosphere in Subseasonal to Seasonal Prediction: 2. Predictability Arising From Stratosphere-Troposphere Coupling. In *Journal of Geophysical Research: Atmospheres* (Vol. 125, Issue 2). https://doi.org/10.1029/2019jd030923

Domeisen, D. I. V., Sun, L., & Chen, G. (2013). The role of synoptic eddies in the tropospheric response to stratospheric variability. In *Geophysical Research Letters* (Vol. 40, Issue 18, pp. 4933–4937). https://doi.org/10.1002/grl.50943

Dong, B., & Dai, A. (2015). The influence of the Interdecadal Pacific Oscillation on Temperature and Precipitation over the Globe. In *Climate Dynamics* (Vol. 45, Issues 9-10, pp. 2667–2681). https://doi.org/10.1007/s00382-015-2500-x

Dunkerton, T. (1978). On the Mean Meridional Mass Motions of the Stratosphere and Mesosphere. In *Journal of the Atmospheric Sciences* (Vol. 35, Issue 12, pp. 2325–2333). https://doi.org/10.1175/1520-0469(1978)035<2325:otmmmm>2.0.co;2

Dunkerton, T., Hsu, C.-P. F., & McIntyre, M. E. (1981). Some Eulerian and Lagrangian Diagnostics for a Model Stratospheric Warming. In *Journal of the Atmospheric Sciences* (Vol. 38, Issue 4, pp. 819–844). https://doi.org/10.1175/1520-0469(1981)038<0819:sealdf>2.0.co;2

Dunkerton, T. J., & Baldwin, M. P. (1991). Quasi-biennial Modulation of Planetary-Wave Fluxes in the Northern Hemisphere Winter. In *Journal of the Atmospheric Sciences* (Vol. 48, Issue 8, pp. 1043–1061). https://doi.org/10.1175/1520-0469(1991)048<1043:qbmopw>2.0.co;2

Edmon, H. J., Hoskins, B. J., & McIntyre, M. E. (1980). Eliassen-Palm Cross Sections for the Troposphere. In *Journal of the Atmospheric Sciences* (Vol. 37, Issue 12, pp. 2600–2616). https://doi.org/10.1175/1520-0469(1980)037<2600:epcsft>2.0.co;2

Eguchi, N., Kodera, K., & Nasuno, T. (2015). A global non-hydrostatic model study of a downward coupling through the tropical tropopause layer during a stratospheric sudden warming. In *Atmospheric Chemistry and Physics* (Vol. 15, Issue 1, pp. 297–304). https://doi.org/10.5194/acp-15-297-2015

Eichelberger, S. J., & Hartmann, D. L. (2007). Zonal Jet Structure and the Leading Mode of Variability. In *Journal of Climate* (Vol. 20, Issue 20, pp. 5149–5163). https://doi.org/10.1175/jcli4279.1

Elsbury, D., Peings, Y., Saint-Martin, D., Douville, H., & Magnusdottir, G. (2019). The Atmospheric Response to Positive IPV, Positive AMV, and Their Combination in Boreal Winter. In *Journal of Climate* (Vol. 32, Issue 14, pp. 4193–4213). https://doi.org/10.1175/jcli-d-18-0422.1

Enfield, D. B., Mestas-Nuñez, A. M., & Trimble, P. J. (2001). The Atlantic Multidecadal Oscillation and its relation to rainfall and river flows in the continental U.S. In *Geophysical Research Letters* (Vol. 28, Issue 10, pp. 2077–2080). https://doi.org/10.1029/2000gl012745

England, M. H., McGregor, S., Spence, P., Meehl, G. A., Timmermann, A., Cai, W., Gupta, A. S., McPhaden, M. J., Purich, A., & Santoso, A. (2014). Recent intensification of wind-driven circulation in the Pacific and the ongoing warming hiatus. In *Nature Climate Change* (Vol. 4, Issue 3, pp. 222–227). https://doi.org/10.1038/nclimate2106

Fletcher, C. G., & Kushner, P. J. (2011). The Role of Linear Interference in the Annular Mode Response to Tropical SST Forcing. In *Journal of Climate* (Vol. 24, Issue 3, pp. 778–794). https://doi.org/10.1175/2010jcli3735.1

García-Serrano, J., Cassou, C., Douville, H., Giannini, A., & Doblas-Reyes, F. J. (2017). Revisiting the ENSO Teleconnection to the Tropical North Atlantic. In *Journal of Climate* (Vol. 30, Issue 17, pp. 6945–6957). https://doi.org/10.1175/jcli-d-16-0641.1

Garfinkel, C. I., & Hartmann, D. L. (2011a). The Influence of the Quasi-Biennial Oscillation on the Troposphere in Winter in a Hierarchy of Models. Part II: Perpetual Winter WACCM Runs. In *Journal of the Atmospheric Sciences* (Vol. 68, Issue 9, pp. 2026–2041). https://doi.org/10.1175/2011jas3702.1

Garfinkel, C. I., & Hartmann, D. L. (2011b). The Influence of the Quasi-Biennial Oscillation on the Troposphere in Winter in a Hierarchy of Models. Part I: Simplified Dry GCMs. In *Journal of the Atmospheric Sciences* (Vol. 68, Issue 6, pp. 1273–1289). https://doi.org/10.1175/2011jas3665.1

Garfinkel, C. I., Schwartz, C., Domeisen, D. I. V., Son, S., Butler, A. H., & White, I. P. (2018). Extratropical atmospheric predictability from the quasi-biennial oscillation in subseasonal forecast models. *Journal of Geophysical Research*, *123*(15), 7855–7866.

Garfinkel, C. I., Shaw, T. A., Hartmann, D. L., & Waugh, D. W. (2012). Does the Holton–Tan Mechanism Explain How the Quasi-Biennial Oscillation Modulates the Arctic Polar Vortex? In *Journal of the Atmospheric Sciences* (Vol. 69, Issue 5, pp. 1713–1733). https://doi.org/10.1175/jas-d-11-0209.1

Garfinkel, C. I., White, I., Gerber, E. P., Jucker, M., & Erez, M. (2020). The Building Blocks of Northern Hemisphere Wintertime Stationary Waves. In *Journal of Climate* (Vol. 33, Issue 13, pp. 5611–5633). https://doi.org/10.1175/jcli-d-19-0181.1

Gerber, E. P., Baldwin, M. P., Akiyoshi, H., Austin, J., Bekki, S., Braesicke, P., Butchart, N., Chipperfield, M., Dameris, M., Dhomse, S., Frith, S. M., Garcia, R. R., Garny, H., Gettelman, A., Hardiman, S. C., Karpechko, A., Marchand, M., Morgenstern, O., Eric Nielsen, J., … Smale, D. (2010). Stratosphere-troposphere coupling and annular mode variability in chemistry-climate models. In *Journal of Geophysical Research* (Vol. 115). https://doi.org/10.1029/2009jd013770

Giannini, A., Chiang, J. C. H., Cane, M. A., Kushnir, Y., & Seager, R. (2001). The ENSO Teleconnection to the Tropical Atlantic Ocean: Contributions of the Remote and Local SSTs to Rainfall Variability in the Tropical Americas. *Journal of Climate*, *14*(24), 4530–4544.

Gray, L. J. (2003). The influence of the equatorial upper stratosphere on stratospheric sudden warmings. In *Geophysical Research Letters* (Vol. 30, Issue 4). https://doi.org/10.1029/2002gl016430

Gray, L. J., Anstey, J. A., Kawatani, Y., Lu, H., Osprey, S., & Schenzinger, V. (2018). Surface impacts of the Quasi Biennial Oscillation. In *Atmospheric Chemistry and Physics* (Vol. 18, Issue 11, pp. 8227–8247). https://doi.org/10.5194/acp-18-8227-2018

Gray, L. J., Drysdale, E. F., Lawrence, B. N., & Dunkerton, T. J. (2001). Model studies of the interannual variability of the northern-hemisphere stratospheric winter circulation: The role of the quasi-biennial oscillation. In *Quarterly Journal of the Royal Meteorological Society* (Vol. 127, Issue 574, pp. 1413–1432). https://doi.org/10.1002/qj.49712757416

Haigh, J. D., Blackburn, M., & Day, R. (2005). The Response of Tropospheric Circulation to Perturbations in Lower-Stratospheric Temperature. In *Journal of Climate* (Vol. 18, Issue 17, pp. 3672–3685). https://doi.org/10.1175/jcli3472.1

Hansen, F., Matthes, K., & Gray, L. J. (2013). Sensitivity of stratospheric dynamics and chemistry to QBO nudging width in the chemistry-climate model WACCM. In *Journal of Geophysical Research: Atmospheres* (Vol. 118, Issue 18, pp. 10,464–10,474). https://doi.org/10.1002/jgrd.50812

Haynes, P., Hitchcock, P., Hitchman, M., Yoden, S., Hendon, H., Kiladis, G., Kodera, K., & Simpson, I. (2021). The Influence of the Stratosphere on the Tropical Troposphere. In *Journal of the Meteorological Society of Japan. Ser. II*. https://doi.org/10.2151/jmsj.2021-040

Haynes, P. H., & McIntyre, M. E. (1987). On the Evolution of Vorticity and Potential Vorticity in the Presence of Diabatic Heating and Frictional or Other Forces. In *Journal of the Atmospheric Sciences* (Vol. 44, Issue 5, pp. 828–841). https://doi.org/10.1175/1520-0469(1987)044<0828:oteova>2.0.co;2

Henley, B. J., Gergis, J., Karoly, D. J., Power, S., Kennedy, J., & Folland, C. K. (2015). A Tripole Index for the Interdecadal Pacific Oscillation. In *Climate Dynamics* (Vol. 45, Issues 11-12, pp. 3077–3090). https://doi.org/10.1007/s00382-015-2525-1

Henley, B. J., & King, A. D. (2017). Trajectories toward the 1.5°C Paris target: Modulation by the Interdecadal Pacific Oscillation. In *Geophysical Research Letters* (Vol. 44, Issue 9, pp. 4256–4262). https://doi.org/10.1002/2017gl073480

Hersbach, H., Bell, B., Berrisford, P., Hirahara, S., Horányi, A., Muñoz-Sabater, J., Nicolas, J., Peubey, C., Radu, R., Schepers, D., Simmons, A., Soci, C., Abdalla, S., Abellan, X., Balsamo, G., Bechtold, P., Biavati, G., Bidlot, J., Bonavita, M., … Jean-Noël Thépaut. (2020). The ERA5 global reanalysis. In *Quarterly Journal of the Royal Meteorological Society* (Vol. 146, Issue 730, pp. 1999–2049). https://doi.org/10.1002/qj.3803

Hitchcock, P., & Haynes, P. H. (2016). Stratospheric control of planetary waves. In *Geophysical Research Letters* (Vol. 43, Issue 22). https://doi.org/10.1002/2016gl071372

Hitchcock, P., Shepherd, T. G., Taguchi, M., Yoden, S., & Noguchi, S. (2013). Lower-Stratospheric Radiative Damping and Polar-Night Jet Oscillation Events. In *Journal of the Atmospheric Sciences* (Vol. 70, Issue 5, pp. 1391–1408). https://doi.org/10.1175/jas-d-12-0193.1

Hitchcock, P., & Simpson, I. R. (2014). The Downward Influence of Stratospheric Sudden Warmings. *Journal of the Atmospheric Sciences*, *71*(10), 3856–3876.

Hitchcock, P., & Simpson, I. R. (2016). Quantifying eddy feedbacks and forcings in the tropospheric response to stratospheric sudden warmings. *Journal of the Atmospheric Sciences*. https://journals.ametsoc.org/view/journals/atsc/73/9/jas-d-16-0056.1.xml

Hitchman, M. H., & Huesmann, A. S. (2009). Seasonal Influence of the Quasi-Biennial Oscillation on Stratospheric Jets and Rossby Wave Breaking. In *Journal of the Atmospheric Sciences* (Vol. 66, Issue 4, pp. 935–946). https://doi.org/10.1175/2008jas2631.1

Hitchman, M. H., Yoden, S., Haynes, P. H., Kumar, V., & Tegtmeier, S. (2021). An Observational History of the Direct Influence of the Stratospheric Quasi-biennial Oscillation on the Tropical and

Subtropical Upper Troposphere and Lower Stratosphere. In *Journal of the Meteorological Society of Japan. Ser. II* (Vol. 99, Issue 2, pp. 239–267). https://doi.org/10.2151/jmsj.2021-012

Holton, J. R., & Mass, C. (1976). Stratospheric Vacillation Cycles. In *Journal of the Atmospheric Sciences* (Vol. 33, Issue 11, pp. 2218–2225). https://doi.org/10.1175/1520-0469(1976)033<2218:svc>2.0.co;2

Holton, J. R., & Tan, H.-C. (1980). The Influence of the Equatorial Quasi-Biennial Oscillation on the Global Circulation at 50 mb. In *Journal of the Atmospheric Sciences* (Vol. 37, Issue 10, pp. 2200–2208). https://doi.org/10.1175/1520-0469(1980)037<2200:tioteq>2.0.co;2

Holton, J. R., & Tan, H.-C. (1982). The Quasi-Biennial Oscillation in the Northern Hemisphere Lower Stratosphere. In *Journal of the Meteorological Society of Japan. Ser. II* (Vol. 60, Issue 1, pp. 140–148). https://doi.org/10.2151/jmsj1965.60.1_140

Horel, J. D., & Wallace, J. M. (1981). Planetary-Scale Atmospheric Phenomena Associated with the Southern Oscillation. In *Monthly Weather Review* (Vol. 109, Issue 4, pp. 813–829). https://doi.org/10.1175/1520-0493(1981)109<0813:psapaw>2.0.co;2

Huang, B., Banzon, V. F., Freeman, E., Lawrimore, J., Liu, W., Peterson, T. C., Smith, T. M., Thorne, P. W., Woodruff, S. D., & Zhang, H.-M. (2015). Extended Reconstructed Sea Surface Temperature Version 4 (ERSST.v4). Part I: Upgrades and Intercomparisons. In *Journal of Climate* (Vol. 28, Issue 3, pp. 911–930). https://doi.org/10.1175/jcli-d-14-00006.1

Huang, B., Hu, Z.-Z., Kinter, J. L., Wu, Z., & Kumar, A. (2012). Connection of stratospheric QBO with global atmospheric general circulation and tropical SST. Part I: methodology and composite life cycle. In *Climate Dynamics* (Vol. 38, Issues 1-2, pp. 1–23). https://doi.org/10.1007/s00382-011-1250-7

Hurrell, J. W., & Van Loon, H. (1997). Decadal Variations in Climate Associated with the North Atlantic Oscillation. In *Climatic Change at High Elevation Sites* (pp. 69–94). https://doi.org/10.1007/978-94-015-8905-5_4

Inoue, M., & Takahashi, M. (2013). Connections between the stratospheric quasi-biennial oscillation and tropospheric circulation over Asia in northern autumn: QBO-TROPOSPHERE RELATIONSHIP OVER ASIA. *Journal of Geophysical Research*, *118*(19), 10,740–10,753.

Inoue, M., Takahashi, M., & Naoe, H. (2011). Relationship between the stratospheric quasi-biennial oscillation and tropospheric circulation in northern autumn: QBO-TROPOSPHERE RELATIONSHIP IN AUTUMN. *Journal of Geophysical Research*, *116*(D24). https://doi.org/10.1029/2011jd016040

Jia, L., Yang, X., Vecchi, G., Gudgel, R., Delworth, T., Fueglistaler, S., Lin, P., Scaife, A. A., Underwood, S., & Lin, S.-J. (2017). Seasonal Prediction Skill of Northern Extratropical Surface Temperature Driven by the Stratosphere. In *Journal of Climate* (Vol. 30, Issue 12, pp. 4463–4475). https://doi.org/10.1175/jcli-d-16-0475.1

Joshi, M. K., & Rai, A. (2015). Combined interplay of the Atlantic multidecadal oscillation and the interdecadal Pacific oscillation on rainfall and its extremes over Indian subcontinent. In *Climate Dynamics* (Vol. 44, Issues 11-12, pp. 3339–3359). https://doi.org/10.1007/s00382-014-2333-z

Kalnay, E., Kanamitsu, M., Kistler, R., Collins, W., Deaven, D., Gandin, L., Iredell, M., Saha, S., White, G., Woollen, J., Zhu, Y., Chelliah, M., Ebisuzaki, W., Higgins, W., Janowiak, J., Mo, K. C., Ropelewski, C., Wang, J., Leetmaa, A., … Joseph, D. (1996). The NCEP/NCAR 40-Year Reanalysis Project. *Bulletin of the American Meteorological Society*, *77*(3), 437–472.

Karl, T. R., Nicholls, N., & Ghazi, A. (1999). CLIVAR/GCOS/WMO Workshop on Indices and Indicators for Climate Extremes Workshop Summary. In *Weather and Climate Extremes* (pp. 3–7). https://doi.org/10.1007/978-94-015-9265-9_2

Kerr, R. A. (2000). A north atlantic climate pacemaker for the centuries. *Science*, *288*(5473), 1984–1985.

Kidston, J., Scaife, A. A., Hardiman, S. C., Mitchell, D. M., Butchart, N., Baldwin, M. P., & Gray, L. J. (2015). Stratospheric influence on tropospheric jet streams, storm tracks and surface weather. In *Nature Geoscience* (Vol. 8, Issue 6, pp. 433–440). https://doi.org/10.1038/ngeo2424

Kim, H., Richter, J. H., & Martin, Z. (2019). Insignificant QBO-MJO prediction skill relationship in the SubX and S2S subseasonal reforecasts. *Journal of Geophysical Research*, *124*(23), 12655–12666.

Kim, W. M., Yeager, S., Chang, P., & Danabasoglu, G. (2018). Low-Frequency North Atlantic Climate Variability in the Community Earth System Model Large Ensemble. In *Journal of Climate* (Vol. 31, Issue 2, pp. 787–813). https://doi.org/10.1175/jcli-d-17-0193.1

Kinoshita, T., Sato, K., Ishijima, K., Takigawa, M., & Yamashita, Y. (2019). Formulation of Three-Dimensional Quasi-Residual Mean Flow Balanced with Diabatic Heating Rate and Potential Vorticity Flux. In *Journal of the Atmospheric Sciences* (Vol. 76, Issue 3, pp. 851–863). https://doi.org/10.1175/jas-d-18-0085.1

Knight, J. R. (2005). A signature of persistent natural thermohaline circulation cycles in observed climate. In *Geophysical Research Letters* (Vol. 32, Issue 20). https://doi.org/10.1029/2005gl024233

Knudsen, M. F., Jacobsen, B. H., Seidenkrantz, M.-S., & Olsen, J. (2014). Evidence for external forcing of the Atlantic Multidecadal Oscillation since termination of the Little Ice Age. *Nature Communications*, *5*, 3323.

Knudsen, M. F., Seidenkrantz, M.-S., Jacobsen, B. H., & Kuijpers, A. (2011). Tracking the Atlantic Multidecadal Oscillation through the last 8,000 years. *Nature Communications*, *2*, 178.

Kodera, K., Mukougawa, H., Maury, P., Ueda, M., & Claud, C. (2016). Absorbing and reflecting sudden stratospheric warming events and their relationship with tropospheric circulation. In *Journal of Geophysical Research: Atmospheres* (Vol. 121, Issue 1, pp. 80–94). https://doi.org/10.1002/2015jd023359

Kodera, K., Yamazaki, K., Chiba, M., & Shibata, K. (1990). Downward propagation of upper stratospheric mean zonal wind perturbation to the troposphere. In *Geophysical Research Letters* (Vol. 17, Issue 9, pp. 1263–1266). https://doi.org/10.1029/gl017i009p01263

Kosaka, Y., & Xie, S.-P. (2013). Recent global-warming hiatus tied to equatorial Pacific surface cooling. *Nature*, *501*(7467), 403–407.

Kren, A. C., Marsh, D. R., Smith, A. K., & Pilewskie, P. (2016). Wintertime Northern Hemisphere Response in the Stratosphere to the Pacific Decadal Oscillation Using the Whole Atmosphere Community Climate Model. In *Journal of Climate* (Vol. 29, Issue 3, pp. 1031–1049). https://doi.org/10.1175/jcli-d-15-0176.1

Kretschmer, M., Cohen, J., Matthias, V., Runge, J., & Coumou, D. (2018). The different stratospheric influence on cold-extremes in Eurasia and North America. In *npj Climate and Atmospheric Science* (Vol. 1, Issue 1). https://doi.org/10.1038/s41612-018-0054-4

Kuroda, Y., & Kodera, K. (2001). Variability of the polar night jet in the northern and southern hemispheres. In *Journal of Geophysical Research: Atmospheres* (Vol. 106, Issue D18, pp. 20703–20713). https://doi.org/10.1029/2001jd900226

Kushner, P. J. (2010). Annular modes of the troposphere and stratosphere. In *The Stratosphere: Dynamics, Transport, and Chemistry* (pp. 59–91). https://doi.org/10.1029/2009gm000924

Labe, Z. M. (2020). *The effects of Arctic sea-ice thickness loss and stratospheric variability on mid-latitude cold spells* [UC Irvine]. https://escholarship.org/uc/item/778982rr

Labitzke, K. (2005). On the solar cycle–QBO relationship: a summary. In *Journal of Atmospheric and Solar-Terrestrial Physics* (Vol. 67, Issues 1-2, pp. 45–54). https://doi.org/10.1016/j.jastp.2004.07.016

Lau, K.-M., & Yang, S. (2003). Walker Circulation. In *Encyclopedia of Atmospheric Sciences* (pp. 2505–2510). https://doi.org/10.1016/b0-12-227090-8/00450-4

Lawrence, Z. D., Perlwitz, J., Butler, A. H., Manney, G. L., Newman, P. A., Lee, S. H., & Nash, E. R. (2020). The Remarkably Strong Arctic Stratospheric Polar Vortex of Winter 2020: Links to Record-Breaking Arctic Oscillation and Ozone Loss. In *Journal of Geophysical Research: Atmospheres* (Vol. 125, Issue 22). https://doi.org/10.1029/2020jd033271

Leovy, C. B., Sun, C.-R., Hitchman, M. H., Remsberg, E. E., Russell, J. M., Gordley, L. L., Gille, J. C., & Lyjak, L. V. (1985). Transport of Ozone in the Middle Stratosphere: Evidence for Planetary Wave Breaking. In *Journal of the Atmospheric Sciences* (Vol. 42, Issue 3, pp. 230–244). https://doi.org/10.1175/1520-0469(1985)042<0230:tooitm>2.0.co;2

Limpasuvan, V., Thompson, D. W. J., & Hartmann, D. L. (2004). The Life Cycle of the Northern Hemisphere Sudden Stratospheric Warmings. In *Journal of Climate* (Vol. 17, Issue 13, pp. 2584–2596). https://doi.org/10.1175/1520-0442(2004)017<2584:tlcotn>2.0.co;2

Lim, Y., Son, S.-W., Marshall, A. G., Hendon, H. H., & Seo, K.-H. (2019). Influence of the QBO on MJO prediction skill in the subseasonal-to-seasonal prediction models. *Climate Dynamics*, *53*(3), 1681–1695.

Liu, C., Tian, B., Li, K.-F., Manney, G. L., Livesey, N. J., Yung, Y. L., & Waliser, D. E. (2014). Northern Hemisphere mid-winter vortex-displacement and vortex-split stratospheric sudden warmings: Influence of the Madden-Julian Oscillation and Quasi-Biennial Oscillation. *Journal of Geophysical Research*, *119*(22), 12,599–12,620.

Li, Y., Yang, S., Deng, Y., Hu, X., Cai, M., & Zhou, W. (2019). Detection and attribution of upper-tropospheric warming over the tropical western Pacific. *Climate Dynamics*, *53*(5), 3057–3068.

Lorenz, D. J., & Hartmann, D. L. (2001). Eddy–Zonal Flow Feedback in the Southern Hemisphere. In *Journal of the Atmospheric Sciences* (Vol. 58, Issue 21, pp. 3312–3327). https://doi.org/10.1175/1520-0469(2001)058<3312:ezffit>2.0.co;2

Lorenz, D. J., & Hartmann, D. L. (2003). Eddy–Zonal Flow Feedback in the Northern Hemisphere Winter. In *Journal of Climate* (Vol. 16, Issue 8, pp. 1212–1227). https://doi.org/10.1175/1520-0442(2003)16<1212:effitn>2.0.co;2

Lubis, S. W., Matthes, K., Omrani, N.-E., Harnik, N., & Wahl, S. (2016). Influence of the Quasi-Biennial Oscillation and Sea Surface Temperature Variability on Downward Wave Coupling in the Northern Hemisphere. In *Journal of the Atmospheric Sciences* (Vol. 73, Issue 5, pp. 1943–1965). https://doi.org/10.1175/jas-d-15-0072.1

Lu, H., Baldwin, M. P., Gray, L. J., & Jarvis, M. J. (2008). Decadal-scale changes in the effect of the QBO on the northern stratospheric polar vortex. In *Journal of Geophysical Research* (Vol. 113, Issue D10). https://doi.org/10.1029/2007jd009647

Lu, H., Bracegirdle, T. J., Phillips, T., Bushell, A., & Gray, L. (2014). Mechanisms for the Holton-Tan relationship and its decadal variation. In *Journal of Geophysical Research: Atmospheres* (Vol. 119, Issue 6, pp. 2811–2830). https://doi.org/10.1002/2013jd021352

Lu, H., Hitchman, M. H., Gray, L. J., Anstey, J. A., & Osprey, S. M. (2020). On the role of Rossby wave breaking in the quasi-biennial modulation of the stratospheric polar vortex during boreal winter. In *Quarterly Journal of the Royal Meteorological Society* (Vol. 146, Issue 729, pp. 1939–1959). https://doi.org/10.1002/qj.3775

Mantua, N. J., Hare, S. R., Zhang, Y., Wallace, J. M., & Francis, R. C. (1997). A Pacific Interdecadal Climate Oscillation with Impacts on Salmon Production. In *Bulletin of the American Meteorological Society* (Vol. 78, Issue 6, pp. 1069–1079). https://doi.org/10.1175/1520-0477(1997)078<1069:apicow>2.0.co;2

Manzini, E., Karpechko, A. Y., Anstey, J., Baldwin, M. P., Black, R. X., Cagnazzo, C., Calvo, N., Charlton-Perez, A., Christiansen, B., Davini, P., Gerber, E., Giorgetta, M., Gray, L., Hardiman, S. C., Lee, Y.-Y., Marsh, D. R., McDaniel, B. A., Purich, A., Scaife, A. A., … Zappa, G. (2014). Northern winter climate change: Assessment of uncertainty in CMIP5 projections related to stratosphere-troposphere coupling. *Journal of Geophysical Research*, *119*(13), 7979–7998.

Marsh, D. R., Mills, M. J., Kinnison, D. E., Lamarque, J.-F., Calvo, N., & Polvani, L. M. (2013). Climate Change from 1850 to 2005 Simulated in CESM1(WACCM). In *Journal of Climate* (Vol. 26, Issue 19, pp. 7372–7391). https://doi.org/10.1175/jcli-d-12-00558.1

Martineau, P., Chen, G., Son, S., & Kim, J. (2018). Lower-Stratospheric Control of the Frequency of Sudden Stratospheric Warming Events. In *Journal of Geophysical Research: Atmospheres* (Vol. 123, Issue 6, pp. 3051–3070). https://doi.org/10.1002/2017jd027648

Martin, Z., Wang, S., Nie, J., & Sobel, A. (2019). The Impact of the QBO on MJO Convection in Cloud-Resolving Simulations. In *Journal of the Atmospheric Sciences* (Vol. 76, Issue 3, pp. 669–688). https://doi.org/10.1175/jas-d-18-0179.1

Ma, T., Chen, W., Huangfu, J., Song, L., & Cai, Q. (2021). The observed influence of the Quasi-Biennial Oscillation in the lower equatorial stratosphere on the East Asian winter monsoon during early boreal winter. *International Journal of Climatology*, *joc.7192*. https://doi.org/10.1002/joc.7192

Matsuno, T. (1970). Vertical Propagation of Stationary Planetary Waves in the Winter Northern Hemisphere. In *Journal of the Atmospheric Sciences* (Vol. 27, Issue 6, pp. 871–883). https://doi.org/10.1175/1520-0469(1970)027<0871:vpospw>2.0.co;2

Matthes, K., Marsh, D. R., Garcia, R. R., Kinnison, D. E., Sassi, F., & Walters, S. (2010). Role of the QBO in modulating the influence of the 11 year solar cycle on the atmosphere using constant forcings. In *Journal of Geophysical Research* (Vol. 115, Issue D18). https://doi.org/10.1029/2009jd013020

Matthias, V., & Kretschmer, M. (2020). The Influence of Stratospheric Wave Reflection on North American Cold Spells. In *Monthly Weather Review* (Vol. 148, Issue 4, pp. 1675–1690). https://doi.org/10.1175/mwr-d-19-0339.1

McIntyre, M. E. (1982). How Well do we Understand the Dynamics of Stratospheric Warmings? In *Journal of the Meteorological Society of Japan. Ser. II* (Vol. 60, Issue 1, pp. 37–65). https://doi.org/10.2151/jmsj1965.60.1_37

McIntyre, M. E. (1992). Atmospheric dynamics: Some fundamentals, with observational implications. *The Use of EOS for Studies of Atmospheric Physics*, *313*, 386.

McIntyre, M. E., & Palmer, T. N. (1983). Breaking planetary waves in the stratosphere. In *Nature* (Vol. 305, Issue 5935, pp. 593–600). https://doi.org/10.1038/305593a0

McIntyre, M. E., & Palmer, T. N. (1984). The “surf zone” in the stratosphere. In *Journal of Atmospheric and Terrestrial Physics* (Vol. 46, Issue 9, pp. 825–849). https://doi.org/10.1016/0021-9169(84)90063-1

Meehl, G. A., Arblaster, J. M., Chung, C. T. Y., Holland, M. M., DuVivier, A., Thompson, L., Yang, D., & Bitz, C. M. (2019). Sustained ocean changes contributed to sudden Antarctic sea ice retreat in late 2016. *Nature Communications*, *10*(1), 14.

Meehl, G. A., Hu, A., Arblaster, J. M., Fasullo, J., & Trenberth, K. E. (2013). Externally Forced and Internally Generated Decadal Climate Variability Associated with the Interdecadal Pacific Oscillation. In *Journal of Climate* (Vol. 26, Issue 18, pp. 7298–7310). https://doi.org/10.1175/jcli-d-12-00548.1

Meehl, G. A., Hu, A., Santer, B. D., & Xie, S.-P. (2016). Contribution of the Interdecadal Pacific Oscillation to twentieth-century global surface temperature trends. In *Nature Climate Change* (Vol. 6, Issue 11, pp. 1005–1008). https://doi.org/10.1038/nclimate3107

Mundhenk, B. D., Barnes, E. A., Maloney, E. D., & Baggett, C. F. (2018). Skillful empirical subseasonal prediction of landfalling atmospheric river activity using the Madden–Julian oscillation and quasi-biennial oscillation. *Npj Climate and Atmospheric Science*, *1*(1), 20177.

Naito, Y., & Yoden, S. (2006). Behavior of Planetary Waves before and after Stratospheric Sudden Warming Events in Several Phases of the Equatorial QBO. In *Journal of the Atmospheric Sciences* (Vol. 63, Issue 6, pp. 1637–1649). https://doi.org/10.1175/jas3702.1

Naoe, H., & Shibata, K. (2010). Equatorial quasi-biennial oscillation influence on northern winter extratropical circulation. In *Journal of Geophysical Research* (Vol. 115, Issue D19). https://doi.org/10.1029/2009jd012952

Newman, P. A., & Nash, E. R. (2005). The Unusual Southern Hemisphere Stratosphere Winter of 2002. In *Journal of the Atmospheric Sciences* (Vol. 62, Issue 3, pp. 614–628). https://doi.org/10.1175/jas-3323.1

Nie, J., Wang, P., Yang, W., & Tan, B. (2008). Northern hemisphere storm tracks in strong AO anomaly winters. *Atmospheric Science Letters*, *9*(3), 153–159.

Noguchi, S., Kuroda, Y., Kodera, K., & Watanabe, S. (2020). Robust Enhancement of Tropical Convective Activity by the 2019 Antarctic Sudden Stratospheric Warming. In *Geophysical Research Letters* (Vol. 47, Issue 15). https://doi.org/10.1029/2020gl088743

Omrani, N.-E., Keenlyside, N. S., Bader, J., & Manzini, E. (2014). Stratosphere key for wintertime atmospheric response to warm Atlantic decadal conditions. In *Climate Dynamics* (Vol. 42, Issues 3-4, pp. 649–663). https://doi.org/10.1007/s00382-013-1860-3

O'Reilly, C. H., Huber, M., Woollings, T., & Zanna, L. (2016). The signature of low-frequency oceanic forcing in the Atlantic Multidecadal Oscillation. In *Geophysical Research Letters* (Vol. 43, Issue 6, pp. 2810–2818). https://doi.org/10.1002/2016gl067925

Otterå, O. H., Bentsen, M., Drange, H., & Suo, L. (2010). External forcing as a metronome for Atlantic multidecadal variability. In *Nature Geoscience* (Vol. 3, Issue 10, pp. 688–694). https://doi.org/10.1038/ngeo955

Pahlavan, H. A., Fu, Q., Wallace, J. M., & Kiladis, G. N. (2021). Revisiting the Quasi-Biennial Oscillation as Seen in ERA5. Part I: Description and Momentum Budget. In *Journal of the Atmospheric Sciences* (Vol. 78, Issue 3, pp. 673–691). https://doi.org/10.1175/jas-d-20-0248.1

Peings, Y., Cattiaux, J., & Magnusdottir, G. (2019). The Polar Stratosphere as an Arbiter of the Projected Tropical Versus Polar Tug of War. In *Geophysical Research Letters* (Vol. 46, Issue 15, pp. 9261–9270). https://doi.org/10.1029/2019gl082463

Peings, Y., & Magnusdottir, G. (2014). Forcing of the wintertime atmospheric circulation by the multidecadal fluctuations of the North Atlantic ocean. In *Environmental Research Letters* (Vol. 9, Issue 3, p. 034018). https://doi.org/10.1088/1748-9326/9/3/034018

Peings, Y., & Magnusdottir, G. (2016). Wintertime atmospheric response to Atlantic multidecadal variability: effect of stratospheric representation and ocean–atmosphere coupling. In *Climate Dynamics* (Vol. 47, Issues 3-4, pp. 1029–1047). https://doi.org/10.1007/s00382-015-2887-4

Perlwitz, J., & Graf, H.-F. (1995). The Statistical Connection between Tropospheric and Stratospheric Circulation of the Northern Hemisphere in Winter. In *Journal of Climate* (Vol. 8, Issue 10, pp. 2281–2295). https://doi.org/10.1175/1520-0442(1995)008<2281:tscbta>2.0.co;2

Planetary-scale atmospheric phenomena associated with the Southern Oscillation. (1981). In *Deep Sea Research Part B. Oceanographic Literature Review* (Vol. 28, Issue 12, p. 862). https://doi.org/10.1016/0198-0254(81)91145-6

Plumb, R. A., & Alan Plumb, R. (1985). On the Three-Dimensional Propagation of Stationary Waves. In *Journal of the Atmospheric Sciences* (Vol. 42, Issue 3, pp. 217–229). https://doi.org/10.1175/1520-0469(1985)042<0217:ottdpo>2.0.co;2

Plumb, R. A., & Alan Plumb, R. (2010). Planetary waves and the extratropical winter stratosphere. In *The Stratosphere: Dynamics, Transport, and Chemistry* (pp. 23–41). https://doi.org/10.1029/2009gm000888

Plumb, R. A., Alan Plumb, R., & Bell, R. C. (1982). A model of the quasi-biennial oscillation on an equatorial beta-plane. In *Quarterly Journal of the Royal Meteorological Society* (Vol. 108, Issue 456, pp. 335–352). https://doi.org/10.1002/qj.49710845604

Poli, P., Hersbach, H., Dee, D. P., Berrisford, P., Simmons, A. J., Vitart, F., Laloyaux, P., Tan, D. G. H., Peubey, C., Jean-Noël Thépaut, Trémolet, Y., Hólm, E. V., Bonavita, M., Isaksen, L., & Fisher, M. (2016). ERA-20C: An Atmospheric Reanalysis of the Twentieth Century. In *Journal of Climate* (Vol. 29, Issue 11, pp. 4083–4097). https://doi.org/10.1175/jcli-d-15-0556.1

Polvani, L. M. (2002). Tropospheric response to stratospheric perturbations in a relatively simple general circulation model. In *Geophysical Research Letters* (Vol. 29, Issue 7). https://doi.org/10.1029/2001gl014284

Polvani, L. M., Sun, L., Butler, A. H., Richter, J. H., & Deser, C. (2017). Distinguishing Stratospheric Sudden Warmings from ENSO as Key Drivers of Wintertime Climate Variability over the North Atlantic and Eurasia. *Journal of Climate*, *30*(6), 1959–1969.

Rao, J., Garfinkel, C. I., & White, I. P. (2020a). How Does the Quasi-Biennial Oscillation Affect the Boreal Winter Tropospheric Circulation in CMIP5/6 Models? In *Journal of Climate* (Vol. 33, Issue 20, pp. 8975–8996). https://doi.org/10.1175/jcli-d-20-0024.1

Rao, J., Garfinkel, C. I., & White, I. P. (2020b). Impact of the Quasi-Biennial Oscillation on the Northern Winter Stratospheric Polar Vortex in CMIP5/6 Models. In *Journal of Climate* (Vol. 33, Issue 11, pp. 4787–4813). https://doi.org/10.1175/jcli-d-19-0663.1

Rayner, N. A. (2003). Global analyses of sea surface temperature, sea ice, and night marine air temperature since the late nineteenth century. In *Journal of Geophysical Research* (Vol. 108, Issue D14). https://doi.org/10.1029/2002jd002670

Richter, J. H., Anstey, J. A., Butchart, N., Kawatani, Y., Meehl, G. A., Osprey, S., & Simpson, I. R. (2020). Progress in Simulating the Quasi-Biennial Oscillation in CMIP Models. In *Journal of Geophysical Research: Atmospheres* (Vol. 125, Issue 8). https://doi.org/10.1029/2019jd032362

Röthlisberger, M., Frossard, L., Bosart, L. F., Keyser, D., & Martius, O. (2019). Recurrent Synoptic-Scale Rossby Wave Patterns and Their Effect on the Persistence of Cold and Hot Spells. *Journal of Climate*, *32*(11), 3207–3226.

Röthlisberger, M., Pfahl, S., & Martius, O. (2016). Regional-scale jet waviness modulates the occurrence of midlatitude weather extremes. In *Geophysical Research Letters* (Vol. 43, Issue 20, pp. 10,989–10,997). https://doi.org/10.1002/2016gl070944

Santer, B. D., Solomon, S., Pallotta, G., Mears, C., Po-Chedley, S., Fu, Q., Wentz, F., Zou, C.-Z., Painter, J., Cvijanovic, I., & Bonfils, C. (2017). Comparing Tropospheric Warming in Climate Models and Satellite Data. *Journal of Climate*, *30*(1), 373–392.

Sardeshmukh, P. D., & Hoskins, B. J. (1988). The Generation of Global Rotational Flow by Steady Idealized Tropical Divergence. In *Journal of the Atmospheric Sciences* (Vol. 45, Issue 7, pp. 1228–1251). https://doi.org/10.1175/1520-0469(1988)045<1228:tgogrf>2.0.co;2

Scaife, A. A., Arribas, A., Blockley, E., Brookshaw, A., Clark, R. T., Dunstone, N., Eade, R., Fereday, D., Folland, C. K., Gordon, M., Hermanson, L., Knight, J. R., Lea, D. J., MacLachlan, C.,

Maidens, A., Martin, M., Peterson, A. K., Smith, D., Vellinga, M., … Williams, A. (2014). Skillful long-range prediction of European and North American winters. *Geophysical Research Letters*, *41*(7), 2514–2519.

Scaife, A. A., Comer, R. E., Dunstone, N. J., Knight, J. R., Smith, D. M., MacLachlan, C., Martin, N., Andrew Peterson, K., Rowlands, D., Carroll, E. B., Belcher, S., & Slingo, J. (2017). Tropical rainfall, Rossby waves and regional winter climate predictions. In *Quarterly Journal of the Royal Meteorological Society* (Vol. 143, Issue 702, pp. 1–11). https://doi.org/10.1002/qj.2910

Scaife, A. A., Spangehl, T., Fereday, D. R., Cubasch, U., Langematz, U., Akiyoshi, H., Bekki, S., Braesicke, P., Butchart, N., Chipperfield, M. P., Gettelman, A., Hardiman, S. C., Michou, M., Rozanov, E., & Shepherd, T. G. (2012). Climate change projections and stratosphere–troposphere interaction. *Climate Dynamics*, *38*(9), 2089–2097.

Scinocca, J. F., & Haynes, P. H. (1998). Dynamical Forcing of Stratospheric Planetary Waves by Tropospheric Baroclinic Eddies. In *Journal of the Atmospheric Sciences* (Vol. 55, Issue 14, pp. 2361–2392). https://doi.org/10.1175/1520-0469(1998)055<2361:dfospw>2.0.co;2

Scott, R. K., & Haynes, P. H. (1998). Internal interannual variability of the extratropical stratospheric circulation: The low-latitude flywheel. In *Quarterly Journal of the Royal Meteorological Society* (Vol. 124, Issue 550, pp. 2149–2173). https://doi.org/10.1002/qj.49712455016

Scott, R. K., & Polvani, L. M. (2004). Stratospheric control of upward wave flux near the tropopause. In *Geophysical Research Letters* (Vol. 31, Issue 2). https://doi.org/10.1029/2003gl017965

Scott, R. K., & Polvani, L. M. (2006). Internal Variability of the Winter Stratosphere. Part I: Time-Independent Forcing. In *Journal of the Atmospheric Sciences* (Vol. 63, Issue 11, pp. 2758–2776). https://doi.org/10.1175/jas3797.1

Shaw, T. A., & Perlwitz, J. (2014). On the Control of the Residual Circulation and Stratospheric Temperatures in the Arctic by Planetary Wave Coupling. In *Journal of the Atmospheric Sciences* (Vol. 71, Issue 1, pp. 195–206). https://doi.org/10.1175/jas-d-13-0138.1

Simpkins, G. R., Peings, Y., & Magnusdottir, G. (2016). Pacific Influences on Tropical Atlantic Teleconnections to the Southern Hemisphere High Latitudes. *Journal of Climate*, *29*(18), 6425–6444.

Simpson, I. R., Blackburn, M., & Haigh, J. D. (2009). The Role of Eddies in Driving the Tropospheric Response to Stratospheric Heating Perturbations. In *Journal of the Atmospheric Sciences* (Vol. 66, Issue 5, pp. 1347–1365). https://doi.org/10.1175/2008jas2758.1

Simpson, I. R., Blackburn, M., & Haigh, J. D. (2012). A Mechanism for the Effect of Tropospheric Jet Structure on the Annular Mode–Like Response to Stratospheric Forcing. In *Journal of the Atmospheric Sciences* (Vol. 69, Issue 7, pp. 2152–2170). https://doi.org/10.1175/jas-d-11-0188.1

Simpson, I. R., Hitchcock, P., Seager, R., Wu, Y., & Callaghan, P. (2018). The Downward Influence of Uncertainty in the Northern Hemisphere Stratospheric Polar Vortex Response to Climate Change. In *Journal of Climate* (Vol. 31, Issue 16, pp. 6371–6391). https://doi.org/10.1175/jcli-d-18-0041.1

Smith, D. M., Screen, J. A., Deser, C., Cohen, J., Fyfe, J. C., García-Serrano, J., Jung, T., Kattsov, V., Matei, D., Msadek, R., Peings, Y., Sigmond, M., Ukita, J., Yoon, J.-H., & Zhang, X. (2019). The Polar Amplification Model Intercomparison Project (PAMIP) contribution to CMIP6: investigating the causes and consequences of polar amplification. In *Geoscientific Model Development* (Vol. 12, Issue 3, pp. 1139–1164). https://doi.org/10.5194/gmd-12-1139-2019

Smith, K. L., Fletcher, C. G., & Kushner, P. J. (2010). The Role of Linear Interference in the Annular Mode Response to Extratropical Surface Forcing. In *Journal of Climate* (Vol. 23, Issue 22, pp. 6036–6050). https://doi.org/10.1175/2010jcli3606.1

Smith, K. L., Neely, R. R., Marsh, D. R., & Polvani, L. M. (2014). The Specified Chemistry Whole Atmosphere Community Climate Model (SC-WACCM). In *Journal of Advances in Modeling Earth Systems* (Vol. 6, Issue 3, pp. 883–901). https://doi.org/10.1002/2014ms000346

Son, S.-W., Lim, Y., Yoo, C., Hendon, H. H., & Kim, J. (2017). Stratospheric Control of the Madden–Julian Oscillation. In *Journal of Climate* (Vol. 30, Issue 6, pp. 1909–1922). https://doi.org/10.1175/jcli-d-16-0620.1

Sun, C., Kucharski, F., Li, J., Jin, F.-F., Kang, I.-S., & Ding, R. (2017). Western tropical Pacific multidecadal variability forced by the Atlantic multidecadal oscillation. *Nature Communications*, *8*, 15998.

Sutton, R. T., & Hodson, D. L. R. (2005). Atlantic Ocean forcing of North American and European summer climate. *Science*, *309*(5731), 115–118.

Tandon, N. F., & Kushner, P. J. (2015). Does External Forcing Interfere with the AMOC's Influence on North Atlantic Sea Surface Temperature? In *Journal of Climate* (Vol. 28, Issue 16, pp. 6309–6323). https://doi.org/10.1175/jcli-d-14-00664.1

Tegtmeier, S., Anstey, J., Davis, S., Ivanciu, I., Jia, Y., McPhee, D., & Kedzierski, R. P. (2020). Zonal Asymmetry of the QBO Temperature Signal in the Tropical Tropopause Region. In *Geophysical Research Letters* (Vol. 47, Issue 24). https://doi.org/10.1029/2020gl089533

Terray, L. (2012). Evidence for multiple drivers of North Atlantic multi-decadal climate variability. In *Geophysical Research Letters* (Vol. 39, Issue 19). https://doi.org/10.1029/2012gl053046

The latitudinal structure of the quasi-biennial oscillation. (n.d.). https://doi.org/10.1002/qj.49712455206

Thompson, D. W. J., & Wallace, J. M. (1998). The Arctic oscillation signature in the wintertime geopotential height and temperature fields. In *Geophysical Research Letters* (Vol. 25, Issue 9, pp. 1297–1300). https://doi.org/10.1029/98gl00950

Thompson, D. W. J., & Wallace, J. M. (2000). Annular Modes in the Extratropical Circulation. Part I: Month-to-Month Variability*. In *Journal of Climate* (Vol. 13, Issue 5, pp. 1000–1016). https://doi.org/10.1175/1520-0442(2000)013<1000:amitec>2.0.co;2

Ting, M., Kushnir, Y., Seager, R., & Li, C. (2009). Forced and Internal Twentieth-Century SST Trends in the North Atlantic*. In *Journal of Climate* (Vol. 22, Issue 6, pp. 1469–1481). https://doi.org/10.1175/2008jcli2561.1

Trenberth, K. E., & Shea, D. J. (2006). Atlantic hurricanes and natural variability in 2005. In *Geophysical Research Letters* (Vol. 33, Issue 12). https://doi.org/10.1029/2006gl026894

Vimont, D. J., & Kossin, J. P. (2007). The Atlantic Meridional Mode and hurricane activity. In *Geophysical Research Letters* (Vol. 34, Issue 7). https://doi.org/10.1029/2007gl029683

Wallace, J. M., & Gutzler, D. S. (1981). Teleconnections in the Geopotential Height Field during the Northern Hemisphere Winter. In *Monthly Weather Review* (Vol. 109, Issue 4, pp. 784–812). https://doi.org/10.1175/1520-0493(1981)109<0784:titghf>2.0.co;2

Wang, C. (2004). ENSO, Atlantic Climate Variability, and the Walker and Hadley Circulations. In *Advances in Global Change Research* (pp. 173–202). https://doi.org/10.1007/978-1-4020-2944-8_7

Wang, C., Dong, S., Evan, A. T., Foltz, G. R., & Lee, S.-K. (2012). Multidecadal Covariability of North Atlantic Sea Surface Temperature, African Dust, Sahel Rainfall, and Atlantic Hurricanes. In *Journal of Climate* (Vol. 25, Issue 15, pp. 5404–5415). https://doi.org/10.1175/jcli-d-11-00413.1

Wang, J., Kim, H.-M., & Chang, E. K. M. (2018). Interannual Modulation of Northern Hemisphere Winter Storm Tracks by the QBO. In *Geophysical Research Letters* (Vol. 45, Issue 6, pp. 2786–2794). https://doi.org/10.1002/2017gl076929

Watson, P. A. G., Weisheimer, A., Knight, J. R., & Palmer, T. N. (2016). The role of the tropical West Pacific in the extreme Northern Hemisphere winter of 2013/2014. In *Journal of Geophysical Research: Atmospheres* (Vol. 121, Issue 4, pp. 1698–1714). https://doi.org/10.1002/2015jd024048

White, I., Garfinkel, C. I., Gerber, E. P., Jucker, M., Aquila, V., & Oman, L. D. (2019). The Downward Influence of Sudden Stratospheric Warmings: Association with Tropospheric Precursors. *Journal of Climate*, *32*(1), 85–108.

White, I. P., Garfinkel, C. I., Cohen, J., Jucker, M., & Rao, J. (2021). The impact of split and displacement sudden stratospheric warmings on the troposphere. In *Journal of Geophysical Research: Atmospheres*. https://doi.org/10.1029/2020jd033989

White, I. P., Lu, H., Mitchell, N. J., & Phillips, T. (2015). Dynamical Response to the QBO in the Northern Winter Stratosphere: Signatures in Wave Forcing and Eddy Fluxes of Potential Vorticity. In *Journal of the Atmospheric Sciences* (Vol. 72, Issue 12, pp. 4487–4507). https://doi.org/10.1175/jas-d-14-0358.1

White, R. H., Battisti, D. S., & Sheshadri, A. (2018). Orography and the boreal winter stratosphere: The importance of the Mongolian mountains. *Geophysical Research Letters*, *45*(4), 2088–2096.

Woo, S.-H., Sung, M.-K., Son, S.-W., & Kug, J.-S. (2015). Connection between weak stratospheric vortex events and the Pacific Decadal Oscillation. In *Climate Dynamics* (Vol. 45, Issues 11-12, pp. 3481–3492). https://doi.org/10.1007/s00382-015-2551-z

Yamashita, Y., Akiyoshi, H., & Takahashi, M. (2011). Dynamical response in the Northern Hemisphere midlatitude and high-latitude winter to the QBO simulated by CCSR/NIES CCM. In *Journal of Geophysical Research* (Vol. 116, Issue D6). https://doi.org/10.1029/2010jd015016

Zhang, J., & Rothrock, D. A. (2003). Modeling Global Sea Ice with a Thickness and Enthalpy Distribution Model in Generalized Curvilinear Coordinates. In *Monthly Weather Review* (Vol. 131, Issue 5, pp. 845–861). https://doi.org/10.1175/1520-0493(2003)131<0845:mgsiwa>2.0.co;2

Zhang, J., Xie, F., Ma, Z., Zhang, C., Xu, M., Wang, T., & Zhang, R. (2019). Seasonal Evolution of the Quasi-biennial Oscillation Impact on the Northern Hemisphere Polar Vortex in Winter. In *Journal of Geophysical Research: Atmospheres* (Vol. 124, Issue 23, pp. 12568–12586). https://doi.org/10.1029/2019jd030966

Zhang, L., & Wang, C. (2013). Multidecadal North Atlantic sea surface temperature and Atlantic meridional overturning circulation variability in CMIP5 historical simulations. In *Journal of Geophysical Research: Oceans* (Vol. 118, Issue 10, pp. 5772–5791). https://doi.org/10.1002/jgrc.20390

Zhang, R., & Delworth, T. L. (2007). Impact of the Atlantic Multidecadal Oscillation on North Pacific climate variability. In *Geophysical Research Letters* (Vol. 34, Issue 23). https://doi.org/10.1029/2007gl031601

McIntyre, M. E. (1992). Atmospheric dynamics: Some fundamentals, with observational implications. *The use of EOS for studies of atmospheric physics*, *313*, 386.